Amphiphilic Block Copolymers: Application in Gene Delivery and *In-vitro* Biological Evaluation

Chaitra Shetty

A Thesis

in

The Department

of

Chemistry and Biochemistry

Presented in Partial Fulfilment of the Requirements

For the Degree of Master of Science (Chemistry) at

Concordia University

Montreal, Quebec, Canada

May 2020

CONCORDIA UNIVERSITY

School of Graduate Studies

This is to certify that the thesis prepared

By: Chaitra Shetty

Entitled: Amphiphilic Block Copolymers: Application in Gene Delivery and *In-vitro* Biological

and submitted in partial fulfilment of the requirements for the degree of

Master of Science (Chemistry)

complies with the regulation of the University and meets the accepted standards with respect to originality and quality.

Signed by the final examining committee:

Dr. Cameron Skinner Chair

Dr. Rafik Naccache Examiner

Dr. Louis Cuccia Examiner

Dr. John Oh Supervisor

Dr. Christopher Wilds Supervisor

Approved by:

Dr. Yves Gélinas
Graduate Program Director

Dr. André G. Roy
Dean of Faculty

Abstract

Amphiphilic Block Copolymers: Application in Gene Delivery and *In-vitro* Biological Evaluation

Chaitra Shetty

Gene therapy holds a great promise in the treatment of acquired genetic disorders such as cancer because it shows fewer side effects compared to chemotherapy. In order for gene therapy to be successful, however, it is crucial to develop efficient and non-toxic gene carriers to overcome poor in vivo stability and low cellular uptake of nucleic acid therapeutic agents. My Master's thesis research mainly focuses on the development of a new approach exploring a combination of hydrophobic modification with stimuli-responsive degradation (SRD) to synthesize novel amphiphilic block copolymer-based nanocarriers for controlled gene delivery. The block copolymer synthesized by atom transfer radical polymerization is designed with an acid-labile acetal linkage at the block junction and pendant disulfide group in a hydrophobic block. The incorporation of labile linkages enables both dual-location dual-acid/reduction-responsive degradation (DL-DSRD) and in situ disulfide-core-crosslinking. Further, the disulfide pendants integrated as hydrophobic moieties facilitate to condense the nucleic acids into nanometer-sized micelleplexes through electrostatic interaction of pendant dimethylamino groups with the anionic phosphate groups of the nucleic acids. Our results demonstrate that the hydrophobic modification approach through DL-DSRD is a robust platform in the development of gene delivery systems with enhanced colloidal stability, reduced cytotoxicity, and improved gene transfection efficiency.

Further, my research is interested in the biological evaluation of delivery nanocarriers to investigate their cellular interactions with various biological systems for tumor-targeted delivery. Four SRD-exhibiting amphiphilic block copolymer micelles were chosen for not only their various chemical compositions but also different positions of labile linkages cleavable in response to acidic pH and glutathione. The results from cytotoxicity and cellular uptake assays reveal that polymer composition and arrangement of monomers play an important role to determine the biological fate of SRD-exhibiting nanocarriers.

Acknowledgments

I would like to express my gratitude to my supervisors, Dr. John Oh and Dr. Christopher Wilds, for their valuable guidance and encouragement throughout my Master's program. The door to their office was always open whenever I ran into a trouble spot or had a question about my research or writing. Their immense knowledge and continuous support have helped me at all times during my Masters research and writing this thesis.

I would also like to extend my gratitude to my committee members Dr. Louis Cuccia and Dr. Rafik Naccache for their support and valuable inputs that helped me guide my research forward.

In addition, I would like to thank Dr. Anne Noronha for training me with skills necessary for gel electrophoresis and providing me with all the nucleic acid samples, both of which were crucial for my research project. I would also like to acknowledge Dr. Chris Law for training and assisting me with fluorescence microscope.

These acknowledgments would not be complete without mentioning my fellow lab-mates in Oh and Wilds research group. I would like to thank to Arman Jazani for training me with the skills for polymerization and Kamaljeet Bawa for instrumentation. Special thanks to Newsha Arezi, Kamaljeet Bawa, Twinkal Patel and Keaton Maruya-Li, for all their help and moral support. Their presence created a positive and constructive environment in the lab that helped me be more productive, survive stress and tackle research problems with ease. I am also grateful to Farshid Effaty, our friend in the adjoining lab for his kind help.

My appreciation also extends to my friends Ajinkya Ghagre and Dushyant Jahagirdar for their motivation, support and for reminding me to take breaks when I have been stressed out.

Last but not the least, I would like to thank my parents whose unconditional love and support has helped me overcome every challenge in life.

List of Publications

1. Maruya-Li, K., Shetty, C., Jazani, A.M., Arezi, N., and Oh, J.K., Dual Reduction/Acid-Responsive Disassembly and Thermoresponsive Tunability of Degradable Double Hydrophilic Block Copolymer. *ACS Omega*, **2020**. *5*, 3734-3742.
2. Jazani, A.M., Arezi, N., Shetty, C., Hong, S.H., Li, H., Wang, X., and Oh, J.K., Tumor-targeting intracellular drug delivery based on dual acid/reduction-degradable nanoassemblies with ketal interface and disulfide core locations. *Polymer Chemistry*, **2019**. *10*, 2840-2853.
3. Bawa, K.K., Jazani, A.M., Shetty, C., and Oh, J.K., PLA-Based Triblock Copolymer Micelles Exhibiting Dual Acidic pH/Reduction Responses at Dual Core and Core/Corona Interface Locations. *Macromolecular Rapid Communications*, **2018**. *39*, 1800477.

Contribution of Authors

The majority of the research presented in this thesis was conducted independently by the author of this thesis under the supervision of Dr. John Oh and Dr. Christopher Wilds at Concordia University. The chapters 1 and 2 were reproduced in part from the original article with approval from the publisher.

In chapter 3, DNA samples were synthesized by Dr. Anne Noronha and RNA samples were synthesized by Dr. Anne Noronha and Alex Pontarelli from Dr. Wilds' research group.

In chapter 4, the polymers were synthesized by my colleagues in Dr. Oh's research group. P1 was synthesized by Kamaljeet Bawa, P3 by Keaton Maruya-Li, P2 and P4 by Arman Jazani.

Table of Contents

List of Figures

List of Tables

List of Abbreviations

^{1}H-NMR	Proton Nuclear Magnetic Resonance
A549	Human lung cancer cell line
ACN	Acetonitrile
ATP	Adenosine triphosphate
ATRP	Atom transfer radical polymerization
BCA	Bicinchoninic acid
BSA	Bovine serum albumin
CD	β-cyclodextrin
CDI	1,1′-Carbonyldiimidazole
CRP	Controlled radical polymerization
$CuBr_2$	Copper (II) bromide
Đ	Dispersity
DBU	Diazabicyclo(5.4.0)undec-7-ene
DCM	Dichloromethane
DL-DSRD	Dual-location dual stimuli-responsive degradation
DLS	Dynamic light scattering
DMAEMA	2-Dimethylaminoethyl methacrylate
DMEM	Dulbecco's modified Eagle medium
DMF	Dimethylformamide
DMF/LiBr	DMF containing 0.1 mol% lithium bromide
DMSO	Dimethyl sulfoxide
DMSO-d_6	Hexadeuterodimethyl sulfoxide
DNA	Deoxyribonucleic acid

Dox	Doxorubicin
DP	Degree of polymerization
dsDNA	Double stranded DNA
DTT	1,4-Dithiothreitol
ECM	Extracellular matrix
EDTA	Ethylenediaminetetraacetic acid
EGFP	Enhanced green fluorescent protein
EO	Ethylene oxide
EPR	Enhanced permeation and retention effect
Et_3N	Triethylamine
FBS	Fetal bovine serum
GPC	Gel permeation chromatography
GSH	Glutathione
GSH-OEt	Glutathione reduced ethyl ester
H_2O_2	Hydrogen peroxide
HCl	Hydrochloric acid
HeLa	Human cervical cancer cell line
HeLa/EGFP	HeLa cells constitutively expressing EGFP
HEPES	4-(2-Hydroxyethyl)-1-piperazineethanesulfonic acid
HepG2	Human liver cancer cell line
HF	Hydrofluoric acid
HMssDMA	Pendant disulfide and tertiary amino group bearing methacrylate monomer
HMssEt	Pendant disulfide group bearing methacrylate monomer

MCF-7	Human breast cancer cell line
MMP	Matrix metalloproteinases
M_n	Number average molecular weight
M-PD	Polyplex of PD
M-PDss	Micelleplex of PDss
MTT	3-(4,5-Dimethylthiazol-2-yl)-2,5-diphenyltetrazolium bromide
N/P	Nitrogen/Phosphate
NADH	Nicotinamide adenine dinucleotide (reduced form)
NADPH	Nicotinamide adenine dinucleotide phosphate (reduced form)
NP	Nanoparticles
NR	Nile Red
PAGE	Polyacrylamide gel electrophoresis
PBS	Phosphate buffered saline
PC-3	Prostate cancer cell line
PD	PEG-AC-PDMAEMA
PDMAEMA	Poly(2-dimethylaminoethyl methacrylate)
pDNA	Plasmid DNA
PDss	PEG-AC-P(HMssEt-co-DMAEMA)
PEG	Poly(ethylene glycol)
PEG-AC-Br	PEG and acetal containing macroinitiator for ATRP
PEG-CA-RAFT	PEG and cyclic acetal linkage containing macroinitiator for RAFT
PEI	Polyethyleneimine
PEO	Poly(ethylene oxide)
PLA	Polylactide

POEOMA	Poly(oligo(ethylene oxide) monomethyl ether methacrylate)
PPTS	Pyridinium p-toluenesulfonate
RAFT	Reversible addition-fragmentation chain transfer
RAW264.7	Abelson murine leukemia virus-induced tumor
RNA	Ribonucleic acid
ROS	Reactive oxygen species
scRNA	scrambled RNA
siRNA	Small interfering RNA
$Sn(II)EH_2$	Tin(II) 2-ethylhexanoate
SRD	Stimuli-responsive degradation
TBDMS	*tert*-butyldimethylsilyl
TBE	Tris/borate/EDTA
TEM	Transmission electron microscopy
THF	Tetrahydrofuran
TPMA	Tris(2-pyridylmethyl)amine
TRAIL	TNF-related apoptosis inducing ligand
Tris	Tris(hydroxymethyl)aminomethane
xM-PDss	Core-crosslinked micelleplex of PDss
ζ-potential	Zeta-potential

Chapter 1

Introduction

1.1. Cancer gene therapy

Cancer is a complex disease arising due to numerous changes in the normal physiology of cells that culminate in the abrupt multiplication of normal cells. The resultant abnormal cell possesses several capabilities such as insensitivity to normal growth regulators, evasion of programmed cell death pathway (apoptosis), unlimited cell replication, induction of angiogenesis, invasion of healthy tissue, and metastasis to a different body part. These capabilities lead to morbidity and mortality in cancer patients.[1] Most cancers present as localized solid mass (except hematological malignancies such as leukemia and lymphoma) which are primarily eliminated by surgery and radiotherapy. However often these solid cancers exhibit metastatic spread to distant sites that cannot be treated by these means. Thus, the current treatment strategy advances to the combination of chemotherapy with surgery and or radiotherapy intending to eliminate both solid and metastatic cancer.[2,3] However, these therapeutic options, especially chemotherapy, have side effects ranging from nausea and cognitive impairment to increased probability of other types of cancer.[3,4] These side-effects make cancer and its treatment a burden to not only patients but also health-care systems.[5] Despite recent advances in reducing the severity of these undesirable effects,[6,7] cancer remains as one of the leading causes of death all over the world irrespective of a country's economic development.[8] In 2018, there were approximately 18.1 million new cases of cancer and 9.5 million deaths from cancer globally.[9] With these numbers expected to rise in the following years,[10] it is necessary to explore alternative strategies to mitigate the suffering and death caused by cancer.

The most commonly employed cancer treatment strategy, chemotherapy, aims to kill all rapidly proliferating cells. However, since small molecule chemotherapeutic agents are not cancer-specific, they damage normal cells during the treatment process which leads to undesired toxicity.[3] Thus, if a novel cancer-specific therapeutic strategy is to be formulated, it is crucial to acquire a sound understanding of the cause for normal cell transformation to the cancer cell. Extensive research into cancer origin has revealed that multiple gene mutations cause various signaling

pathways inside normal cells to go awry, thus transforming them into cancer cells. In the last decade, elaborate research into cancer genomics has led to the identification of more than 300 genes and their alterations associated with cancer, and elucidation of the various pathways they govern.[11,12] In general, these genes can be segregated into three classes: oncogene, tumor suppressor, or stability genes. Oncogenes are activated when mutations occur in the normal version of the gene, also called a proto-oncogene, that tightly controls cell proliferation, survival, and spread. On the other hand, tumor suppression genes are responsible for inhibition of cell proliferation and survival; and their mutations result in its deactivation. Finally, mutations in stability genes incapacitate them from rectifying gene damage.[13,14] This recent understanding of cancer at the molecular level has been exploited to develop novel therapeutic strategies, particularly gene therapy.[15]

Gene therapy is a treatment modality that employs nucleic acid fragments to repair, replace, regulate, or suppress a defective gene and thereby cure or prevent the progression of genetic-defect induced diseases.[16,17] Some examples of nucleic acids used in gene therapy include plasmid DNA (pDNA), antisense oligonucleotides, messenger RNA (mRNA), small interfering RNA (siRNA), small hairpin RNA (shRNA), micro RNA (miRNA)[18] and clustered regularly interspaced short palindromic repeats (CRISPR-Cas9).[19] Since cancer is an acquired genetic disease, this strategy is especially beneficial for treatment because unlike chemotherapy, gene therapy is cancer-specific, targets the defects in the cancer cell, and is non-cytotoxic.[20] Strategies involved in cancer gene therapy can be broadly classified into three categories: a direct attack on cancer cells, upskill normal cells or manipulate immune cells to respond to cancer cell antigen.[21-23] Nucleic acid therapeutics can directly be targeted towards cancer cells to 1) block oncogene expression; 2) replace defective tumor suppressor genes with the wild type gene; 3) express genes in cancer cells that can induce apoptosis or increase sensitivity to conventional therapy or enhance immunogenicity to trigger an immune response. MYC and K-Ras are some examples of oncogenes whose expression has been attempted to be suppressed. Genes have been delivered to cancer cells in an attempt to restore the function of some tumor suppressor genes such as p53, retinoblastoma gene Rb, and PTEN. Apoptosis has been induced in cancer cells by introducing genes such as TNF-related apoptosis inducing ligand (TRAIL), caspases, and Interleukin-24 (IL-24). By introducing genes encoding for enzymes such as thymidine kinase, cancer cells can be made sensitive to chemotherapeutic agents by enabling conversion of non-cytotoxic prodrug to toxic

metabolites inside cancer cells.[23] Delivery of immunostimulatory genes such as those encoding for cytokines can boost the immunogenicity of cancer cells thereby making them recognizable by immune cells.[21] Besides, gene therapy can be used to deliver genes to normal cells which can confer capabilities to protect itself from damage from chemotherapeutic drugs.[24] Instead of targeting cancer or normal cells, the immune system and immune response can be harnessed to target and eliminate cancer cells. Immune cells can be engineered to recognize antigens specific to particular cancer types thereby enabling them to initiate an immune reaction to and eradicate cancer cells.[21] Despite significant progress in targeting strategies and treatment modalities, the efficiency of cancer gene therapy strongly relies on safe and efficient delivery of a functional gene to the target cancer site.[23,25] Nucleic acids are susceptible to biochemical degradation, cleared rapidly by kidney and unable to pass through the cell membrane due to their large size and high charge density. These limitations have driven the need to develop sophisticated delivery systems to overcome these challenges.[26-28]

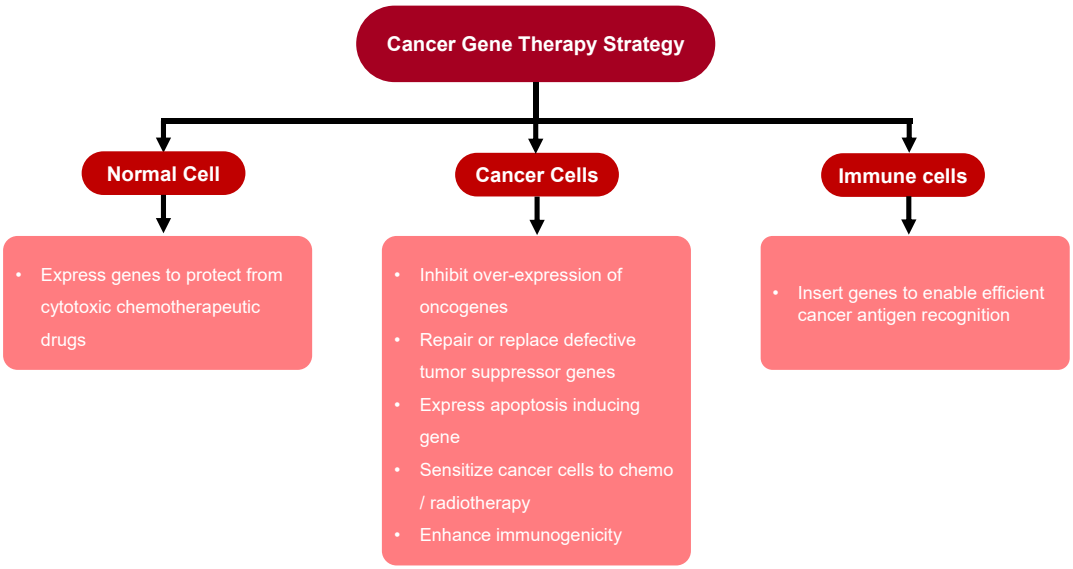

Figure 1.1. Strategies employed in cancer-gene therapy.

1.2. Tumor microenvironment

The nucleic acid carriers should not only condense and protect the nucleic acid but also deliver it specifically to the tumor site. This specificity can be achieved by exploiting the unique features of cancer tissues.[29] The dynamic interaction of cancer cells with the surrounding vascular tissue, immune cells, cytokines, and the extracellular matrix (ECM) creates a complex tumor microenvironment that dictates the survival, growth, proliferation, and metastasis of the cancer

cell.[30,31] Recent investigations of tumor microenvironment have disclosed several features unique to tumor tissue which are significantly different from the normal tissue microenvironment (Figure. 1.2). Rapidly proliferating tumor cells have an ever-increasing need for nutrients and oxygen, and this demand can only be met if a dedicated blood vessel is present. Thus, tumors secrete certain factors that induce rapid formation and maintenance of blood vessels. However, this rapid formation results in blood vessels with poorly aligned endothelial cells separated by wide fenestrations (200 – 800 nm)[32] and elevated levels of vascular permeability factors such as bradykinin, nitric oxide, matrix metalloproteinases (MMPs) and vascular endothelial growth factor (VEGF) which result in vasculature that are 3-10 times more leaky compared to normal tissue. Moreover, the growing tumor compresses the lymph vessel causing it to collapse and the resulting decrease in lymphatic drainage allows the macromolecules to be retained in the tumor microenvironment. This entrapment of leaked macromolecules in the tumor site is referred as enhanced permeation and retention (EPR) effect. This effect has been extensively exploited to passively target nanocarriers to tumor tissue.[32-34]

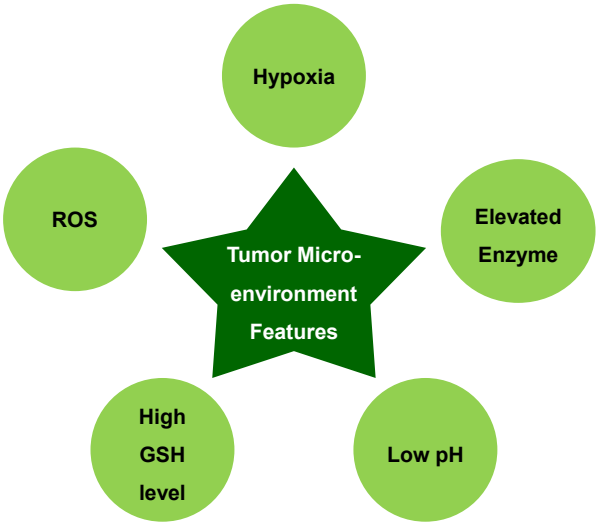

Figure 1.2. Unique characteristics exhibited by cancer cells in their microenvironment.

Architecturally defective and impaired blood vessels result in inconsistent blood supply to all cells in tumor tissue. This leads to some sites being deprived of oxygen thereby creating a hypoxic environment.[35] Moreover, cancer cells alter or enhance their metabolic pathway to achieve and sustain their rapid proliferative capacity even in the presence of low oxygen supply. A major proportion of the cancer cell's energy requirement is fulfilled by less-efficient aerobic glycolysis rather than oxidative phosphorylation. This aerobic glycolysis also referred to as the Warburg

effect, which involves the metabolism of glucose in the presence of oxygen resulting in the production of lactic acid. The elevated production of lactic acid results in an increase in acidity of the tumor microenvironment. Thus, the extracellular environment of the tumor has a pH of 6.5 – 6.8 compared to pH 7.4 for normal tissues.[36] In addition to altered metabolic pathways, cancer cells exhibit abnormalities in mitochondrial oxygen metabolism which is normally involved in the generation of energy through oxidative phosphorylation. Impairment of this pathway can lead to the formation of reactive oxygen species (ROS) and since cancer cells exhibit mitochondrial dysfunction, they contain elevated levels of ROS.[37,38] High levels of ROS can damage nucleic acids, lipids, and protein thereby diminishing cell viability. To counter this, cancer cells increase the production of glutathione (GSH) which detoxifies the ROS. Cancer cells have approximately 10 times higher GSH concentration than normal cells (2 – 10 mM).[39] Since cancer cells rely on glycolysis for their energy requirement, they exhibit elevated levels of associated enzymes. In addition to this, enzymes associated with the metabolism of lipids and amino acids such as serine, methionine, and arginine are also over-expressed.[40] Apart from metabolic enzymes, MMPs, which are involved in remodeling of various structural proteins in ECM, are also overexpressed. Remodeling of ECM structure by MMPs has been known to regulate cancer cell survival, proliferation, differentiation, migration, and invasion.[41] These unique intracellular features offered by tumor tissues including hypoxia, acidic pH, redox potential, elevated ROS, and elevated enzymes have potential as precise triggers because they are responsive to the specific environment of cancer cells. Thus, by taking advantage of these characteristics an efficient and cancer-specific nucleic acid carrier can be developed which is inactive in the presence of normal tissue but turns active in tumor sites.[42]

1.3. Polymer-based therapeutic delivery systems

In nature, viruses have acquired the ability to overcome biological barriers and introduce nucleic acids into host cells with high specificity and efficiency. These attributes make viral vectors ideal candidates for nucleic acid delivery.[43,44] However, their application is restricted due to their limited nucleic acid carrying capacity, inherent immunogenicity, inflammatory response, carcinogenesis, toxicity, broad tropism, poor reproducibility, and high cost.[45-47] These drawbacks have prompted researchers to explore non-viral strategies for nucleic acid delivery because of their low safety risk, low immunogenicity, design flexibility, unrestricted nucleic acid cargo size, and low cost. Taking advantage of the negatively charged nature of nucleic acids, various positively

charged biomaterials such as lipids, peptides, polysaccharides and polymers (Figure. 1.3) have been widely explored to package and deliver nucleic acid therapeutics.[48-50] Among these cationic lipids and cationic polymers have been extensively studied. Despite their simple structure and easy synthesis, cationic lipids exhibit limitations such as difficulty to functionalize with various modifications, poor *in-vivo* stability, and low entrapment efficiency.[51,52] On the other hand, cationic polymers offer diversity in structure, composition, and functional groups which enable the easy synthesis of a wide range of polymers exhibiting different physiochemical properties. This property makes cationic polymers an ideal candidate as a non-viral nucleic acid carrier.[53,54]

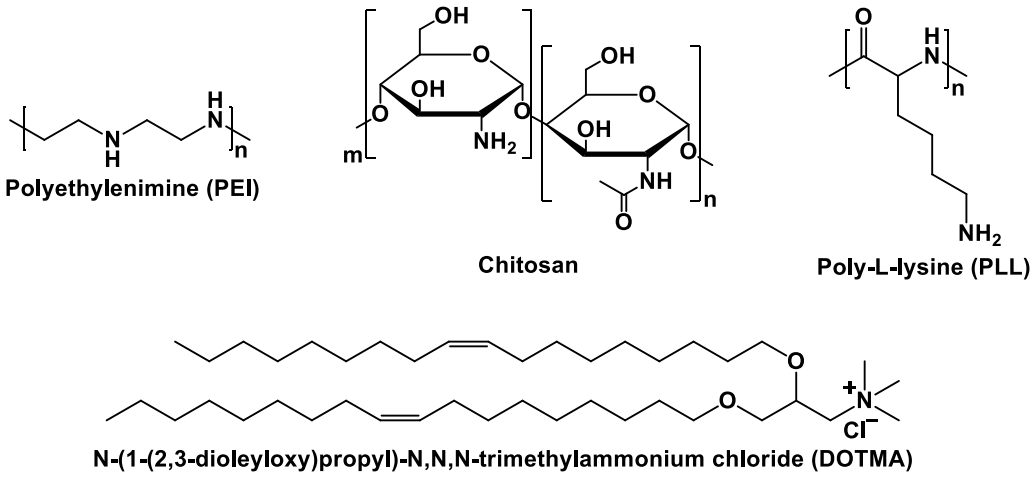

Figure 1.3. Examples of polycations used in gene therapy.

Complexation of nucleic acids with polycations makes it inaccessible for degradation by nucleases; however, a polyplex needs to overcome various extracellular and intracellular barriers for successful gene delivery (Figure 1.4). Upon intravenous administration, positively charged polyplexes interact with anionic blood proteins which lead to either disassembly or aggregation of the nanocarrier. Once the polyplexes are coated by proteins for phagocytosis, also known as opsonization, the mononuclear phagocytic system (MPS) is activated leading to clearance of these particles from circulation. Shielding the positive charge of the polyplex with neutral polymers like poly(ethylene glycol) (PEG) can avoid opsonization and prolong the nanocarrier's circulation time. The next barrier is extravasation into the target tissue which is directly related to the size and permeability of the vascular endothelium at the target site. Since tumor tissues have leaky vasculature, polyplexes with a size less than the fenestrae can extravasate into the tumor tissue.[55] After overcoming these extracellular barriers, the polyplexes encounter intracellular barriers. The

first barrier is the endocytosis of the polyplex. This cellular uptake pathway is dependent on the surface charge, size, and targeting-ligands on the surface of the polyplex. Irrespective of the uptake pathway, all polyplexes will be localized in the early endosome. Early endosome undergoes rapid acidification (from pH 6 to 5) and slowly merges with other sorting vesicles; maturing into the late endosome. These late endosomes are finally trafficked to the lysosome that further acidifies (pH ~4.5) and activate various degradative enzymes which result in rapid degradation of contents in the vesicle i.e. nucleic acid. Thus, the polyplex must escape the endosome before the degradation sequence is initiated.[56] Cationic polymers are believed to escape the endosome by the proton sponge effect wherein a large number of amine groups in the polymer undergo protonation during endosomal acidification and thus promote a rapid influx of protons and the counterion Cl^-. This increased uptake of ions is compensated by the intake of water, causing osmotic swelling and subsequent rupture of the endosomal membrane. Alternatively, protonation of polymer and its tight juxtaposition with the inner membrane of the endosome is also believed to lead to permeabilization of the endosomal membrane and thus allow the release of nucleic acid into the cytosol.[57] Finally, the escaped nucleic acid should be transported to their site of action in the cell i.e. cytoplasm or nucleus.[56] Thus, the chemical and functional versatility offered by polymers should be used to judiciously design a delivery system capable of bypassing all the biological barriers and deliver the nucleic acid to the target cell with high transfection efficiency and low cytotoxicity.[58,59]

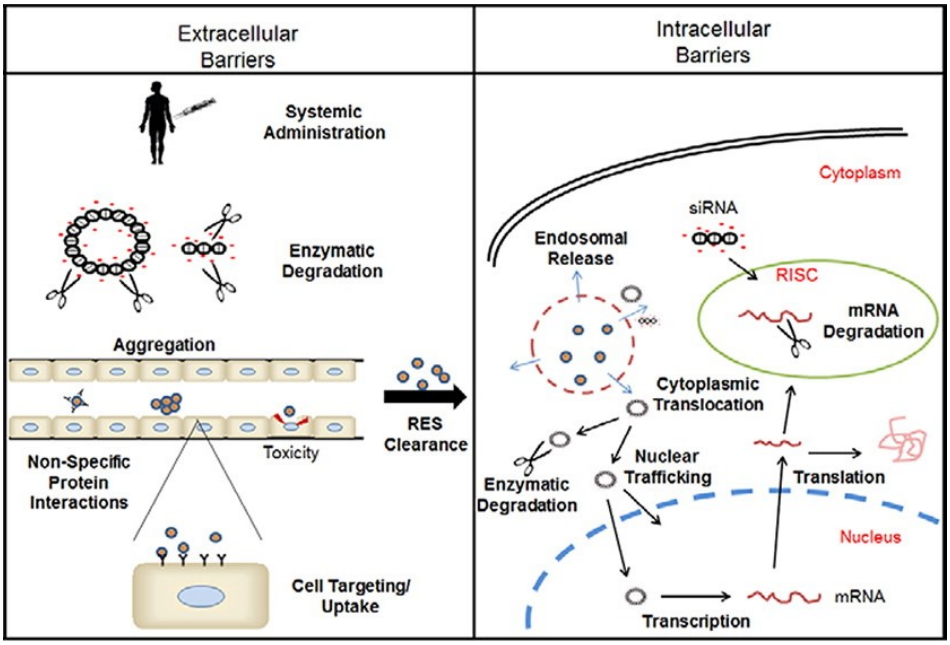

Figure 1.4. Extracellular and intracellular barriers for non-viral gene delivery.[56]

As a result of extensive research, it has been found that the performance of polymeric nucleic acid carriers is dependent on architecture, composition, molecular weight, dispersity, surface properties, charge density, and size of the polyplex. Thus, the utilization of procedures that offer tight control over synthesis is crucial to obtain polymers with a high degree of uniformity and well-defined physiochemical properties.[59,60] Controlled/living radical polymerization (CRP) techniques such as atom transfer radical polymerization (ATRP) and reversible addition-fragmentation chain transfer (RAFT) enable precise control over polymer synthesis thereby resulting in carriers of well-defined architecture, size, shape, and functionality.[59-63] In addition to this, introduction of hydrophobic segments in the polymer has been shown to influence polymer-based nucleic acid carrier's performance. Hydrophobization of polycations has been shown to improve gene delivery efficiency by increasing nucleic acid loading, boosting cellular uptake, enhancing endosomal escape ability, preventing disassembly in serum, and decreasing cytotoxicity.[64,65] The performance of these carriers can be enhanced further by introducing functionalities that respond to extra- or intracellular factors specific to stimuli presented in a cancer cell or its micro-environment. This stimuli-responsive nature regulates the assembly and disassembly behavior of the polymer in the presence of cancer-specific stimuli which in turn could help in improving not only the gene transfection ability and biocompatibility but also the carrier's stability, target specificity, cellular uptake and endosomal escape ability.[66,67]

Apart from gene therapy, significant efforts have been undertaken to either synthesize new chemotherapeutic agents or improve the existing ones.[68] Recent advancement in processes associated with drug design, drug discovery, biotechnology and pharmaceutical studies have led to the identification of several drugs that are highly effective in cancer treatment. However, despite being highly efficient in killing cancer cells, their clinical application is impeded due to low stability, rapid degradation *in-vivo*, bioavailability, rapid clearance from blood circulation, lack of specificity and unacceptable systemic toxicity.[69-74] Since the processes involved in new drug development is both time consuming and financially draining, the current research focus is directed towards alleviating these limitations by developing strategies to deliver these drugs safely, efficiently, and specifically to tumor tissues. Encapsulating these drugs in polymers responsive to cancer-specific stimuli is an ideal strategy for their safe administration.[66] With the increasing application of polymers in the biomedical area, it has become imperative to determine the effect of polymer characteristics on its interaction with biological systems. Based on the requirement,

polymers have been designed such that the resulting nanocarriers have different sizes, shapes, and surface chemistry. This has been shown to influence tissue permeability, carrier uptake and intracellular metabolism. Thus, there is a need for a detailed investigation of polymer structure-activity relationships so as to unleash the full potential of polymer-based nanocarriers for therapeutic applications.[75-78]

1.4. Research objectives and scope of thesis

My Master's research focuses on exploring two aspects of stimuli-responsive degradable amphiphilic block copolymers; a) assess their ability to complex and deliver therapeutic nucleic acids to target cells and b) evaluate the influence of polymer composition on the nanocarrier's interaction with cells.

The primary objective of my Master's research is to explore dual location dual-stimuli responsive degradation (DL-DSRD) and amphiphilicity in the design and synthesis of an amphiphilic block copolymer and its micelleplex for efficient gene delivery and transfection. To achieve this objective, recent strategies that have been explored for the development of acid and reduction-responsive polymeric nanocarriers for gene delivery are mapped and summarized in Chapter 2.

Chapter 3 describes the synthesis and characterization of a novel acid and reduction-responsive micelleplex for gene silencing. A novel block copolymer composed of a hydrophilic PEG block bridged by an acetal linkage to a hydrophobic cationic block bearing pendant tertiary amine and disulfide groups is synthesized by ATRP technique. Through mutual ionic interactions of cationic protonated amine groups with anionic nucleic acids, the block copolymer formed nanometre-sized micelloplexes which contain acid-responsive cleavable acetal linkages at core/corona interface and reduction-responsive cleavable disulfide linkages in the core, thus displaying the property of dual-acid/reduction degradation at dual locations. The neutral PEG corona conferred stealth properties to the micelleplex whereas the crosslinked core prevented destabilization of the micelleplex in the presence of competing polyanions. In the presence of both acid and reduction stimuli, these micelleplexes were found to disassemble and release nucleic acid. Moreover, the copolymer and its micelleplex with siRNA was demonstrated to be non-cytotoxic and the micelleplex exhibited gene silencing in the presence of both the stimuli.

The second objective of my Master's research is to investigate the cellular interaction of various stimuli-responsive degradable amphiphilic block copolymer micelles for drug delivery. Chapter 4 provides detailed studies on the exploration of the significance of polymer architecture on the cellular interaction of nanocarriers. The influence of different nanocarriers on cancer cells was evaluated by a combination of cytotoxicity assays and microscopy techniques. Upon comparative analysis of the results, a relationship between polymer composition and cellular interaction was observed.

Finally, chapter 5 presents a concise summary of knowledge acquired during the research (concluding remarks) and potential improvement to the design strategy for a gene carrier (future directions).

Chapter 2

Recent Advances in Cationic Polymer-Based Gene Delivery Vectors: Stimuli-Responsive Degradation and Hydrophobic Modification

For the development of effective cationic polymers for gene delivery, an integration of stimuli-responsive degradation (SRD) and hydrophobic moieties is a promising platform to reduce cytotoxicity and enhance release of encapsulated therapeutic genes. SRD involves the incorporation of labile linkages into the design of cationic polymers that are cleaved in response to specific stimuli. Acidic pH, GSH, ROS, and enzymes are promising endogenous stimuli found in tumor tissues and cancer cells. On the other hand, an incorporation of hydrophobic moieties into the framework of a polycation modulates its charge density and interaction with the cell membrane; thereby facilitating cellular uptake, endosomal escape and gene release. This chapter describes recent advances in the development of cationic polymers with SRD or hydrophobic modifications for gene delivery.

2.1. SRD-exhibiting nucleic acid delivery systems

2.1.1. pH-responsive systems

Polymers can be engineered to be dynamic, capable of undergoing changes to their chemical structures and properties in response to a pH change in their environments. These polymers are generally synthesized by incorporation of pH-labile or pH-responsive functional groups that are susceptible to modification in pathological tissue environment. The extracellular microenvironment of normal healthy tissues is maintained very close to pH = 7.4; however, tumor tissues exhibit an acidic microenvironment (pH = 6.5 - 6.9) as a result of elevated lactic acid production. Also, cells contain acidic environments within compartments such as endosomes or lysosomes.[79-81] Moreover, the introduction of these functionalities at different locations in the polymer enables the preparation of nanocarriers with unique features that ultimately contribute to enhancement in gene-delivery efficacy of the carrier. These differences can be considered to design novel pH-responsive nanocarriers for cancer-gene delivery.[82,83] This section summarizes pH-responsive cationic polymers for gene delivery with two important categories based on a pH-

responsive degradation mechanism: chemical degradation through linkage cleavage and physical degradation through charge balance.

Chemical degradation through cleavage of a linkage

After intravenous injection, the undesired interactions of cationic polyplexes with anionic blood components can be alleviated by shielding positive charges with neutral hydrophilic polymers such as PEG (covalent attachment) and anionic polymers (ionic interaction). However, this approach often hinders their cellular uptake, thus decreasing transfection efficiency. A promising solution is to introduce acidic pH-responsive degradable linkages such as ketal, acetal, imine, hydrazone, and orthoester into the design of cationic polymers. Upon the cleavage of these linkages in acidic pH, the protective layers can be shed or the polyplexes can be disintegrated at tumor sites.[84]

Guan et al. synthesized a pH-responsive PEG-detachable gene delivery nanocarrier by conjugation of an aldehyde-terminated PEG with PEI/DNA polyplexes through the formation of acidic pH-cleavable imine linkages. The conjugation allows for the formation of colloidally-stable complexes with the diameter < 200 nm, thus decreasing their zeta-potential and reducing cytotoxicity compared to their PEI/DNA counterparts. Cellular uptake and transfection efficiency of PEG/PEI/DNA was significantly lower than PEI/DNA at pH 7.4; however, at pH 6.8 it increased and became similar to PEI/DNA. This enhancement was attributed to acid-catalyzed hydrolysis of the junction imine linkages that can expose positive charges. Further, PEG/PEI/DNA showed higher accumulation and gene transfection efficiency at tumor tissues in tumor-bearing mice compared to PEI/DNA.[85]

Yang et al. designed an acid-labile star-shaped polymer (A-CD-PGEA) composed of a β-cyclodextrin (CD) core linked via an acid-labile acetal linkage to ethanolamine-functionalized poly(glycidyl methacrylate) (PGEA) (Figure 2.1). A-CD-PGEA could condense DNA into nanocarriers that are stable at physiological pH but rapidly release the DNA at endosomal pH = 5.5. Despite similar cellular uptake, A-CD-PGEA exhibited significantly higher transfection efficiency compared to CD-PGEA (polymer devoid of acetal linkage).[86] These studies suggest that acid-responsive de-shielding or separation of polycation components leads to an enhancement in gene delivery efficacy of a nanocarrier.

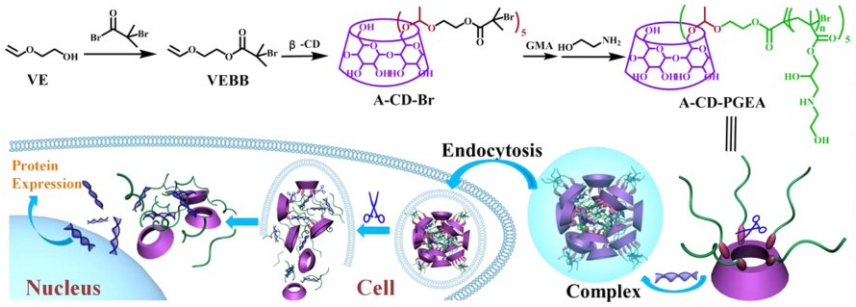

Figure 2.1. Scheme for the synthesis of A-CD-PGEA and illustration of its intracellular gene release mechanism.[86]

Apart from the junction, pH-responsive linkages can also be introduced into the core of the polyplex to enhance its stability and facilitate nucleic acid release. Leber et al. developed an acid-responsive cationic nanohydrogel crosslinked by acid-labile ketal containing linkers. Self-assembled micelles prepared from an amphiphilic block copolymer of oligo(ethylene oxide) methyl ether methacrylate and pentafluorophenyl (PFP) methacrylate, was crosslinked by switching the hydrophobic reactive PFP ester with a spermine analogue crosslinker bearing a ketal linkage. The resulting nanohydrogel consists of a cationic cage capable of loading siRNA by electrostatic interaction. siRNA loaded nanohydrogel was stable at pH 7.4 but released the encapsulated siRNA rapidly in acidic pH. The acid-responsive nanohydrogel exhibited higher cellular uptake and transfection efficiency *in-vitro* compared to the nanohydrogel crosslinked with non-degradable spermine. In murine liver fibrosis model, acid-labile nanohydrogel exhibited enhanced accumulation in fibrotic tissue; however, its transfection efficiency decreased and was similar to non-degradable nanohydrogel. Nevertheless, the pronounced clearance of acid-labile nanohydrogel indicated its superior biocompatibility and *in-vivo* tolerance compared to non-degradable nanohydrogel.[87]

In addition to acid-responsive linkages, pH-dependent association and dissociation between host-guest moieties can be harnessed to enhance gene delivery efficacy of nanocarriers. Kim et al. exploited the pH-dependent affinity of phenylboronic acid (PBA) with cis-diols to develop a pH-responsive PEI-based nucleic acid carrier. The interaction between PBA modified PEI and galactose modified PEI (1.8 kDa) resulted in the formation of CrossPEI which was further coated with PBA modified PEG (PBA-PEG) (Figure 2.2). Since the binding affinity of PBA increases in the order glucose < galactose < ribose, the polyplex was stable during blood circulation even in

the presence of glucose. However, this affinity between PBA and galactose weakened at low pH environments and in the presence of the ribose sugar of ATP. Thus, the polyplex was found to release nucleic acid only in presence of low pH or high ATP concentration, which in turn resulted in higher luciferase expression than PEI 25 k in MCF-7, HeLa, and PC-3 cell lines. Moreover, PBA can act as a cancer targeting ligand due to its ability to bind to sialylated glycoprotein receptors overexpressed in various tumors. Thus, when injected into MCF-7-xenografted mice, PBA-PEG-CrossPEI accumulated twice as much as PEG-CrossPEI in the tumor. Also, the release of pDNA coding a soluble fragment of VEGF receptor Flt-1 (sFlt-1) from PBA-PEG-CrossPEI in fast-growing CT-26 colon cancer cells in mice resulted in inhibition of tumor growth after 7 days. Thus, the ability of sialylated receptors to recognize PBA enabled the development of a cancer-specific carrier with high transfection efficiency due to pH-dependent PBA-sugar disassociation and low toxicity.[88]

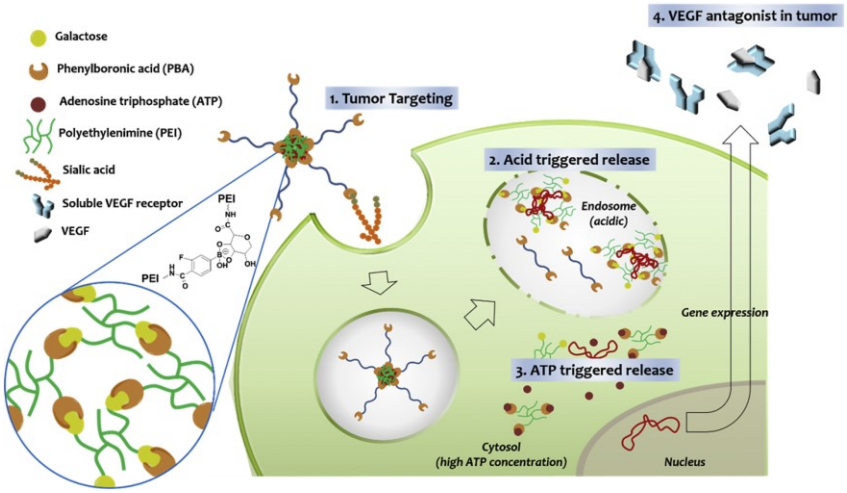

Figure 2.2. Schematic illustration of tumor-targeting by PBA-PEG-CrossPEI and subsequent release of anti-angiogenic gene in response to acid and ATP.[88]

Physical degradation through charge balance

An ionizable group capable of undergoing reversible protonation and deprotonation in response to changes in pH can be incorporated to impart pH-responsive nature into the polymer. Depending on the pH, these transitions dictate a polymer's hydrophobic/hydrophilic or ionic/non-ionic characteristics in a given environment. Thus, such polymers enable preparation of nanocarriers capable of undergoing a pH-triggered transition, thereby offering enhancement in cellular uptake, endosomal escape and nucleic acid release.[89]

The endosome represents an important barrier which nanocarriers need to overcome for successful gene transfection. One way to overcome this barrier is by incorporation of substituents that are hydrophobic at physiological pH but switch to a hydrophilic state in the acidic pH of the endosome due to protonation. The consumption of protons during this switch contributes to the proton sponge effect and thus enhances the nanocarrier's ability to escape the endosome.[90] Ye et al. developed a PEG-coated double-network nanogel consisting of silane-crosslinked PEI (PEI-S) as the first network and pH-responsive poly(2-(hexamethyleneimino) ethyl methacrylate) polymer (PC7A) as the second network (Figure 2.3). Incorporation of PC7A (with or without PEG) into PEI-S polyplex resulted in the compaction of nanoparticles to a size of ~50 nm. PEI-S with a low extent of crosslinking (silane:PEI (25 kDa) = 4:1) brought about a 3-fold increase in transfection efficiency compared to PEI (25 kDa). Incorporation of PC7A to this crosslinked formulation enabled nanogels to achieve transfection efficiency significantly higher than lipofectamine which was retained even after PEGylation. These results suggested that hydrophobicity of PC7A at physiological pH played an important role in enhancing DNA condensation and nanocarrier stability whereas its hydrophobic to hydrophilic transition below pH 6.8 facilitated endosomal escape and DNA release. They further went on to explore the influence of PC7A on transfection efficiency of other commonly used polycations such as polyarginine, poly(2-dimethylaminoethyl methacrylate) (PDMAEMA), poly(N-(2-aminoethyl)aspartamide) (PAsp(EDA)), and poly (N′-(N-(2-aminoethyl)-2-aminoethyl)-aspartamide) (Psp(DET)). The addition of PC7A showed a dramatic increase in the transfection efficiency of all the polycations. These results suggest that pH-responsive PC7A could be used as an additive to enhance the transfection efficiency of different systems.[91]

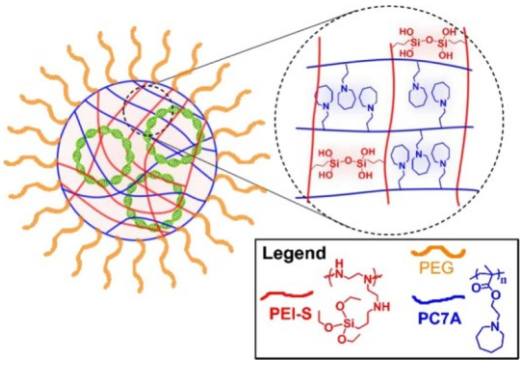

Figure 2.3. Schematic illustration of a double-network nanogel.[91]

Similarly, Cheng et al. designed a pH-sensitive polymer (SP) in which the cationic block was composed of poly((oligo(ethylene oxide) monomethyl ether methacrylate)-co-DMAEMA) (POEOMA-co-DMAEMA) and a pendant benzoic imine group bearing poly(propargyl methacrylate)-graft-poly(propyl-(4-methoxy-benzylidene)-amine)) (PMA-g-PMBA) formed the hydrophobic block capable of undergoing a pH-triggered transition to the hydrophilic state. At pH 5.5, SP exhibited a rapid decrease in size and a higher DNA release compared to pH insensitive polymer (IP). Furthermore, SP polyplexes exhibited significantly higher endosomal escape and luciferase activity in HeLa cells compared to IP and P(OEOMA-co-DMAEMA). These results indicate that the consumption of H^+ for the cleavage of the benzoic imine group augment the proton sponge effect of DMAEMA and thus facilitate endosomal membrane rupture. Moreover, the primary amines produced due to hydrolysis of benzoic imine group enable the polymer to switch from hydrophobic to hydrophilic properties thereby enhancing its gene release. On the other hand, despite having a hydrophobic component, IP exhibited impaired DNA release in the cytoplasm which highlights the importance of the stimuli-assisted hydrophilic transition of polymer for efficient gene delivery.[92]

The other way to overcome the endosomal barrier is to employ membrane-active peptides; however, they exhibit non-specific toxicity. To reduce the toxicity of the membrane-active peptide melittin, Cheng et al. designed a virus-inspired amphiphilic polymer that undergoes a conformational change in the acidic environment of the endosome to expose the otherwise hidden melittin and bring about the selective disruption of the endosomal membrane. This virus-inspired polymer for endosomal release (VIPER) consisted of a hydrophilic cationic block for complexation with nucleic acid, and a pH-sensitive block capable of unveiling melittin by undergoing a pH-triggered transition from hydrophobic to hydrophilic state (Figure 2.4). Block copolymer P(OEOMA-co-DMAEMA) formed the hydrophilic cationic block whereas block copolymer of pH-responsive 2-diisopropylaminoethyl methacrylate (DIPAMA) and pyridyl disulfide ethyl methacrylate (PDSEMA) formed the pH-sensitive block. Melittin was conjugated to the PDSEMA block in VIPER by disulfide exchange reaction. Control polymer complex without melittin (CP/DNA) did not exhibit hemolysis at any pH, whereas VIPER/DNA polyplex induced significant hemolysis only at pH 5.4, thereby indicating VIPER's ability to expose melittin in response to an acidic environment. This ability enabled VIPER to escape from the endosome

effectively, lower its cytotoxicity, and enhance transfection efficiency. Compared to PEI, VIPER exhibited 11 % and 3 % higher transfection efficiency *in-vitro* and *in-vivo* respectively.[93]

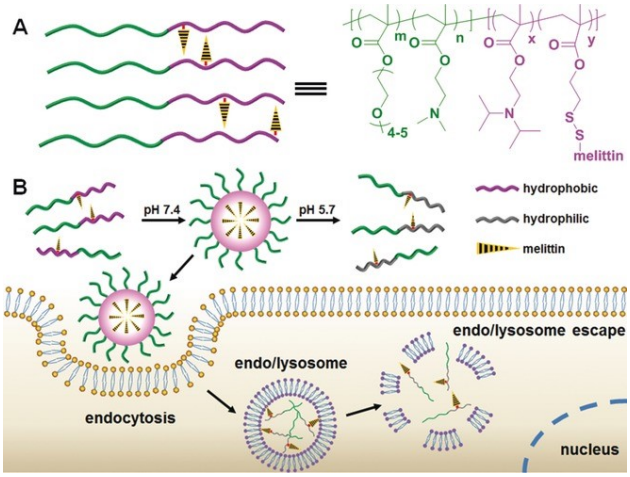

Figure 2.4. Structure **a)** and schematic illustration of cellular uptake and endosomal escape of VIPER **b)**.[93]

Shielding of polyplex with neutral or anionic polymer avoids non-specific interactions and prolongs circulation time; however, it can hinder cellular uptake at the tumor site. Thus, it is desirable to develop a nanocarrier that is neutral or anionic during blood circulation but switches to a positive charge at the tumor site, thereby enhancing cellular uptake, endosomal escape, and transfection efficiency. Guo et al. developed a pH-responsive charge-convertible ternary system comprising of a cationic PEI/DNA core coated with a pH-responsive anionic polymer made of 1,2-cyclohexanedicarboxylic anhydride (CCA) and folic acid (FA) grafted PEI (FA-PEI-CCA). The addition of anionic FA-PEI-CCA to PEI/DNA complex did not impair the complex and helped to decrease the cytotoxicity of PEI/DNA at pH 7.4. FA-PEI-CCA/PEI/DNA exhibited lower transfection efficiency than PEI/DNA at pH 7.4; however, at pH 6.8 FA-PEI-CCA/PEI/DNA exhibited transfection efficiency similar to PEI/DNA. This increase in transfection efficiency was attributed to acid-triggered hydrolysis of amides with β-carboxylic acids leading to regeneration of positively charged amine and hence positively charged complex.[94]

Similarly, taking advantage of the susceptibility of amides with β-carboxylic acids to acid-trigged hydrolysis, Ooi et al. developed a pH-responsive surface charge switchable ternary system CD-OEI/pDNA/PPD_9+PPS_1 comprising of a positively charged core for DNA complexation coated with an anionic polymer to prevent non-specific interaction with blood components (Figure

2.5). The core consists of oligoethylenimine (OEI) conjugated β-CD whereas the anionic polymer consists of PEG, pH-sensitive PPD (2,3-dimethylmaleic anhydride (DMA) modified poly(2-aminoethyl methacrylate hydrochloride) (PAEMA) and a small amount of pH insensitive PPS (succinic anhydride-modified PAEMA). At N/P ratios 10 - 50, the ternary system condensed DNA into a neutral or negatively charged nanocarrier with a size range of 100 - 200 nm. CD-OEI/pDNA/PPD_9+PPS_1 exhibited lower cellular uptake and transfection efficiency at physiological pH when compared to CD-OEI. However, the cellular uptake and transfection efficiency increased significantly at pH 6.5 owing to a switch from negative to positive charge due to the exposed primary amine generated by pH triggered hydrolysis of the amide bond in PPD.[95]

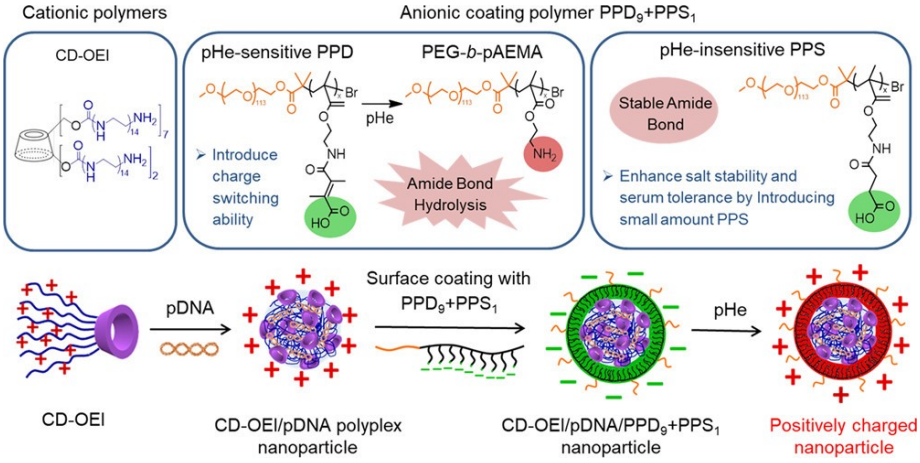

Figure 2.5. Structure of CD-OEI/pDNA/PPD_9+PPS_1 and schematic illustration of its assembly and pH-responsive disassembly.[95]

2.1.2. Glutathione (GSH)-responsive systems

Glutathione (GSH) is an attractive stimulus due to a significant difference in its concentration in the extracellular environment compared to the intracellular environment. GSH concentration in the intracellular environment ranges from 1-10 mM which is 100-1000 times higher than GSH concentration of 1-10 μM in the extracellular environment. In addition, cancer cells have a higher GSH concentration than normal cells which makes the development of GSH-responsive nanocarriers a promising strategy for cancer gene delivery.[96-99]

Incorporation of disulfide linkages into the framework of polymers results in nanocarriers that can be degraded in the presence of a high level of intracellular GSH. Such GSH-responsive degradation can promote the intracellular release of nucleic acids from nanocarriers, thus

enhancing gene transfection efficiency.[100] Ullah et al. synthesized a PEGylated bioreducible cationic polymer PEG-b-poly(disulfide-L-lysine) (PEG-SSL) by Michael addition reaction of PEG tetra-acrylate with amine-terminated PEG-SSL. PEG-SSL/pDNA complexes exhibit no significant size change upon incubation with DTT (2 μM); whereas, their size increased drastically in the presence of DTT (5 mM); confirming the redox-responsive nature of PEG-SSL polymer. Compared with PEI, PEG-SSL/pDNA polyplexes had significantly lower cytotoxicity and further similar transfection efficiency. These results indicate that the inclusion of GSH-responsive linkages enhanced gene release.[101]

A series of galactose-based hyperbranched polymers (HRRP) composed of disulfide-bond bearing cross-linker N,N′-bis(methacryloyl)cystamine (BMAC) and varying ratios of 2-lactobionamidoethylmethacrylamide (LAEMA) and 2-aminoethyl methacrylate (AEMA), were synthesized and evaluated by Peng et al. for the rapid release of siRNA in the cytosol in response to elevated GSH concentration (Figure 2.6). Polymers containing a higher LAEMA:AEMA ratio displayed a lower zeta-potential and lower toxicity. Compared to other HRRPs and lipofectamine, HRRP with a LAEMA:AEMA ratio of 1.5 exhibited enhanced serum stability, the lowest cytotoxicity, less non-specific EGFR silencing, and the highest specific EGFR silencing. Upon redox-responsive degradation, a higher sugar to cation ratio resulted in lower charge distribution making the polyplex unstable and thus enhancing the release of siRNA.[102]

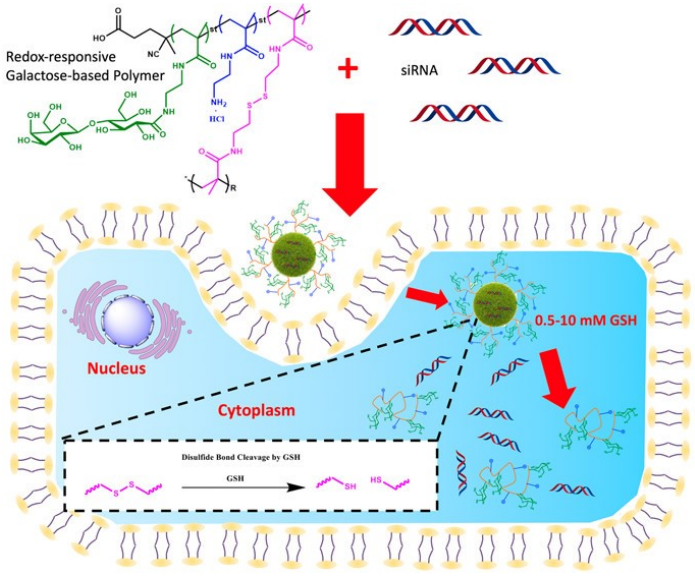

Figure 2.6. Schematic illustration of HRRP-siRNA complex formation, cellular uptake and GSH-responsive intracellular release of siRNA from the polyplex.[102]

Gao et al. developed redox-responsive backbone degradable single-chain cyclized polymeric nanoparticles for gene delivery. The P(DMAEMA-co-MDTD-co-TEGDA) synthesized via RAFT was composed of DMAEMA for electrostatic complexation with DNA, tri(ethyleneglycol) diacrylate (TEGDA) for formation of intrachain cyclization and 3-methylidene1,9-dioxa-5,12,13-trithiacyclopentadecane-2,8-dione (MDTD) for incorporation of disulfide and ester linkages in the polymer backbone (Figure 2.7). P(DMAEMA-co-MDTD-co-TEGDA) exhibited rapid degradation in the presence of GSH (20 mM) which resulted in higher gene transfection efficiency than PEI. Also, P(DMAEMA-co-MDTD-co-TEGDA) was found to be significantly less cytotoxic than PEI.[103]

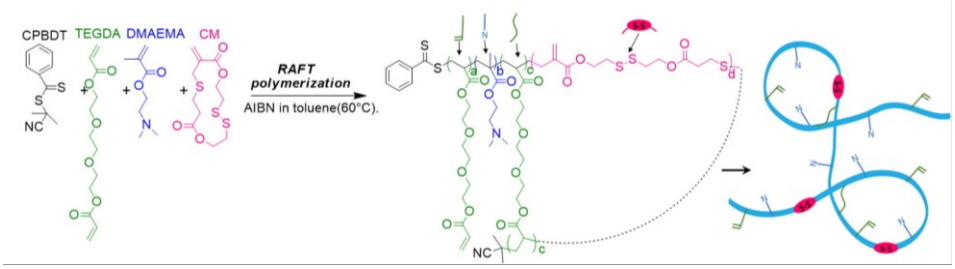

Figure 2.7. Synthesis of backbone-degradable single-chain cyclized polymer poly(DMAEMA-co-MDTD-co-TEGDA) by RAFT polymerization.[103]

A novel system for co-delivery of docetaxel (DTX), gambogic acid (GA), and matrix metalloproteinase-9 (MMP-9) short hairpin RNA (shRNA) was developed by Kang et al. by conjugating GA with bioreducible poly(amido amine)s (PAA) through amide bond formation. The resulting amphiphilic block copolymer (PAG) self-assembled into micelles with a hydrophobic GA core for encapsulation of DTX and hydrophilic PAA shell for complexation with MMP-9 shRNA. In the presence of 3 mM DTT, PAG/DTX-shRNA exhibited rapid release of shRNA, DTX (80 % in 24 hr) and GA (79.7 % in 24 hr) whereas in absence of DTT no shRNA, and low DTX (52 % in 24 hr) and GA (16.5 % in 24 hr) release was observed. PAG/DTX-shRNA transfected a higher number of cells than PEI and resulted in an 83.7% decrease in MMP-9 expression. Moreover, the tumor inhibitory rate of PAG/DTX-shRNA and commercial anti-cancer drug Taxotere® in MCF-7 tumor-bearing mice was 45.6 % and 24.9 % respectively. These results indicated that PAG/DTX-shRNA could co-deliver three anti-cancer agents to tumor tissues and release them rapidly in the presence of a high redox environment.[104]

Based on the observation that the lack of positive charge prompts gene release from viruses, Jiang et al. designed a novel polymeric carrier to enhance gene release by employing a similar strategy (Figure 2.8). The polymer was synthesized by copolymerizing pyridyl disulfide ethyl methacrylate (PDS) and POEOMA, followed by N-methylation of PDS units (MPDS). The positively charged MPDS promoted the interaction of the polymer with DNA and the subsequent core-crosslinking in presence of DTT resulted in the loss of the cationic unit and entrapment of DNA in a non-cationic cage. This non-cationic complex was non-cytotoxic, stable in low GSH levels (10 μM), and released DNA only in the presence high GSH levels (10 mM). Also, this carrier exhibited efficient knockdown of Tuba1a and decreased the development of highly sensitive mouse embryos.[105]

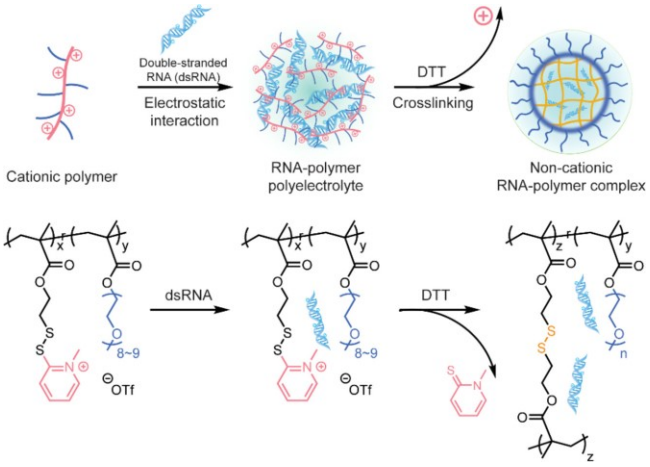

Figure 2.8. Schematic illustration of the formation of non-cationic MPDS/siRNA complex.[105]

To exert their therapeutic effect, different nucleic acids need to be delivered to the specific compartments within the cell. For example, targeting of DNA versus messenger RNA (mRNA) with a therapeutic nucleic acid requires translocation into the nucleus for the former and the cytosol for the latter. Thus, a delivery system should be meticulously designed such that it not only protects but also delivers the therapeutic agent to the right compartment in the cell. Wang et al. synthesized poly(N,N′-bis(acryloyl)cystamine-co-triethylenetetramine) (p(BAC-TET))-based polymers to design bioreducible nanocarriers capable of delivering DNA, mRNA, Cas9 ribonucleoprotein (RNP), and S1mplex. p(BAC-TET), a type of poly(N,N′-bis-(acryloyl) cystamine–poly(aminoalkyl)) (PBAP) polymer, consists of disulfide linkages in its backbone for redox-responsive release of therapeutic agents and imidazole (Im) group for endosomal escape. PBAP was modified with either CD or adamantane (AD) and mixed together to form cross-linked

PBAP (CLPBAP) due to host guest-interaction between the CD and AD. The complex was coated with PEG conjugates PBAP (PEG-PBAP-PEG) for serum stability and prolonged circulation time. CLPBAP/PEG-CLPBAP-PEG/mRNA exhibited higher transfection efficiency compared to Lipo 2000. Since the site of action of DNA, Cas9 RNP and S1mplex is the nucleus, they were loaded into PBAP together with nuclear localization signal (NLS) peptide to induce nuclear translocation, followed by crosslinking and PEG-PBAP-PEG coating. CLPBAP/PEG-CLPBAP-PEG/DNA exhibited similar transfection efficiency compared to lipofectamine and inclusion of small amounts of NLS increased transfection efficiency significantly. In cells treated with CLPBAP/PEG-CLPBAP-PEG/DNA, DNA was found to escape endosomes within 2 hrs and localize in DNA within 6 hrs in the presence of NLS. CLPBAP/PEG-CLPBAP-PEG/RNP and CLPBAP/PEG-CLPBAP-PEG/S1mplex exhibited similar gene correction efficiency to Lipo 2000. Also, CLPBAP was significantly less cytotoxic than Lipo 2000. Thus, this study demonstrated the versatility of these bioreducible nanovectors in not only protecting but also delivering the payload to the designated site of action and thereby making it a potential carrier for delivery of various therapeutic agents for a wide range of applications.[106]

Intracellular release from the polyplex is hindered due to the interaction between the cationic polymer and anionic nucleic acid. However, this release can be facilitated if the polymer is capable of switching to the anionic state inside the cell. Thus, Wang et al. designed a novel cationic polymer, poly(N-(2-(acryloyloxy)ethyl)-N-(p-(2,4-dinitrophenoxy)benzyl)-N,N-diethyl ammonium chloride) (PADDAC), capable of switching from a positive to negative surface charge specifically in presence of GSH (Figure 2.9). In the presence of GSH, thiolysis of *p*-dinitrophenyl ether conjugated with a quaternary ammonium moiety results in generation of a polymer containing a tertiary amine that is subsequently hydrolysed to form the negatively charged polymer poly(acrylic acid). Within 1 hr, nearly half of the PADDAC degraded and released DNA in the presence of GSH but not cysteine or homocysteine. These results confirmed the ability of PADDAC to undergo GSH-responsive degradation and thereby release the gene due to charge reversal. PADDAC/DNA complex coated with PEGylated lipid (LPADDAC) showed greater stability, prolonged blood circulation time, and lower cytotoxicity compared to PADDAC. Moreover, LPADDAC/pLuci exhibited 2-4 times higher luciferase expression both *in-vitro* and *in-vivo* compared to PEI/pLuci. Transfection of HeLa, A549, and HepG2 cells with LPADDAC/pTRAIL resulted in 48 % cell death as opposed to 20 % cell death by PEI/pTRAIL.

When injected into HeLa xenograft bearing mice via intravenous administration, the tumor inhibition rate of paclitaxel (PTX), LPADDAC/pTRAIL and Lipo2000/pTRAIL were 77 %, 87 %, and 40 % respectively. Also, PTX treated mice exhibited abnormal spleen hypertrophy and severe loss in body weight, whereas these adverse effects were not observed in LPADDAC/pTRAIL treated mice.[107]

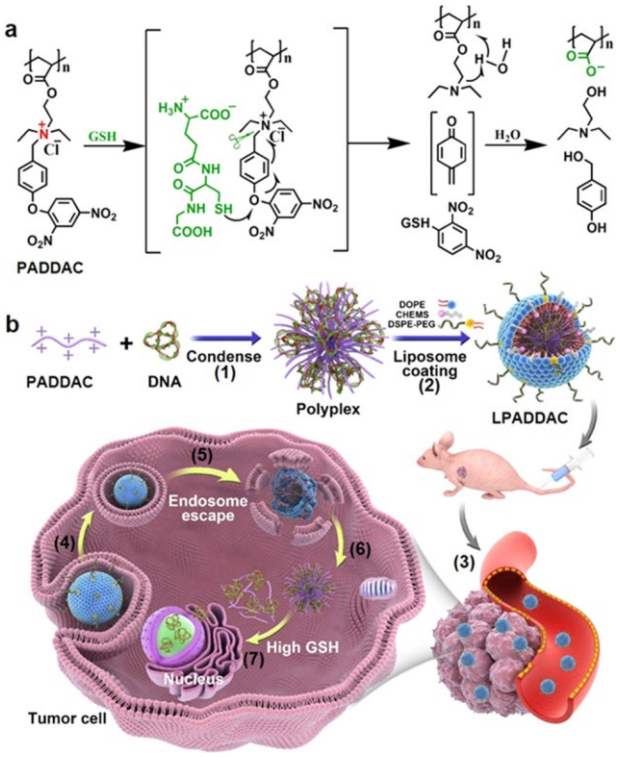

Figure 2.9. Chemical structure of PADDAC and its charge-reversal in presence of GSH **a)** and formation of PADDAC polyplex (1) followed by coating with PEGylated lipid resulting in formation of LPADDAC (2). After LPADDAC administration, the polyplex accumulates at the tumor tissue (3) and is endocytosed by the tumor cell (4). After the endosomal escape (5), the polyplex degrades in presence of GSH (6) and rapidly releases DNA due to charge-reversal (7) **b)**.[107]

2.1.3. Reactive oxygen species (ROS)-responsive systems

In cancer cells, impaired mitochondrial activity and incomplete oxidative phosphorylation results in the generation of reactive oxygen species (ROS), and thus cancer cells exhibit elevated levels of intracellular ROS.[108-110] Taking advantage of the sensitivity of aryl boronates to ROS, Li et al. synthesized a ROS-responsive dendrimer poly(amido amine)-N-(4-boronobenzyl)-N,N-

diethyl-2-(propionyloxy) ethan-1-aminium (PAMAM-(B-DEAEP)$_{16}$) . In presence of ROS (H_2O_2), oxidation of terminal boronate groups led to the conversion of quaternary ammonium to tertiary amine, followed by self-catalyzed hydrolysis of the ester bond to generate negatively charged poly(amido amine)-propionic acid (PAMAM-PAc$_{16}$). This charge-reversal causes complete nucleic acid release from DNA/PAMAM-(B-DEAEP)$_{16}$ complexes in the presence of H_2O_2 (2 mM). Also, PAMAM-(B-DEAEP)16/Cy-5 DNA complexes gained entry into HeLa cells within 30 mins and within 4 hrs significant amount of Cy-5 DNA was found in the nucleus. Moreover, PAMAM-(B-DEAEP)$_{16}$ exhibited 4.5 times higher gene transfection efficiency compared to PEI (25 kDa) and thus indicating the charge reversal due to elevated ROS promoted efficient gene transfection.[111]

Fang et al. developed a ROS responsive gene carrier composed of p-tosyl-L-arginine grafted polylysine (PLL-RT) for DNA complexation and H_2O_2-responsive thioketal dipropane-dioic acid-modified dextran (TDPAD) for coating the polyplex core to shield from extracellular anions (Figure 2.10). TDPAD compressed the nanocarrier, decreased the zeta potential, and enhanced serum stability of the PLL-RT/DNA (PD) polyplex. In the absence of H_2O_2, TDPAD/PLL-RT/pDNA failed to show significant cellular uptake and transfection efficiency; however, the cellular uptake and transfection efficiency increased significantly in the presence of H_2O_2. These results indicate that the shedding of the external coating due to cleavage of thioketal linkages exposed the positively charged polyplex core and thus enhanced cellular uptake and transfection efficiency. Moreover, mercaptopropionic acid (MPA), generated from H_2O_2-responsive degradation of TDPAD induced cancer cell apoptosis and thus enhanced the anti-tumor effect of TDPAD/PLL-RT/pDNA. In 4T1 (mouse breast cancer cell line) bearing mice, TDPAD/PLL-RT/pDNA exhibited prolonged blood circulation time, enhanced tumor accumulation, elevated gene transfection efficiency and higher anti-tumor effect compared to PD.[112]

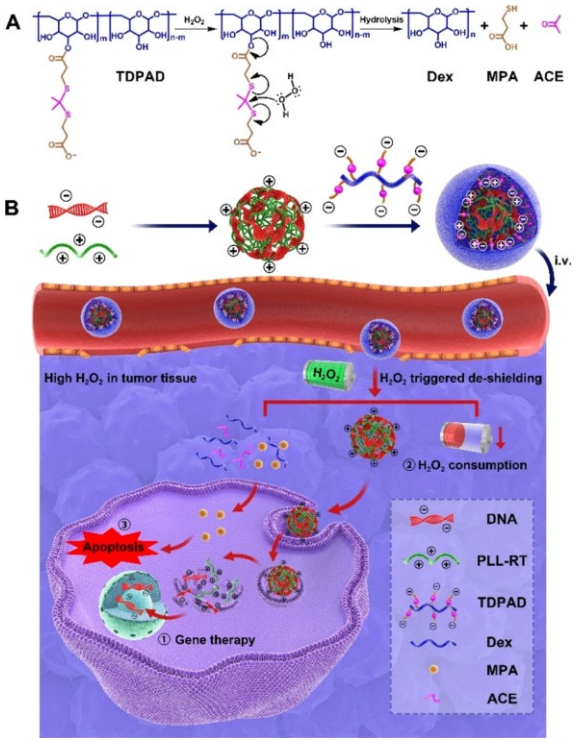

Figure 2.10. Degradation of TDPAD in the presence of ROS **a)** and schematic illustration of ROS-responsive TDPAD degradation inside cells and subsequent release of MPA and DNA **b)**.[112]

2.1.4. Enzyme-responsive systems

Rapidly proliferating cancer cells have an ever-increasing demand for energy and to meet those demands certain enzymes involved in metabolism of nutrients are over-expressed.[113] In addition, cancer cells modulate the expression of enzymes such as esterase[114] and matrix metalloproteinases (MMP)[115] involved in various physiological processes including invasion and migration. It has been reported that damage to fibroblast cells during cancer treatment induces it to secrete WNT16B, which promotes tumor cell survival and metastasis, causes quick tumor relapse and poor prognosis of chemotherapy. Thus, Qui et al. designed a cancer-specific gene delivery system by taking advantage of high esterase expression in cancer cells but low levels in fibroblast cells. An esterase responsive polymer (ERP) was synthesized by the reaction of PEI (10 kDa) with 4-acetoxybenzyl acrylate, followed by quaternization (Figure 2.11). Esterase-catalyzed hydrolysis of 4-acetoxybenzyl ester groups in ERP, triggers its charge-reversal and thus facilitating rapid DNA release. In the presence of 100 U mL^{-1} esterase, ERP underwent complete hydrolysis with complete release of DNA; thereby confirming the esterase-responsive charge-responsive

activity of ERP. The ERP polyplex was then coated with a lipid outer layer containing 3β-N-(dimethylaminoethyl)-carbamate hydrochloride (DC-Chol) and 1,2-dioleoyl-sn-glycero-3-phosphoethanolamine (DOPE) to prevent premature disassociation and gene release in presence of extracellular esterase. The resulting lipid-coated esterase-responsive polyplex (LERP) exhibited higher stability in the presence of serum. While PEI exhibited similar pTRAIL transfection efficiency in both HeLa and NIH3T3, LERP exhibited cancer-cell specific expression with significantly higher TRAIL expression in HeLa compared to mouse embryonic fibroblast cells NIH3T3. Similar results were observed *in-vivo* in mice model bearing cancer cells co-cultured with NIH3T3. LERP/pTRAIL selectively targeted and killed cancer cells with no damage to fibroblasts, whereas PEI/pTRAIL, paclitaxel (PTX), irinotecan (CPT11) and cisplatin (CDDP) failed to distinguish between cancer cells and fibroblasts. Moreover, PTX, CPT, and CDDP significantly stimulated fibroblasts to express WNT16B whereas, LERP/pTRAIL not only avoided fibroblast damage but also suppressed the expression of WNT16B. Also, PTX, CPT, and CDDP treatment resulted in severe toxic effects such as significant weight loss, liver damage, kidney damage, and splenomegaly, which, in contrast, was not observed with LERP/pTRAIL treatment.[116]

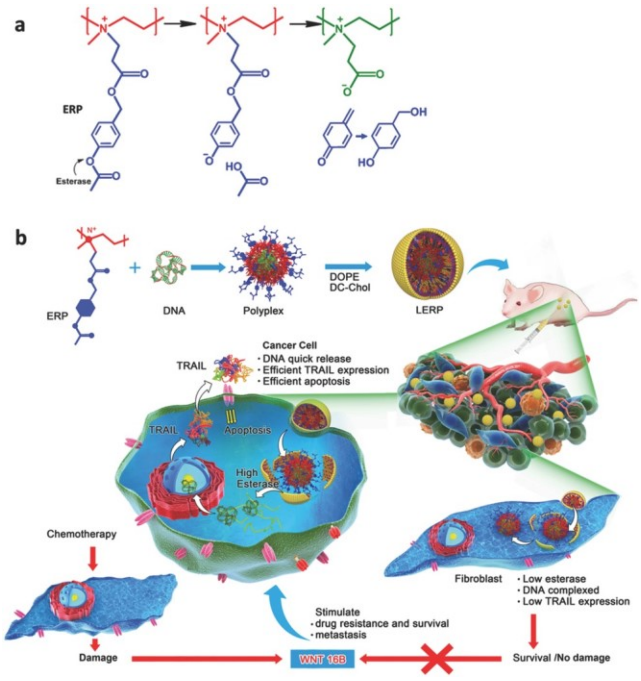

Figure 2.11. Chemical structure of ERP and its cleavage in presence of esterase **a)** and schematic illustration of lipid-coated ERP/pTRAIL complex (LERP/pTRAIL) formation and the difference between the therapeutic action of chemotherapeutic drugs and pTRAIL **b)**.[116]

Zhang et al. developed a surface-mediated matrix metalloproteinase (MMP)-responsive gene delivery system by loading PEI/DNA complex-containing MMP-responsive hydrogel into a micropatterned breath figure (BF) surface. MMP-responsive hydrogels (MDG) were prepared by UV-induced thiol-ene click chemistry between the cysteine residues of the MMP-sensitive peptide GCRD-GPQGIWGQ-DRCG and the acrylate group of the four-armed PEG (PEG-ACRL). When human breast cancer cells (MDA-MB-231) or human normal breast cells (HBL-100) were grown on BF loaded with MDG, cell adhesion was observed on hydrogel-free areas of BF and 40-fold higher gene expression was found in MDA-MB-231 compared to HBL-100. Since PEI/DNA exhibited similar transfection efficiency in both cell lines, the difference in gene expression between cancer and normal cells when treated with BF-MDG was a result PEI/DNA release due to MMP-responsive degradation of MDG.[117]

2.2. Hydrophobic modifications

Charge density influences the interaction of polycations with cell membranes and thus their transfection efficiency and cytotoxicity. An increase in charge density leads to an increase in the transfection efficiency of the polycations but at the cost of higher toxicity. Hence, it is critical to optimize their charge density to maintain the balance of reduced cytotoxicity and higher transfection efficiency.[118] An appealing approach to modulate the charge density of polycations is the hydrophobic modification of cationic copolymers. This approach enables effective condensing of nucleic acids into polyplexes to provide improved carrier stability and elevated cellular uptake. Moreover, the hydrophobic modification facilitates the disruption of endosomal membranes thereby improving the endosomal escape of polyplexes and enhancing gene transfection efficiency.[119]

To investigate hydrophobic modifications for cationic PDMAEMA, Fan et al. explored the incorporation of a hydrophobic poly(L-lactide) (PLLA) block. A triblock copolymer of PDMAEMA-b-PLLA-b-PDMAEMA was synthesized by ATRP of DMAEMA in presence of a PLLA-diBr difunctional initiator (a PLLA bearing bromo groups at both chain ends). The synthesized polymer was partially quarternized with 2-azidoethyl-2-bromopropanoate (AEBP), a bifunctional linker bearing bromopropionyl and azido group. The azido groups were further used for a click-type alkyne-azido cycloaddition reaction to PEGylate the copolymer. The presence of PLLA did not significantly hinder the complexation of DMA-PLLA-DMA or DMA-PLLA-

DMA@PEG with DNA. Moreover, both DMA-PLLA-DMA and DMA-PLLA-DMA@PEG showed reduced cytotoxicity and higher transfection efficiency compared to PDMAEMA which could be a result of not only reduction of charge density but also enhanced cellular interaction due to hydrophobic PLLA.[120] Cheng et al. investigated the integration of polycaprolactone (PCL) as a hydrophobic block into PDMAEMA. CD-g-(PCL-b-PDMAEMA), was synthesized by ring-opening polymerization (ROP) of CL on CD cores, followed by the ATRP of DMAEMA. Compared to PEI and CD-g-PDMAEMA (with no hydrophobic PCL block), CD-g-(PCL-b-PDMAEMA) exhibited greater ability to condense nucleic acids, improved stability, and lower cytotoxicity. Moreover, CD-g-(PCL-b-PDMAEMA) had 10.8 % transfection efficiency in RAW264.7 cells, which is greater than that of 2.4% for CD-g-PDMAEMA and 2.6 % for lipofectamine (a conventional transfection reagent). These results suggest that the enhanced performance of CD-g-(PCL-b-PDMAEMA) is due to the incorporation of hydrophobic PCL.[121]

Despite the advantages, it is crucial to optimize the extent of hydrophobic modification for enhanced gene transfection efficacy. Nelson et al. synthesized a series of PEG-based block copolymers with a random methacrylate copolymer block consisting of cationic DMAEMA and hydrophobic *tert*-butyl methacrylate (*t*BMA), thus forming PEG-b-P(DMAEMA-co-*t*BMA) (PDB) with various densities of BMA units ranging from 0 - 75 mol% (Figure 2.12). The formed PDB with 50 % BMA units exhibited higher cellular uptake, increased stability in blood serum, and extended *in-vivo* circulation time, compared with the PEG-b-PDMAEMA (PD) (no *t*BMA units). It also had resistance against destabilization in the presence of competing for the anionic heparan sulfate in kidneys *in-vivo* and elevated gene silencing both *in-vitro* and *in-vivo*. These results suggested that PDB with 50 % *t*BMA had an optimal balance between cationic and hydrophobic content.[122] Using this information Werfel et al. performed a systematic analysis of a series of ternary nanoparticles that differed in composition (DMAEMA or *t*BMA) and relative quantity of both core and (PEG-containing) corona forming component. The inclusion of *t*BMA in the core was crucial to achieving enhanced stability and improved gene transfection. The systematic study led to the identification of an ideal ternary system, DB4-PDB12 (Core N/P4-Corona, final N/P12) exhibiting efficient cellular uptake, potent endosomal escape, and effective gene silencing *in-vitro*. Compared to binary system PDB, ternary system DB4-PDB12 demonstrated superiority in cellular uptake, stability against heparan sulfate, circulation time, and target gene silencing within tumors. Thus, this study emphasizes the importance of systematic

investigation of the structure-function relationship between the cationic polymer and its hydrophobic substituent to develop ideal gene delivery carriers.[123]

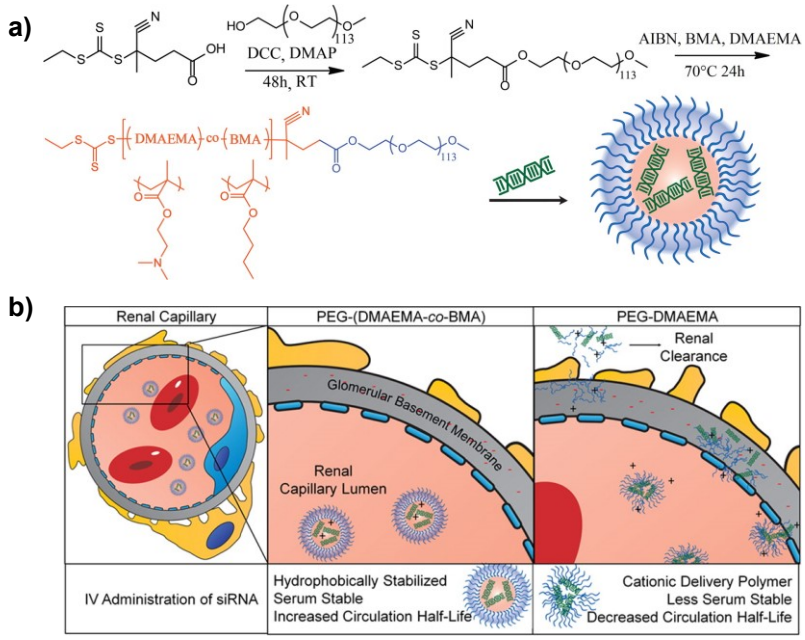

Figure 2.12. Synthesis scheme of PEG-(DMAEMA-co-BMA) and **a)** its merits compared to PEG-DMAEMA **b)**.[122]

To explore the influence of the size of hydrophobic substituent and degree of substitution on gene delivery efficacy of PEI, Teo et al. modified PEI (1.8 kDa) with different hydrophobic functionalities including ethyl, octyl, dodecyl, benzyl, and phenyl groups. Despite a decrease in DNA binding efficiency, the modified PEI polymers were able to condense DNA to polyplexes with the average diameter found to be 96 - 166 nm. These sizes are much smaller than that of the polyplexes (2 µm) formed with unmodified PEI. The transfection efficiency of all modified PEI was higher than that of unmodified PEI. However, among the modified PEI, transfection efficiency decreased with an increasing chain length of the substituent group and increased with the incorporation of an aromatic benzyl compared to an alkyl octyl group. Furthermore, the substitution of all the primary amines was not found to affect the endosomal escape ability of PEI. However, a lower degree of ethyl conjugation (1, 2 or 4 ethyl/PEI) increased the transfection efficiency whereas a higher degree of ethyl conjugation (10 ethyl/PEI) significantly decreased the transfection efficiency.[124] Similarly, Thapa et al. investigated the gene delivery efficacy of various PEI-PrAs synthesized by grafting propionic acid (PrA) onto PEI (1.2 kDa). In comparison to PEI,

PEI-PrA exhibited a decrease in pDNA binding efficiency and buffering capacity as well as an increase in cytotoxicity of the polymer. However, PEI-PrA with a low degree of PrA substitution (< 1.2 PrA/PEI) demonstrated higher transfection efficiency compared to PEI and long-chain linolenic acid substituted PEI (1.2 kDa).[125] Thus, these studies show that enhancement in gene delivery efficacy of a polycation is dependent on both choice of substituent and the degree of substitution.

Chapter 3

Acid-Responsive PEG-Sheddable Micelleplex with Bioreducible Core for Dual-disassembly-mediated Gene Silencing

3.1. Introduction

Sequence-specific target gene silencing by processes such as RNA interference has created a powerful therapeutic intervention strategy that has the promise to treat numerous diseases including cancer.[126,127] Since its discovery 20 years ago, several strategies have been explored for safe and efficient delivery of siRNA into the target site.[128] However, there still remains a number of challenges for this therapeutic strategy. These include stability, nuclease resistance and target specificity of synthetic siRNA which have been improved by introducing various design modifications. Despite these modifications, unmodified siRNA is incapable of entering the cells and thus there is a need for a carrier agent to facilitate endocytosis and promote localization of siRNA in the subcellular compartment.[129,130] Viruses exhibit an ability to introduce a gene into target cells with high specificity and efficiency thus making them ideal gene carriers.[131] However, their limited nucleic acid capacity, high cost of production, immunogenicity and toxicity have motivated researchers to explore non-viral gene carrier systems.[132-134]

A variety of materials such as polymers, peptides, lipids, polysaccharides, and dendrimers carrying positive charge have been developed due to their ability to not only condense siRNA into nanocarriers but also enhance cellular uptake.[49,135,136] Among all of these, cationic polymers have attracted a lot of attention as a result of their chemical versatility, design flexibility, high nucleic acid cargo capacity, low cost, and low immunogenicity.[137,138] Cationic polyplexes formed as a result of electrostatic interaction between the positively charged polymer and negatively charged nucleic acid are susceptible to non-specific interaction with blood components leading to its aggregation and subsequent removal from circulation by opsonization. Moreover, the cationic moieties have been shown to destabilize cell and mitochondrial membranes resulting in cytotoxicity.[139] Masking the positive charge with a neutral, hydrophilic and biocompatible polymer such as PEG has been shown to improve stability, circulation time and biocompatibility of the polyplex by suppressing non-specific interactions.[140,141] Despite their numerous advantages, it is

challenging for polyplexes to reach many targeted sites. Moreover, polyplexes are not degradable and display transfection efficiency which increases with increasing molecular weight of the polycation. Both these attributes increase the cytotoxicity of the polyplex.[142]

Polyplexes can reach the targeted tumor sites by taking advantage of the EPR effect whereby wider fenestrations in the endothelial lining of blood vessels surrounding the rapidly growing tumor tissues lead to easy passage of polyplexes and low lymphatic drainage from tumor lead to their accumulation.[143-145] Once endocytosed into the tumor cell, the polyplex should be capable of releasing the siRNA in the cytoplasm. One way to modulate the binding affinity of siRNA with the polycation is to introduce linkages which degrade in presence of an internal trigger.[146,147] Tumor cells have a slightly acidic (~ pH 6.5-6.8) extracellular matrix[148,149] and high (~10 times) intracellular GSH concentration compared to normal tissue.[150] Moreover, endosome and lysosome inside the cells have a significantly acidic (pH 6.5 - 4) environment. Thus acid-labile linkages such as acetals or ketals and redox responsive linkages such as disulfide can be employed to achieve on-demand release of siRNA.[151] Another widely explored approach involves incorporation of a hydrophobic modification into the design of a polycation. Hydrophobic moieties have been shown to not only enhance polyplex disassembly for siRNA release but also improve siRNA encapsulation, stability, cellular uptake and endosomal escape ability.[64,119] Furthermore, both these approaches have been shown to decrease cytotoxicity by reducing the polycations charge density.

In this study, we have combined both the above-mentioned approaches to develop an intracellular acid and redox potential-responsive micellar gene delivery system (Figure 3.1). A polycation based on DMAEMA was used to complex, condense and deliver siRNA. Hydrophobic modification was introduced into the polycation by copolymerizing DMAEMA with hydrophobic pendant disulfide group bearing methacrylate (HMssEt). ATRP of monomers in presence of a macroinitiator containing PEG and an acid-labile acetal linkage resulted in synthesis of a novel block copolymer PEG-AC-P(HMssEt-co-DMAEMA) (PDss). The electrostatic interaction of anionic dsDNA or dsRNA with cationic DMAEMA and hydrophobicity of HMssEt allows PDss to self-assemble into a micelleplex which consists of acid-labile acetal linkage at the core/corona interface and redox responsive disulfide linkage in the core. *In-situ* disulfide core-crosslinking of the micelleplex to improve the stability of the micelleplex in serum environment. This dual location acid/reduction responsive degradable micelleplex was found to have improved uptake, cell viability and endosomal escape ability. Moreover, the dsDNA release and gene silencing were

found to be higher in response to degradation of micelleplex in presence of both acid and reduction stimuli.

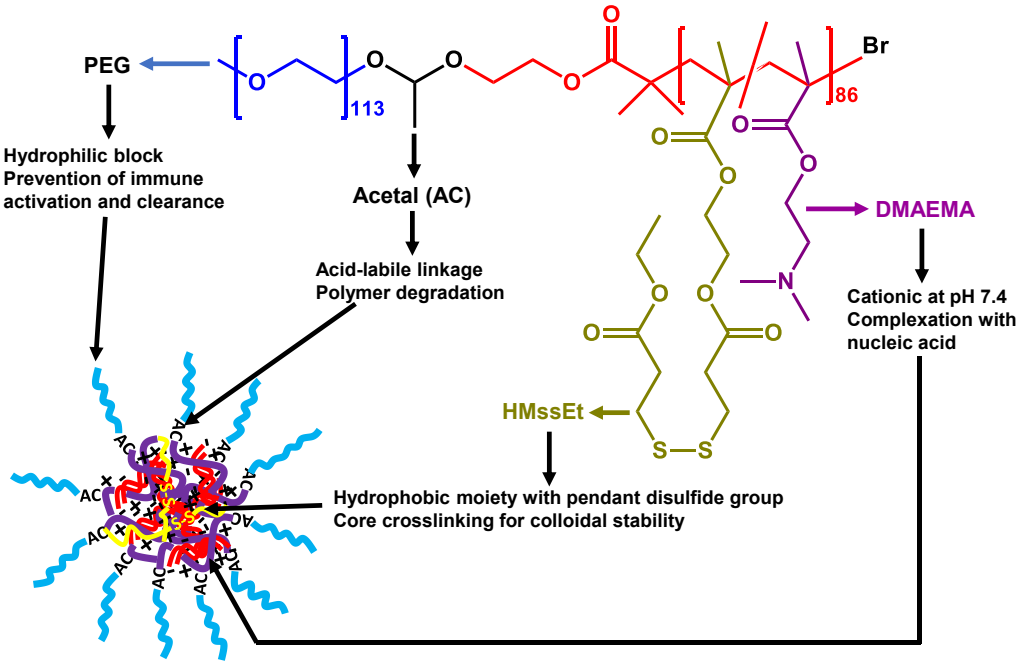

Figure 3.1. Illustration of the novel dual location dual acid/redox responsive block co-polymer PEG-AC-P(HMssEt-co-DMAEMA) (PDss).

3.2. Experimental

3.2.1. Materials

Poly(ethylene glycol) methyl ether (M_n = 5000 g/mol), tris(2-pyridylmethyl)amine (TPMA, 98%), tin(II) 2-ethylhexanoate ($Sn(II)(EH)_2$, >92%), glutathione (GSH, ≥98%), 1,4-dithreithiol (DTT, 98%), bovine serum albumin (BSA, ≥98%), Hoechst 33342 (≥98%) and Stains-all (95 %) were purchased from Sigma-Aldrich; acrylamide (99%), N,N′-methylenebis(acrylamide) (99%), ammonium persulfate (APS, 98%) and N,N,N',N'-tetramethylethylenediamine (TEMED, 99%) were from BioShop; tris/borate/EDTA (TBE, 10x) buffer was from Bio-Rad; Dulbecco's minimal essential media (DMEM) with and without phenol red, fetal bovine serum (FBS), penicillin-streptomycin solution, phosphate-buffered saline (PBS), trypsin and 4-(2-hydroxyethyl)-1-piperazineethanesulfonic acid (HEPES) were acquired from Wisent Bioproducts; Alexa Fluor 488 tagged dsDNA was from Integrated DNA Technologies (IDT); and tris(hydroxymethyl)aminomethane (Tris, 99.9 %), LysoTracker deep red, and Opti-MEM from

Thermo Fisher Scientific were purchased and used as received. 2-Dimethylaminoethyl methacrylate (DMAEMA, 98%) purchased from Sigma-Aldrich was purified by passing through a column filled with basic aluminum oxide to remove inhibitor. A methacrylate labeled with a pendant disulfide (HMssEt) was synthesized according to the procedure described elsewhere.[152]

3.2.2. Instrumentation

^{1}H-NMR spectra were obtained using a 500 MHz Varian spectrometer with $CDCl_3$ at 7.26 ppm as the reference standards. Monomer conversion and degree of polymerization (DP) was determined by ^{1}H-NMR spectroscopy. Molecular weight and molecular weight distribution were determined by an Agilent gel permeation chromatography (GPC) system equipped with a 1260 Infinity Isocratic Pump, two Agilent PL gel mixed-C and mixed-D columns and a RI detector. DMF containing 0.1 mol% LiBr (DMF/LiBr) was used as an eluent at 50 °C at a flow rate of 1.0 mL/min. Molecular weight and molecular weight distribution were calculated relative to linear poly(methyl methacrylate) standards from Fluka. Aliquots of the polymer samples dissolved in DMF/LiBr were filtered through a 0.45 μm PTFE filter to remove any DMF-insoluble species and injected into the GPC with a drop of anisole as a flow rate marker.

Dynamic light scattering (DLS) analysis was performed to determine the sizes and size distributions of micelloplexes with a Malvern Instruments Nano S ZEN1600 equipped with a 633 nm He–Ne gas laser at a fixed scattering angle of 175° at 25 °C.

Transmission electron microscopy (TEM) imaging was conducted with a FEI Tecnai G2 F20 Cryo-STEM, operated at 200 kV equipped with Gatan Ultrascan 4000 4k x 4k CCD camera system model 895. Samples (10 μL) were dropped onto a copper TEM grid (300 mesh, carbon coated) and allowed to dry in air.

Electrophoresis was performed by running the samples at 200V for 80 min on a 20% polyacrylamide gel in mini-protean tetra cell (Bio-Rad). Vertical gel electrophoresis setup was assembled according to manufacturer's protocol. To prepare polyacrylamide gels, acrylamide (19% w/v), N,N′-methylenebis(acrylamide) (1% w/v), ammonium persulfate (0.25% w/v) and N,N,N',N'-tetramethylethylenediamine (TEMED, 0.13% v/v) were dissolved in TBE buffer (1x). The resulting mixture was immediately dispensed into the space between two glass plates and was subjected to redox-initiated free radical polymerization at room temperature for 30 min. To

visualize dsDNA bands on the gel, Stains-all dye solution (0.1% w/v) in formamide was diluted with a solution of tris buffer (20 mM, pH = 8.0)/isopropanol (3/1 v/v) at 1/4 v/v ratio.

3.2.3. Synthesis of nucleic acids

All phosphoramidites and ancillary reagents were obtained from either Glen Research (Sterling, Virginia) or ChemGenes Corporation (Wilmington, Massachusetts). All oligonucleotides were synthesized on 1 μmol scale with an Applied Biosystems Model 3400 synthesizer using standard β-cyanoethylphosphoramidite chemistry with long chain alkylamine controlled pore glass (LCAA-CPG, 500 Å) used as the solid support. The synthesis protocol was supplied by the manufacturer with only minor modifications made to the coupling times. Cleavage of the oligonucleotides from the controlled pore glass and removal of the protecting groups was achieved with ammonium hydroxide (1 mL, 28 % aqueous solution)/ethanol at 3/1 v/v for a minimum of 4 hr at 55 °C. The RNA containing oligonucleotides were subjected to an additional deprotection step which consisted of treatment with $Et_3N•3HF$ (200 μL) at 65 °C for 2 hr to remove the 2′-O-TBDMS protecting group. Crude oligonucleotides were then precipitated from anhydrous methanol (400 μL), then washed twice with anhydrous methanol (400 μL). Oligonucleotides were purified either by preparatory denaturing polyacrylamide gel electrophoresis (PAGE) or ion-exchange (IEX) high performance liquid chromatography (HPLC). Purification by preparatory denaturing PAGE was performed with a 20% acrylamide solution (19/1 acrylamide/N,N′-methylenebis(acrylamide)) in 1x, TBE running buffer on standard 20 × 20 cm glass plates at 450 V until sufficient separation was achieved. The band of interest was excised, placed in a Falcon tube containing 0.1 M sodium acetate (8-10 mL) and shaken overnight to extract the pure oligonucleotide. Purification by IEX-HPLC was performed using a Dionex DNAPAC PA-100 column (0.4 × 25 cm) with a linear gradient of 0–50% buffer B over 30 min (buffer A: 100 mM Tris–HCl, pH 7.5, 10% acetonitrile (ACN) and buffer B: 100 mM Tris–HCl, pH 7.5, 10% ACN, 1 M sodium chloride. The collected fraction was diluted by ¼ with 0.1 M sodium acetate and desalted with a C-18 SEP PAK cartridge. The cartridge was prepared by washing with 10 mL each of HPLC grade ACN, 50% ACN (in water) and finally 0.1 M sodium acetate. The oligonucleotide was adsorbed to the C-18 column then the salt was removed by flushing the column twice with water (10 mL). The sample was eluted from the column with methanol/water/ACN (2/1/1) eluent (3-4 mL). Purity was assessed to be >90% for all synthesized oligonucleotides by analytical

denaturing PAGE and IEX HPLC. All oligonucleotides were quantitated using a Varian Cary Model 3E spectrophotometer. Single strand concentrations were calculated using the Beer–Lambert law from the absorbance measured at 260 nm; molar extinction coefficients were calculated by the nearest neighbour approximation. The purity and identity of oligonucleotides was assessed by mass spectrometry (MS) at the Concordia University Centre for Biological Applications of Mass Spectrometry. 0.1 OD of oligonucleotide was dried down for Electrospray ionization quadrupole time-of-flight (ESI-qTOF) MS analysis on a Micromass qTOF Ultima API. The mass spectrometer was run in full scan, negative ion detection mode. The double stranded DNA (dsDNA) consists of a DNA sequence of 5′-CATTTTCAAAATGCATTTTTG-3′’ paired with its complementary DNA sequence of 3′-GTAAAAGTTTTACGTAAAAAC-5′. The small interfering RNA (siRNA) targeting the enhanced green fluorescent protein (EGFP) messenger RNA (mRNA) consists of the sequence 5′-CAAGCUGACCCUGAAGUUCTT-3′ paired with its complementary sequence 3′-TTGUUCGACUGGGACUUCTTGTT-5′. The scrambled RNA (scRNA) consists of the sequence 5′-GCAAUCCUGCACAGUACGUTT-3′ paired with its complementary sequence 3′-TTCGUUAGGACGUGUCAUGCA-5′.

3.2.4. Synthesis of PDss block copolymer by ATRP

PEG-AC-Br (0.3 g, 57 μmol), DMAEMA (0.45 g, 2.9 mmol), HMssEt (1 g, 2.9 mmol), Cu(II)Br_2/TPMA complex (1.5 mg, 3 μmol), TPMA (2.5 mg, 9 μmol) were dissolved in anisole (4.8 g) in a 10 mL Schlenk flask. The mixture was deoxygenated by purging under nitrogen for 1 hr and then placed in an oil bath preheated at 50 °C. A nitrogen pre-purged solution of Sn(II)$(EH)_2$ (9.3 mg, 0.23 mmol) dissolved in anisole (0.5 g) was injected to initiate polymerization and purged further for 30 mins. After 5.5 hrs, polymerization was stopped by cooling the reaction mixture in an ice bath and exposing it to air.

For purification, the as-prepared polymer solutions were precipitated from hexane. The precipitate was then dissolved in THF and passed through a basic alumina column to remove residual copper species. After the removal of organic solvent by rotary evaporation at room temperature, the product was dried in a vacuum oven set at 50 °C for 12 hrs.

3.2.5. Solution properties of PDss in aqueous solution

PBS (3 mL) was added dropwise (0.2 mL/min) to an organic solution of the purified, dried PDss (3 mg) dissolved in THF (1 mL) under stirring. The resulting solution was stirred for 12 hrs

to allow the evaporation of THF. The resultant aqueous solution was transferred to a quartz cuvette and then sealed with a Teflon stopper. DLS was used to monitor a change in light scattering intensity at an increment of 1 °C/min in the temperature range of 25 - 90 °C.

3.2.6. Complexation of PDss with nucleic acids

A series of organic solutions of PDss at different amounts dissolved in THF (5 μL) was mixed with PBS (2 μL, 1 mM, pH = 7.4). The resulting mixtures were stirred for 3 hrs to remove THF, yielding aqueous dispersions of PDss micelles at different concentrations. The amounts of PDss required to attain various N/P ratios were calculated based on the following equation: N/P ratio = (mole of PDss x 43)/(mole of dsDNA x 40), where 43 is the number of DMAEMA units in PDss and 40 is the number of phosphate groups in dsDNA. Then, the resultant dispersions were mixed with an aqueous solution of dsDNA (0.36 nmol) in acetate buffer (3 μL, 10 mM, pH = 5) for 30 mins, and then PBS (3 μL, 20 mM, pH = 7.4) for 1 hrs under stirring, yielding a series of aqueous M-PDss dispersions with various N/P ratios of 0.8, 1, 2, 4, 6, 8 and 10 at pH = 7.4. Their aliquots (8 μL) were mixed with glycerol (8 μL) for electrophoresis assay.

3.2.7. *In-situ* disulfide core-crosslinking of M-PDss to xM-PDss

An aqueous dispersion of PDss micelles (20 μL, 9 mg/mL) was prepared and mixed with an aqueous solution of dsDNA (0.71 nmol) in acetate buffer (30 μL, 10 mM, pH = 5) and following PBS (40 uL, 20 mM, pH = 7.4) under stirring, yielding M-PDss with N/P = 10/1. Then, it was mixed with an aqueous solution of DTT dissolved in PBS (10 μL, 10 mM, pH = 7.4) at a mole equivalent ratio of DTT/disulfide = 0.4/1 for 3 hrs at room temperature under stirring. The formed xM-PDss was dialyzed using dialysis tubing with MWCO = 3.5 kDa against fresh PBS (10 mM, pH = 7.4) to remove excess DTT.

A similar procedure was used with an aqueous solution of dsRNA. Nuclease free water was used in the preparation of dsRNA containing M-PDss and xM-PDss. An aqueous dispersion of PDss micelles (20 μL, 1.3 mg/mL) was prepared and mixed with an aqueous solution of siRNA or scRNA (100 pmol) in acetate buffer (30 μL, 10 mM, pH = 5) under stirring at 100 rpm and incubated for 30 mins. This was followed by the addition of PBS (40 μL, 20 mM, pH = 7.4) under stirring, yielding siRNA or scRNA containing M-PDss at N/P = 10/1. xM-PDss was prepared by mixing M-PDss with an aqueous solution of DTT dissolved in PBS (10 μL, 10 mM, pH 7.4) at a mole equivalent ratio of DTT/disulfide = 0.4/1 for 3 hrs at room temperature under stirring. This

was followed by dialysis in a dialysis tubing with molecular weight cut-off (MWCO) = 3.5 kDa against fresh PBS (10 mM, pH = 7.4) prepared in nuclease free water to remove excess DTT.

3.2.8. Acid/reduction-responsive degradation of PDss and xM-PDss using DLS and GPC

An aqueous dispersion of xM-PDss with N/P = 10/1 ratio (100 µL, 0.18 mg) was incubated in acetate buffer (10 mM, pH = 5.4) with or without GSH (10 mM). DLS technique was used to monitor changes in their size distribution. Further, the purified and dried PDss (4 mg, 0.14 µmol) was dissolved in DMF (2 mL) and mixed with HCl (15 µL, 12.1 N) or DTT (4.6 mg, 30 µmol). After 24 hrs, aliquots were analyzed using GPC.

3.2.9. Release of dsDNA upon acid/reduction-responsive degradation using gel electrophoresis

xM-PDss was prepared according to the procedure described above. An aliquot of aqueous xM-PDss dispersion (6 µL) was mixed with PBS (2 µL, 40 mM, pH = 7.4) or acetate buffer (2 µL, 40 mM, pH 5.4), with or without GSH (10 mM). After 24 hrs, these samples were mixed with glycerol (8 µL) and then electrophoresed to determine the presence of released dsDNA.

3.2.10. Colloidal stability in presence of proteins

An aqueous dispersion of xM-PDss (1.8 mg/mL) was incubated with BSA (40 mg /mL) for 48 hrs at 37 °C. The resulting mixtures, along with a control (without xM-PDss), was subjected to centrifugation (10,000 rpm × 20 min, room temperature) to remove any aggregates. Quantitative analysis was conducted to estimate the concentration of proteins remaining in supernatants using a bicinchoninic acid (BCA) assay (Pierce BCA Assay Kit), according to the protocol reported in our report, based on the manufacturer's instructions. The absorbance of the resultant supernatants was recorded at λ = 562 nm in triplicates.

3.2.11. Cell culture

Human cervical cancer cell line HeLa was cultured in DMEM containing 10% FBS and 1% Pen-Strep solution. HeLa cells stably expressing enhanced green fluorescent protein (EGFP) were purchased from Cell Biolabs Inc. and cultured in DMEM containing 10% FBS, 0.1 mM minimum essential media (MEM) Non-Essential Amino Acids (NEAA), 2 mM L-glutamine and 1% Pen-Strep solution. The cells were incubated at 37 °C in a humidified atmosphere containing 5% carbon dioxide until the cells reached 95% confluency.

3.2.12. Cell Viability using Alamar blue assay

HeLa cells (10,000 cells/well) were seeded into a 96-well plate and incubated at 37 °C for 24 hrs. Cells were then treated with DMEM (100 µL) containing different concentrations of PDss. Untreated cells were used as controls. After 48 hrs, the media was replaced with DMEM (100 µL) containing 10% Alamar Blue dye (0.15 mg/mL) and incubated at 37 °C for 4 hrs. Absorbance at 570 nm and 600 nm were recorded to calculate the cell viability. Cell viability was calculated as follows:

Cell viability (%) = (A_{570} - (A_{600} x Ro) for test sample x 100) / (A_{570} - (A_{600} x Ro) for control), where A_{570} = Absorbance at 570 nm, A_{600} = Absorbance at 600 nm, Ro = A_{570}/A_{600} of dye

3.2.13. Endosomal escape ability

HeLa cells (50,000 cells/well) were seeded into a 4-well glass bottom plate and incubated at 37°C for 24 hrs. They were then incubated with Alexa Fluor-488 labelled dsDNA (100 nM) complexed with PDss at N/P 10 were mixed with DMEM and added to each well. After 24 hrs, the media was replaced with phenol red free DMEM containing Lysotracker (75 nM) and Hoechst 33342 (36 µM). The cells were incubated in the dark for 1 hr before imaging with Nikon Eclipse TiE inverted epifluorescence microscope. The captured images were processed using ImageJ software.

3.2.14. *In-vitro* EGFP gene silencing

HeLa cells stably expressing EGFP (HeLa/EGFP) were seeded into a 96-well glass bottom plates and incubated at 37 °C until 50% confluency was achieved. An aliquot of xM-PDss polyplex loaded with siRNA (1 µM) targeting EGFP gene or scrambled siRNA (1 µM) mixed with Opti-MEM (20 µL) was added to each well and incubated at 37°C. After 5 hrs, DMEM (80 µL) containing 10 % FBS, 0.1 mM MEM Non-Essential Amino Acids (NEAA), 2 mM L-glutamine and 1% Pen-Strep solution was added to each well. In order to simulate the stimuli-responsive environment, GSH-OEt (10 mM) was added to media. The cells were stained with Hoechst 33342 (36 µM) and imaged by Nikon Eclipse TiE inverted epifluorescence microscope. All images were processed by ImageJ and the gene silencing was analyzed by comparing the fluorescence decrease in xM-PDss treated cells with untreated control.

3.3. Results and discussion

3.3.1. Synthesis and solution properties of PDss

Figure 3.2.a depicts our approach utilizing the ATRP technique to synthesize a well-controlled PDss block copolymer. PEG-AC-Br was employed as an ATRP macroinitiator synthesized according to protocols described elsewhere[153] and further in Appendix A (Figure A1 for the synthesis scheme and ^{1}H-NMR analysis). In the presence of the PEG-AC-Br, ATRP was examined for a mixture of HMssEt and DMAEMA mediated with $CuBr_2$/TPMA complexes in anisole at 50 °C. The initial mole ratio of $[DMAEMA]_o/[HMssEt]_o/[PEG\text{-}AC\text{-}Br]_o$ was selected to be 60/60/1 for the DP to be 120 at complete monomer conversion. The polymerization was stopped at 70 % monomer conversion. After being purified by standard methods, the formed PDss was characterized for its chemical structure using ^{1}H-NMR and molecular weight using GPC.

^{1}H-NMR of the purified PDss in Figure 3.2.b contains signals at 3.6 - 3.7 ppm corresponding to EO protons from the PEO block, the signal at 2.9 ppm corresponds to methylene protons adjacent to disulfide linkage in the PHMssEt units and the signal at 2.3 ppm is due to the methyl protons in the PDMA units. Using their integration ratios with the DP of PEG block = 113, the DP was found to be 43 for PHMssEt unit, 43 for PDMAEMA unit, and thus 86 for P(HMssEt-co-DMAEMA). The GPC chromatograph of PDss in Figure 3.2.c shows the clear shift of molecular weight distribution to a higher value with no significant residual of PEG-AC-Br initiator observed. PDss had a number average molecular weight (M_n) of 23 kg/mol with a dispersity (Đ) = 1.1.

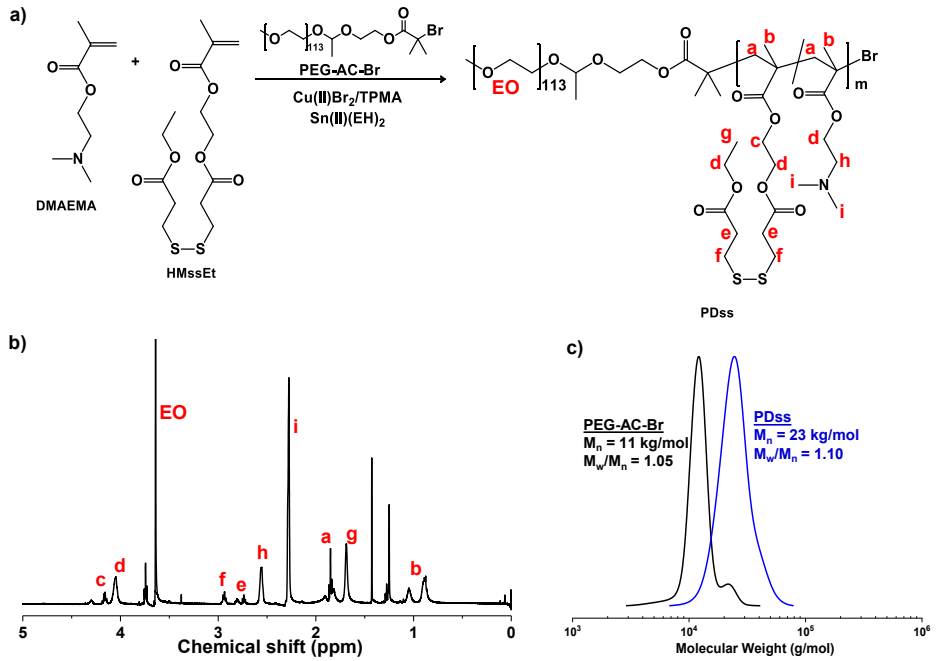

Figure 3.2. Synthesis by ATRP **a)**, ^{1}H-NMR spectra in $CDCl_3$ **b)**, and GPC trace **c)** of PDss.

PDMAEMA has been known to exhibit a coil-globular transition through hydrophobic/hydrophilic switch upon a change in temperature, and thus being thermoresponsive.[154] Since PEG is hydrophilic, PEG-AC-P(HMssEt-co-DMAEMA) block copolymer could be either double hydrophilic or amphiphilic, depending on the mole ratio of HMssEt and DMAEMA units. We have tested the solution property of PDss with 1/1 mole ratio of HMssEt/DMAEMA using DLS. As seen in Figure A2, the z-averaged hydrodynamic diameter kept decreasing over the temperature range, suggesting that the PDss is not thermoresponsive, but amphiphilic.

3.3.2. Complexation and characterization of M-PDss

The PDss contains pendant dimethylamino groups that can interact with anionic phosphate groups in nucleic acids. As illustrated in Figure 3.3.a, such ionic association can lead to the formation of micelleplexes of PDss with nucleic acids (called M-PDss) in aqueous solution. To investigate the micelleplexation of PDss with nucleic acids, well-defined chemically synthesized dsDNA was evaluated. Then, the effect of the N/P ratio was examined for the formed M-PDss using native gel electrophoresis and DLS. Because of the amphiphilicity, the PDss first self-assembled to form micelles in aqueous solutions, which were mixed with dsDNA to form a series

of aqueous dispersions of M-PDss with various N/P ratio ranging from 0.5/1-10/1. Note that the micelleplexation was conducted in acetate buffer at pH = 5, at which the DMAEMA units in PDss would be protonated to facilitate ionic interactions with the dsDNA. This can facilitate the incorporation of dsDNA in PDss micelles through charge complexation. Figure 3.3.b shows the determination of the N/P ratio required for M-PDss formation by native 20% polyacrylamide gel electrophoresis with visualization of species using Stains-all. With N/P ratios < 2/1, a stained band is observed with mobility equivalent to the dsDNA which indicates that the dsDNA are unbound (free), suggesting the incomplete complexation with PDss. When the N/P ratios > 2/1, no stained band equivalent to free dsDNAs was observed, however, a stained band of reduced mobility was observed at the bottom of the loading well, suggesting that most dsDNA molecules are condensed to M-PDss.

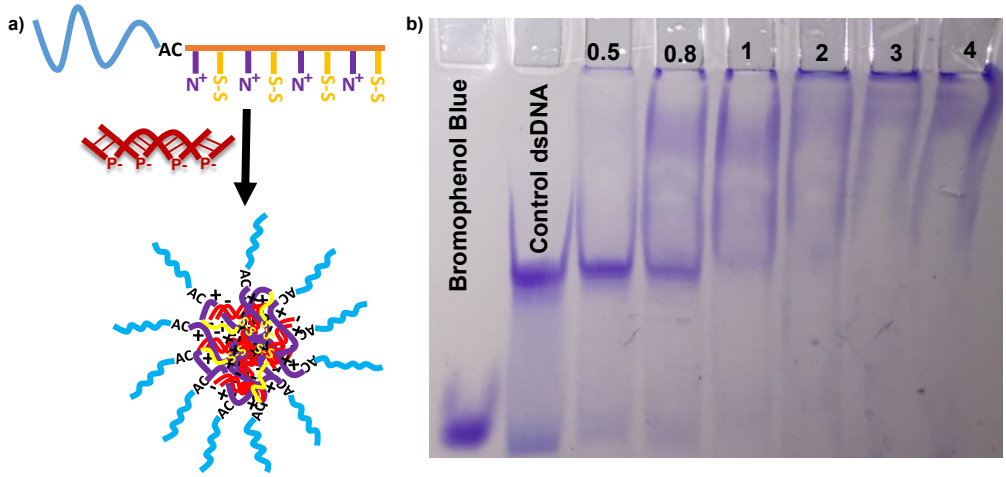

Figure 3.3. Schematic illustration of micelleplex formation as a result of interaction between tertiary amines and dsDNA **a)**, and evaluation of optimum N/P ratio for complete complexation by gel electrophoresis **b)**

3.3.3. Fabrication of *in-situ* disulfide-core-crosslinked xM-PDss

PDss contains pendant disulfide linkages (50 mol%) in the hydrophobic polymethacrylate block, which can be subjected to a click-type disulfide-thiol exchange reaction in the presence of a catalytic amount of a reducing agent. As illustrated in Figure 3.4.a, this process yields disulfide-core-crosslinked micelleplexes (called xM-PDss). To fabricate colloidally-stable xM-PDss, M-PDss was first prepared in PBS with N/P ratio = 10/1. Excess PDss over dsDNA was used because free DMAEMA moieties can improve cellular uptake, endosomal escape and transfection

efficiency of micelleplexes.[123,155,156] Then, the formed M-PDss was incubated with DTT (0.4 mole equivalent to pendant disulfide linkages of PDss) at room temperature to induce intramolecular disulfide-thiol exchange reaction. The formed xM-PDss had the diameter = 83 nm with narrow size distribution by DLS (Figure 3.4.b). Their smaller size suggests that hydrophobic PHMssEt units can enhance the ability of PDMAEMA units to condense dsDNA to form well-defined micelleplexes. Their morphologies were further visualized by TEM analysis (Figure 3.4.c) which shows PDss is capable of condensing dsDNA into a compact structure. Their ζ-potential (Figure 3.4.d) were determined to be -1.2 ± 0.5 mV, which is slightly lower than that (0.8 ± 0.2 mV) for PDss micelles, but much greater than -12.7 ± 2.2 mV of free dsDNA, suggesting the improved condensation ability of PDss to dsDNA.

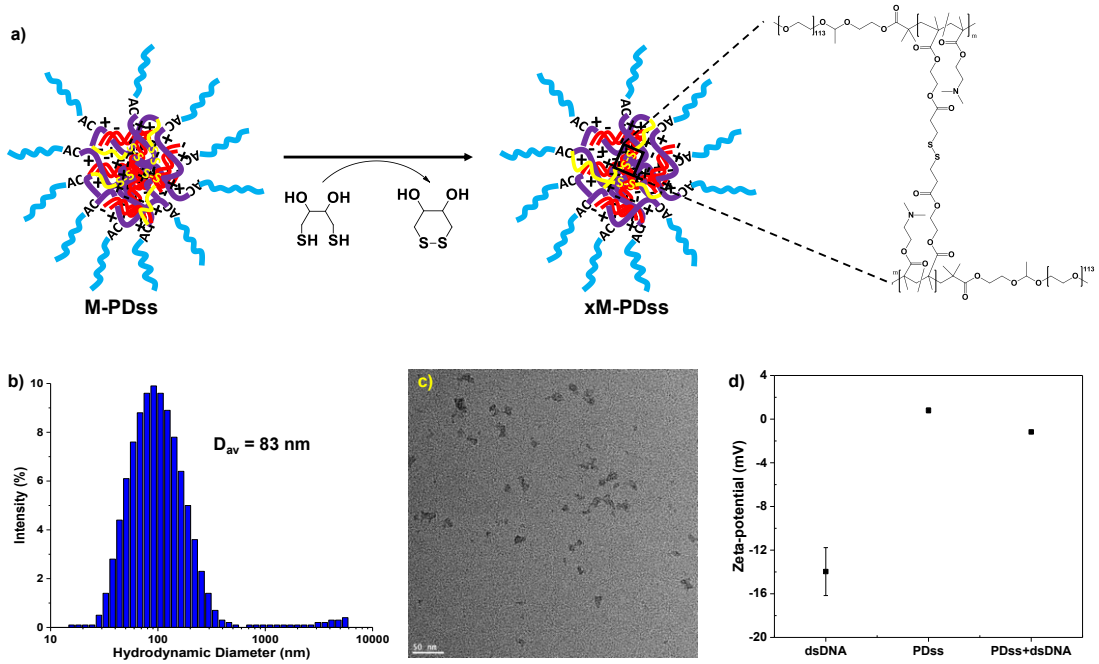

Figure 3.4. Schematic illustration of disulfide core-crosslinking of micelleplex by thiol-exchange reaction in presence of catalytic amount of DTT **a)**, hydrodynamic diameter and size distribution **b)**, TEM image of xM-PDss **c)** and ζ-potential **d)** of dsDNA, PDss and xM-PDss.

3.3.4. Acid/reduction-responsive degradation and dsDNA release

The formed disulfide-core-crosslinked xM-PDss complexed with dsDNA are labelled with reduction-cleavable disulfide linkages as pendant chains and crosslinks in the cores as well as acid-labile acetal linkages at core/corona interfaces. To investigate the responses to reduction and acidic

pH, aliquots of the xM-PDss with the diameter = 83 nm were incubated with acid (pH = 5.4), 10 mM GSH, and both. As seen in Figure 3.5.b, the DLS diagram shows no significant change with the diameter = 85 nm at pH = 7.4 (with no stimuli), suggesting colloidal stability at physiological pH. In the presence of 10 mM GSH, the size distribution became multimodal with the occurrence of large aggregation (diameter >1 μm) in 6 hrs of incubation. Such changes could be caused by degradation of xM-PDss upon the cleavage of pendant disulfide linkages in a reducing environment (Figure 3.5.a). At pH = 5.3, the size distribution became multimodal. Such degradation of xM-PDss at acidic pH could be caused by not only the cleavage of junction acetal linkage but also protonation of PDMAEMA units at acidic pH causing an ionic repulsion between polymer chains in the cores (Figure 3.5.a).

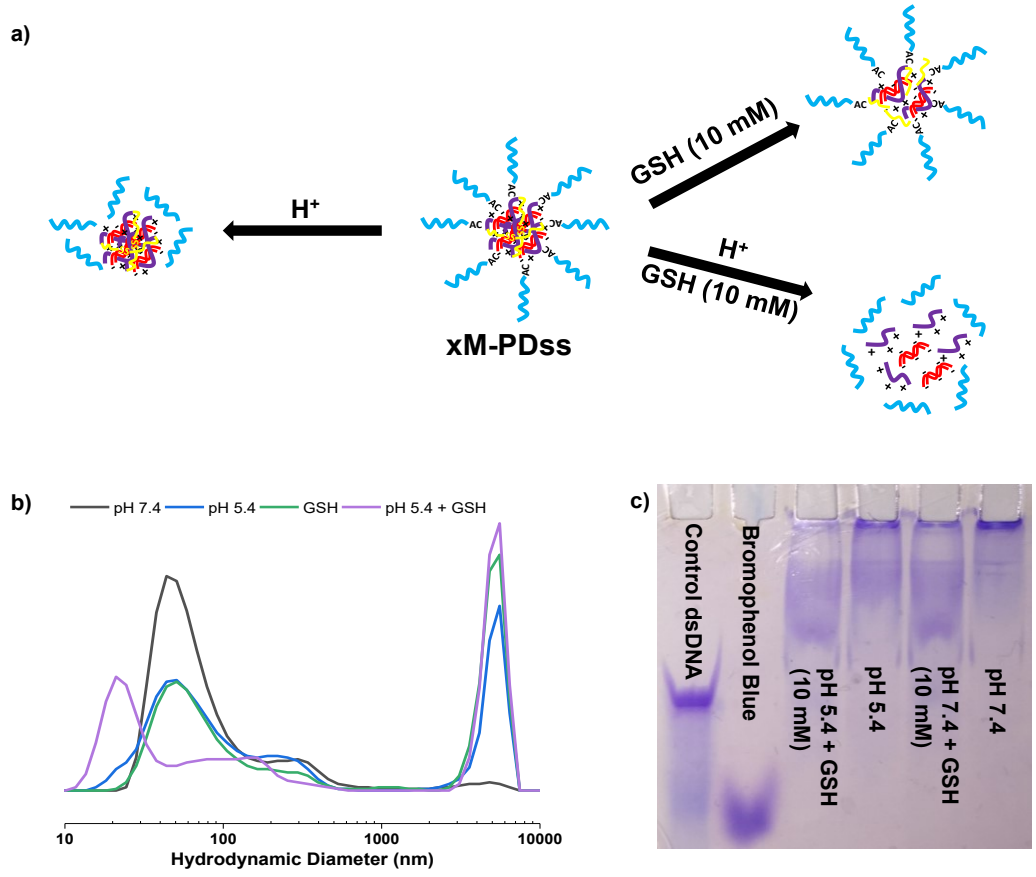

Figure 3.5. Schematic illustration of xM-PDss degradation in presence of stimuli **a)**, DLS signal of change in diameter after 6 hr **b)** and release of dsDNA after 24 hrs **c)** from xM-PDss in response to stimuli.

To further investigate acid and reduction-responsive degradation, the PDss labeled with pendant disulfide and junction acetal linkages was incubated with acid and DTT (a reducing agent) in DMF, a homogeneous solution. Figure 3.6.a shows the schematic illustration of acid and reduction response of the PDss copolymer. As seen in Figure 3.6.b, GPC was used to follow the degradation. When being incubated with acid (HCl), PDss degraded to PEG-OH, acetaldehyde, and P1-OH upon the cleavage of the acetal cleavages at block junctions. GPC analysis confirms the decrease in molecular weight to M_n = 13 kg/mol from M_n = 23 kg/mol, and the shift of GPC trace to a lower molecular weight region between P1-OH and PEG-ac-Br (macroinitiator). A shoulder in the lower molecular weight region corresponds to that of the PEG-AC-Br macroinitiator, confirming the generation of PEG-OH as a degraded product. Upon exposure to DTT (5 mole equivalents), the disulfide pendants in the polymethacrylate block could be cleaved, generating PEG-AC-P2-SH as a possible degraded macromolecular product. Its molecular weight slightly decreased from 23 kg/mol (Đ = 1.1) to 22 kg/mol (Đ = 1.1), confirming reductive cleavage of significant densities of pendant disulfide linkages. These results confirm that the change in size and size distribution of xM-PDss could be attributed to the cleavage of pendant disulfides and junction acetals when being treated with acid and reduction stimulus.

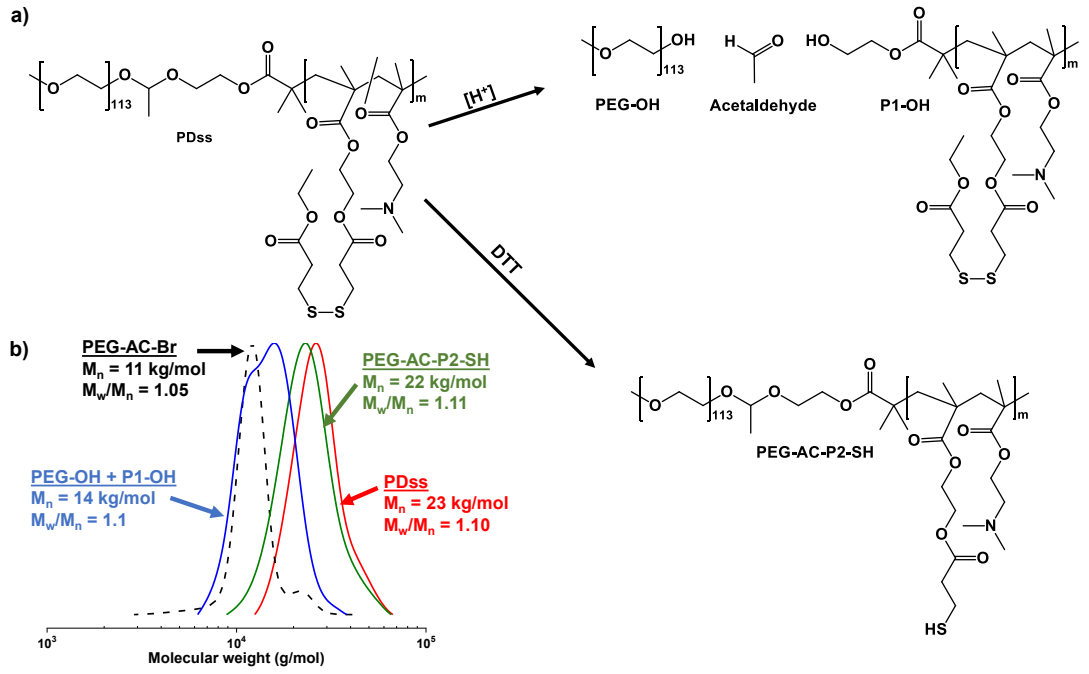

Figure 3.6. Acid and reduction responsive degradation of PDss **a)** and GPC analysis in DMF of the degraded products compared to PEG-AC-Br **b)**.

Acid and reduction-responsive degradation of xM-PDss was further evaluated by gel electrophoresis. As shown in Figure 3.5.c, a dark band near the bottom of the loading well was observed with the absence of a higher mobility band corresponding to free dsDNA at pH = 7.4, suggesting that most dsDNA molecules remain complexed with the xMPDss. For the xMPDss incubated at pH 5.4 or with 10 mM GSH, a broad band was observed between the bottom of the loading well and the position to which the dsDNA migrates (lane 1). This broad band could be plausibly attributed to the degraded polymer products complexed with dsDNA molecules, generated in response to acid or reduction stimulus. Further, this result is promising in that ds-nucleic acids complexed in micelleplex cores could be released in response to acid and reduction stimuli. More interestingly, no significant band near the bottom of the loading well was observed when xM-PDss was incubated in the presence of 10 mM GSH at pH = 5.3. This suggests that the release of ds-nucleic acids could be accelerated in response to dual acid/reduction stimuli.

3.3.5. Colloidal stability, cytotoxicity, cellular uptake and endosomal escape ability

Cationic polymers are known to interact with anionic serum proteins due to their positive charge.[157] Thus, the susceptibility of xM-PDss to interact with serum protein was further analysed by the BCA assay. Their aliquots were incubated with BSA (40 mg/mL) in PBS for 48 hrs. The mixture was subjected to centrifugation and the supernatant was analysed to determine free BSA. Only <2% BSA was adsorbed onto xM-PDss and >98% remain as free in supernatant (Figure 3.7.a). This result suggests that xM-PDss are colloidally stable in the presence of serum proteins. This could be attributed to their ζ potential being close to zero representing their neutral surface, which ensures no significant interactions with serum proteins during blood circulation.

Moreover, polycations have been known to induce cytotoxicity.[158,159] Thus, HeLa cells were incubated with varying concentration of PDss and the cell viability was determined by the Alamar Blue assay. As shown in Figure 3.7.b, PDss was found to be non-cytotoxic with > 95 % cell viability up to 0.9 mg/mL. On the other hand, the block copolymer without HMssEt PEG-AC-PDMAEMA (PD) was found to be cytotoxic with <75% cell viability above 150 µg/mL (refer to Figure B5.a, Appendix B). This shows that incorporation of hydrophobic component reduces the cytotoxicity of polycations by reducing the charge density.

One of the bottlenecks in nucleic acid delivery is the entrapment of polycationic nanocarriers in endosomes due to their inability to endosomal escape.[160,161] Here, colloidally-stable xM-PDss

complexed with Alexa Fluor 488 tagged dsDNA were incubated with HeLa cells and their ability to escape from endosomes/lysosomes was evaluated using fluorescence microscopy to visualize the localization of Alexa Fluor 488 tagged dsDNA inside cells. Alexa Fluor 488 tagged dsDNA was compared as a control. Endosomes/lysosomes were stained with Lysotracker. As seen in Figure 3.7.c, dsDNA alone was not capable of entering HeLa cells whereas xM-PDss were taken up. More promisingly, Alexa Fluor 488 fluorescence was observed outside the LysoTracker fluorescence region for cells incubated with xM-PDss, indicating the significant capability of the xM-PDss to escape endosomes/lysosomes. On the other hand, Alexa Fluor 488 fluorescence was observed to merge with the LysoTracker fluorescence region for cells incubated with M-PD, indicating the inability of M-PD to escape from the endosome (refer Figure B5.b, Appendix B).

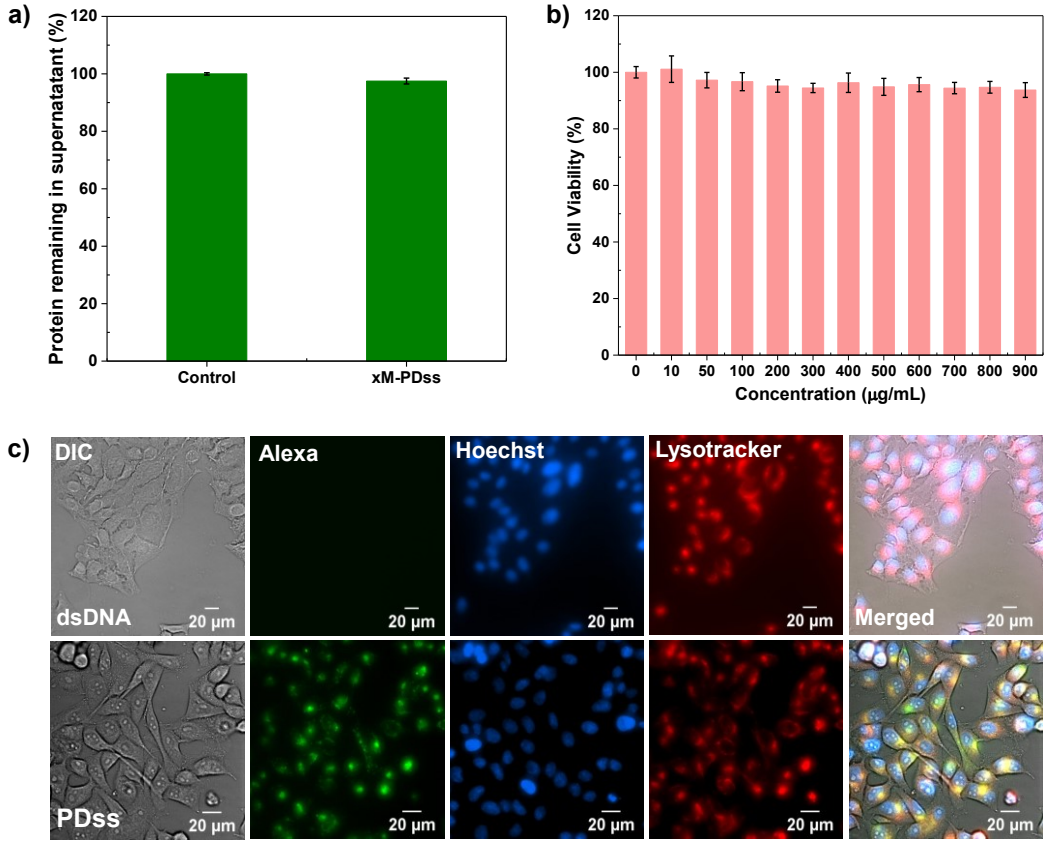

Figure 3.7. Colloidal stability of xM-PDss in the presence of BSA **a)**, cell viability of HeLa cells incubated with different concentrations of empty M-PDss **b)** and fluorescence microscopy images of HeLa cells incubated with M-PDss containing Alexa Fluor 488 tagged dsDNA (100 nM) compared to free Alexa Fluor tagged dsDNA after 24 hr **c)**.

3.3.6. *In-vitro* gene silencing efficiency

We evaluated xM-PDss for gene silencing efficiency with HeLa cells stably expressing EGFP. Gene silencing efficiency was followed with a decrease in EGFP fluorescence signal. Scrambled siRNA and siRNA were synthesized and complexed with M-PDss to xM-PDss/siRNA. We further investigated the effect of acidic pH and cellular GSH on gene silencing. Figure 3.8.a shows the fluorescence microscopy images of cells incubated with xM-PDss/siRNA at pH = 7.4 without and with 10 mM GSH. Note that most cells were dead when incubated at pH = 6.8 (images not shown here). As summarized in Figure 3.8.b, fluorescence intensity was used for the quantitative analysis of gene expression%. At pH = 7.4, gene silencing was estimated at 40% with 10 mM GSH, while it was 30% without GSH. Gene expression for xM-PDss complexed with scrambled siRNA did not change regardless of the presence or absence of 10 mM GSH, suggesting that the reduction of EGFP fluorescence observed with siRNA was not due to non-specific silencing. Also, increased EGFP silencing was observed in the presence of GSH, which suggests that cellular GSH-induced degradation can enhance gene silencing in cancer cells.

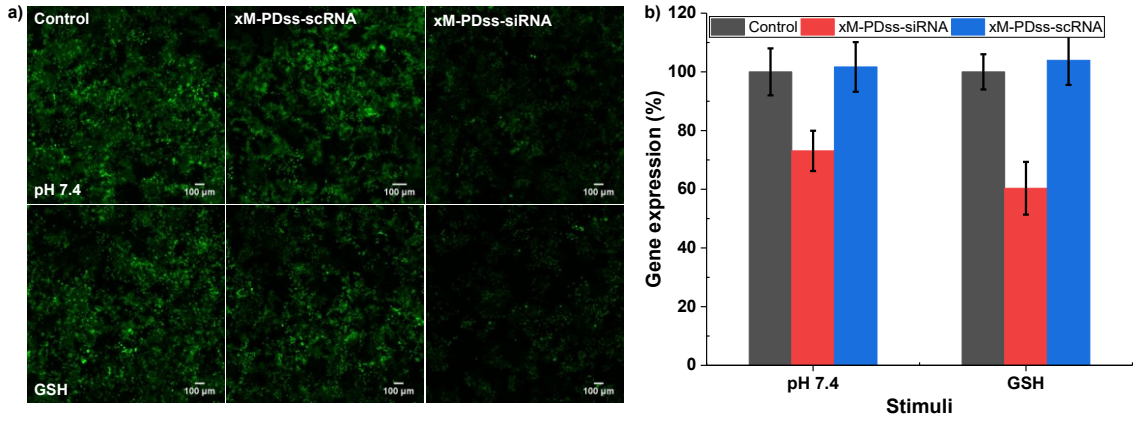

Figure 3.8. Fluorescence microscopy images of HeLa/EGFP cells incubated with xM-PDss containing siRNA or scRNA **a)** and quantification of resulting gene silencing **b)** in presence of stimuli.

3.4. Conclusion

Novel dual location acid/redox responsive block copolymer PDss was synthesized by ATRP and characterized for its siRNA delivery and gene silencing ability. PDss was capable of complete complexation with dsDNA above N/P 2. Micelleplex formed as a result of interaction between

PDss and dsDNA was crosslinked further by the disulfide linkages in the core. This disulfide core-crosslinked micelleplex, xM-PDss, had a hydrodynamic diameter of 83 nm with a surface charge of -1.2 ± 0.2 mV and did not show significant interaction with the serum protein albumin. In the presence of acid or GSH, PDss was found to degrade and xM-PDss was found to disassemble. This disassembly was also found to cause release of dsDNA from xM-PDss with highest release observed in presence of both acid and GSH. Upon incubation with HeLa cells, PDss showed above 95% cell viability up to 900 μg/mL. Moreover, PDss was found to be capable of escaping the endosome and a decrease in fluorescence of HeLa/EGFP cell line upon treatment was observed. EGFP gene silencing was found to be highest (30 %) in the presence of dual stimuli.

Chapter 4

Evaluation of Cellular Interaction of Block copolymer Nanocarriers

4.1. Introduction

Conventional chemotherapy utilizes small drug molecules that suffer from poor solubility, low stability, sensitivity to chemical and enzymatic degradation, and non-specificity, causing undesired side effects and low drug efficacy.[162-165] Polymer-based delivery nanocarriers have paved the way for the clinical application of effective drugs because of their structural, functional, and chemical versatility.[166,167] CRP techniques allow for the synthesis of (co)polymers, particularly amphiphilic block copolymers, with predetermined molecular weights, narrow distributions, various architectures, and functionalities. Further, the techniques can allow for the introduction of SRD into the design of amphiphilic block copolymers.[168,169] The resultant SRD-exhibiting polymers enhances the release of encapsulated therapeutic agents in response to pathological stimuli.[170-172] Further, SRD can influence the stability, biodegradability, biodistribution, and toxicity of nanocarriers. Because of these features, SRD-exhibiting nanocarriers have proved to be a promising strategy in the development of robust intracellular delivery of therapeutic agents.[173]

Once administered through intra-venous injection, these SRD-nanocarriers interact with biological components in the body. It is essential to synthesize robust nanoscale delivery carriers exhibiting not only good therapeutic efficacy but also low cytotoxicity and high uptake by the target cell.[174] Understanding the interactions of these SRD-nanocarriers with cells is crucial to the development of an efficient and biocompatible nanocarrier for therapeutic delivery. Reports describe that cytotoxicity and cellular uptake are dependent on size, shape, surface charge, and core-composition of the polymeric nanocarrier.[75-78] This chapter describes my investigation of biological interactions, particularly cytotoxicity and cellular uptake of four SRD-exhibiting block copolymer-based nanocarriers that have been synthesized in Dr. Oh's laboratory. Their chemical structures are shown in Figure 4.1.

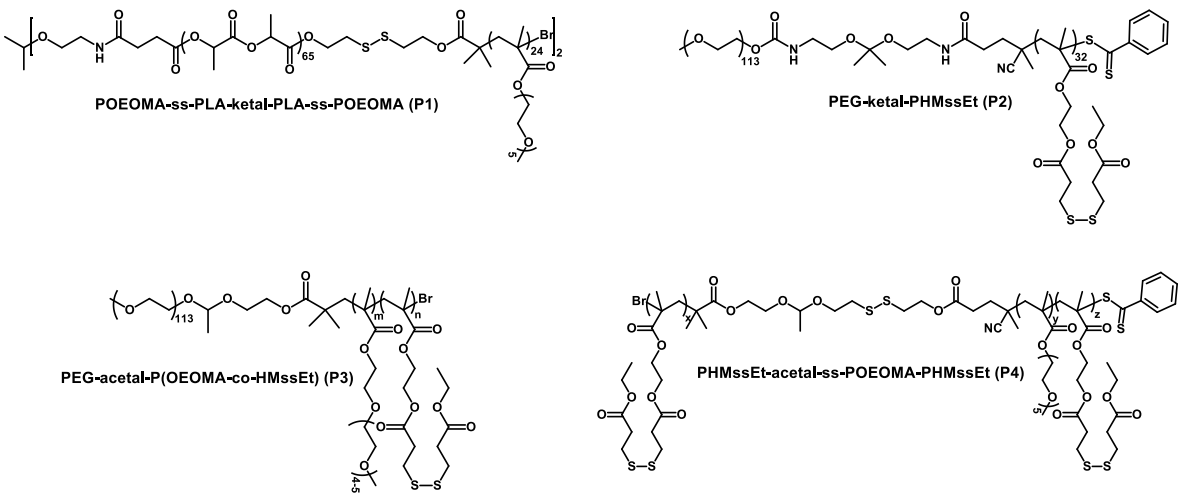

Figure 4.1. Chemical structure of **P1**, **P2**, **P3**, and **P4**.

4.2. Polymer characteristics and experimental methods

Table 4.1 summarizes the characteristics of the copolymers and their doxorubicin (Dox) or Nile Red (NR)-loaded micelles. POEOMA-ss-PLA-ketal-PLA-ss-POEOMA **(P1)**[175] is a polylactide (PLA)-based block copolymer. PLA is known to be hydrophobic and also contains degradable ester linkages in the backbone which confer enhanced biocompatibility and biodegradability.[176,177] The hydrophobic PLA core is stabilized with the hydrophilic corona of POEOMA. PEG-ketal-PHMssEt **(P2)**,[178] PEG-acetal-P(OEOMA-co-HMssEt) **(P3)**[153] and PHMssEt-acetal-ss-POEOMA-PHMssEt **(P4)** are methacrylate-based block copolymers. They consist of a HMssEt as the hydrophobic core and either PEG or POEOMA as the hydrophilic corona.

Table 4.1. Characteristics of SRD-exhibiting block copolymers and their Dox or NR-loaded micelles used in this study.

Polymer	M_n (kg/mol)	Dispersity (Đ)	Diameter (nm)	Drug Loading (%)	Reference
P1	26.0	1.35	31.4	-	[175]
P2	24.6	1,15	116.4	2.5	[178]
P3	27.2	1.12	168	3.3	[153]
P4	23.0	1.23	73.6	0.14	-

For cell culture experiments, **P1** and **P2** were evaluated for cytotoxicity only, while **P3** and **P4** were evaluated for both cellular uptake and cytotoxicity. The cytotoxicity was evaluated with the MTT assay. Cellular uptake was investigated with fluorescence microscopy upon the loading of Dox (or NR) in the micelles.

4.2.1. Cytotoxicity assays

Determination of cell viability relies on the ability of an assay to differentiate between living, dead, and impeded cells. One way to evaluate cell viability is to determine the metabolic activity of the cell by measuring the turnover rate of NADH and NADPH. Colored products obtained as a result of enzymatic reduction of certain compounds such as tetrazolium salts (MTT) in the presence of NADH/NADPH enable colorimetric quantification of cell viability.[179,180] The other way to determine cell viability is by staining the cells using stains specific to live or dead cells and quantifying the number of cells in the images.[181]

MTT assay

Colorless or weakly colored tetrazolium salt, 3-(4,5-dimethylthiazol-2-yl)-2,5-diphenyltetrazolium bromide (MTT), is used in the MTT assay. MTT is freely permeable through the cell membrane as a result of its lipophilic side groups and cationic charge. In viable cells, mitochondrial or cytoplasmic enzymes like oxidoreductases, dehydrogenases, oxidases, and peroxidases reduce MTT using NADH, NADPH, succinate, or pyruvate as the electron donor into a purple-colored water-insoluble formazan, as shown in Figure 4.2. The insoluble formazan forms as a needle-like crystal which damages the cell's integrity ultimately resulting in cell death. Since cell death interrupts further metabolism of MTT, this assay is known as an end-point determination. Estimation of cell viability can be performed by quantifying the formazan crystals using spectroscopic methods. However, before spectroscopic quantification, it is necessary to lyse the cells and dissolve these intracellular crystals in an appropriate solvent.[179,180] In order to investigate the cytotoxicity of the micelles prepared from **P1**, **P2**, **P3,** or **P4**, the following procedure was used. HeLa cells cultured in DMEM containing 10 vol % FBS and 1 vol % penicillin−streptomycin solution was harvested at 80% confluency, and 8×10^3 cells were seeded into each well of a 96 well plate. After incubation at 37 °C for 24 hr, the media was replaced with DMEM (100 μL) containing different concentrations of micellar dispersion, and the cells were further incubated at 37 °C for 48 hr. The media was then replaced with DMEM (100 μL) containing

10% MTT dye (CellTiter 96 Non-Radioactive Cell Proliferation Assay Kit (MTT, Promega)) and incubated at 37 °C. After 4 hr, MTT solution was carefully removed and the formazan crystals were dissolved in dimethyl sulfoxide (DMSO, 200 µL). The absorbance at 570 nm was measured using Tecan Infinite M200 PRO microplate reader, and the cell viability was calculated as the percent ratio of absorbance of cells treated with micelles to control (cells only without NPs).

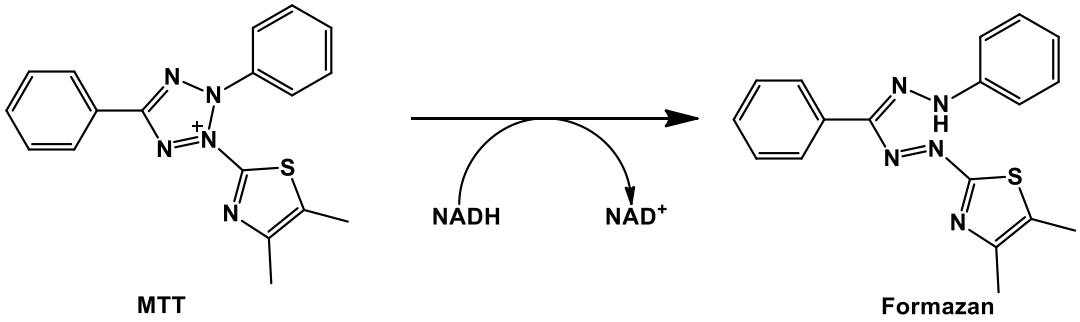

Figure 4.2. Enzymatic reduction of MTT to formazan using NADH as an electron source.

Multi-staining method

Determination of cell viability using assays based on tetrazolium salts is simple, rapid, and high throughput, however, it suffers from one major drawback. MTT can be reduced non-enzymatically by reducing agents such as ascorbic acid, GSH, or co-enzyme A. This increases the chance of errors in data interpretation if proper assay conditions are not maintained.[179,180] This can be overcome by staining the cells with dyes and measuring the number of viable or dead cells to estimate cell viability. Depending on the cell type and assay required one, two or three dyes could be used to stain the cells, and images of these stained cells could be further used to estimate cell viability.[181]

In the current study, a dual-staining system was used to evaluate the effect of the stimuli-responsive release of Dox by Dox-loaded **P2** micelles on the viability of HeLa cells. **P2** polymer system was designed to release Dox in the presence of low pH and glutathione. Since the evaluation of stimuli-responsive release required the cells to be incubated with glutathione, MTT assay could not be used to evaluate cell viability. Thus, two dye-based cell staining method was used to determine cell viability. Abundant esterase activity in live cells results in conversion of freely cell permeable non-fluorescent calcein AM to impermeable fluorescent calcein, thus resulting in only viable cells being stained. Calcein has an excitation maximum at 494 nm and emission maximum at 517 nm. Ethidium homodimer (EthD-1) is unable to enter through the intact

cell membrane of live cells but can easily pass through the damaged cell membrane of the dead cells. In the dead cells, EthD-1 intercalates between the base pairs of the nucleic acid duplex and produces a bright red fluorescence which is 40-fold higher than the unbound EthD-1. EthD-1 has an excitation maximum at 528 and an emission maximum at 617 nm.[182] The following procedure was used to determine the influence of Dox released from degraded **P2** micelles on cell viability. HeLa cells were plated at 1×10^4 cells per well into a 96-well plate and incubated at 37 °C in DMEM (100 μL) containing 10% FBS and 1% antibiotics for 24 hr. Cells were then treated with Dox-NPs to have Dox concentrations at 0.5, 1, and 2 μg/mL in DMEM containing either sodium bicarbonate (1.5 g/L, pH 7.4) for the control or both 10 mM GSH-OEt and 15 mM HEPES buffer (pH = 6.8) for the dual acid/reduction stimuli. Blank samples without Dox-NPs were run simultaneously as controls. Cell viability was measured using the Live/Dead Cell Assay Kit (Invitrogen) according to the manufacturer's protocol. After 48 h incubation at 37 °C, the cells were treated with DMEM (phenol red-free) containing calcein AM (1 μM) and EthD-1 (5 μM) for 30 min. Images were obtained with an inverted fluorescent microscope (Nikon Eclipse TiE inverted epifluorescence microscope), and the number of live cells was counted using ImageJ software. Cell viability was calculated by the percent ratio of the number of live cells incubated with Dox-NPs to control (without Dox-NPs).

4.2.2. Evaluation of cellular uptake by fluorescence microscopy

Widely used methods to investigate cellular uptake involves the use of an imaging or spectroscopic technique to determine the localization of nanocarriers inside the cell.[183] Cellular uptake of **P3** and **P4** micelles were evaluated using the procedure as follows. HeLa cells were seeded at a concentration of 1×10^5 cells/mL into a 35 mm glass-bottom plate and cultured in DMEM. After 24 hr, the media was replaced with DMEM containing either NR-loaded **P4** micelles or Dox-loaded **P3** micelles such that the final concentration of NR or Dox in the micelles was 5 μg/mL or 20 μg/mL respectively. HeLa cells treated with either NR or Dox were kept as control. After a 4 hr incubation, the cells were washed with PBS (3 times) and PBS containing 2 μL of Hoechst 33342 (5 mg/mL) added to the cells to stain the nucleus. After 15 min incubation in the dark, the stain solution was replaced with phenol red-free DMEM and the cells were observed by Nikon Eclipse TiE inverted epifluorescence microscope and the obtained images were processed by ImageJ.

4.3. Biological evaluation of nanocarriers

The results for **P1**, **P2** and **P3** have been described in our publications cited above, adapted from the original source materials.

4.3.1. Cytotoxicity of P1

P1 is an ABA type triblock copolymer which consists of PLA as a hydrophobic block and POEOMA as a hydrophilic block. PLA is an FDA approved polyester which is known to be biocompatible and biodegradable. As shown in Figure 4.3, **P1** was found to demonstrate >75% HeLa cell viability up to 100 µg/mL. These results suggest that since PLA is biocompatible, the polymers containing this should exhibit similar compatibility with cells.

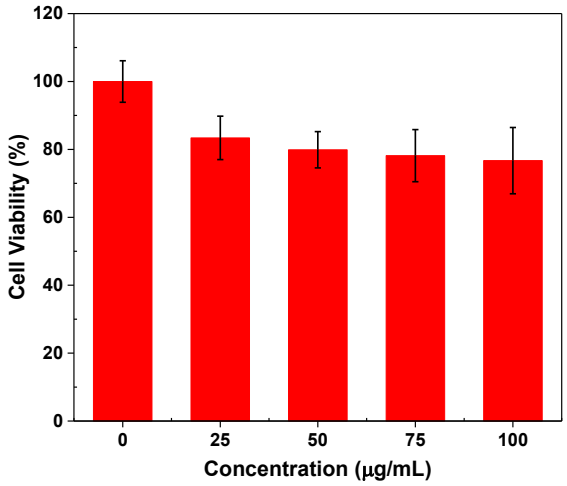

Figure 4.3. HeLa cell viability in the presence of **P1**.

4.3.2. Cytotoxicity of P2

As shown in Figure 4.4.a, the viability of HeLa cells was >80% in the presence of empty **P2** micelles up to 300 µg/mL, suggesting that they are not toxic to HeLa cells. Apart from the cytotoxicity of the polymer, it is important to determine whether the release of the drug in response to SRD of the polymer can produce the desired therapeutic effect in biological systems *in-vitro*. In order to investigate this, HeLa cells were incubated with Dox-loaded **P2** micelle in the presence of appropriate stimuli and the resulting influence on HeLa cell viability was determined by live/dead cell staining assay. **P2** polymer consists of an acid-labile ketal linkage and a redox-labile disulfide linkage which causes it to degrade resulting in the fast release of Dox in low pH and high GSH environment. Thus, various concentrations of Dox-loaded **P2** micelles were incubated with

HeLa cells in an acidic medium (pH 6.8) containing GSH (10 mM) for 48 hrs and the cell death due to released Dox was quantified. In order to evaluate the cell viability, live cells and dead cells stained by calcein-AM and EthD-1, respectively, were visualized using a fluorescence microscope and the percent ratio of live cells in samples treated with Dox-loaded **P2** micelles to control was determined by image analysis. Figure 4.4.b shows the fluorescence microscopy images of live cells incubated with the various amounts of Dox-loaded **P2** micelles in the dual acidic pH = 6.8/GSH condition, compared with the control at pH = 7.4 (no stimuli). For both cases, the density of live cells, i.e., HeLa viability, decreased with an increasing amount of Dox-loaded **P2** micelles. Importantly, the HeLa viability was lower with both acid/GSH, compared to the control with no stimuli at pH = 7.4 (Fig. 4.4.c). The half maximum inhibitor concentration (IC_{50}) value was as low as 0.5 μg/mL with both acid/GSH, which is significantly lower than that (1.04 μg/mL) for the control (pH = 7.4).

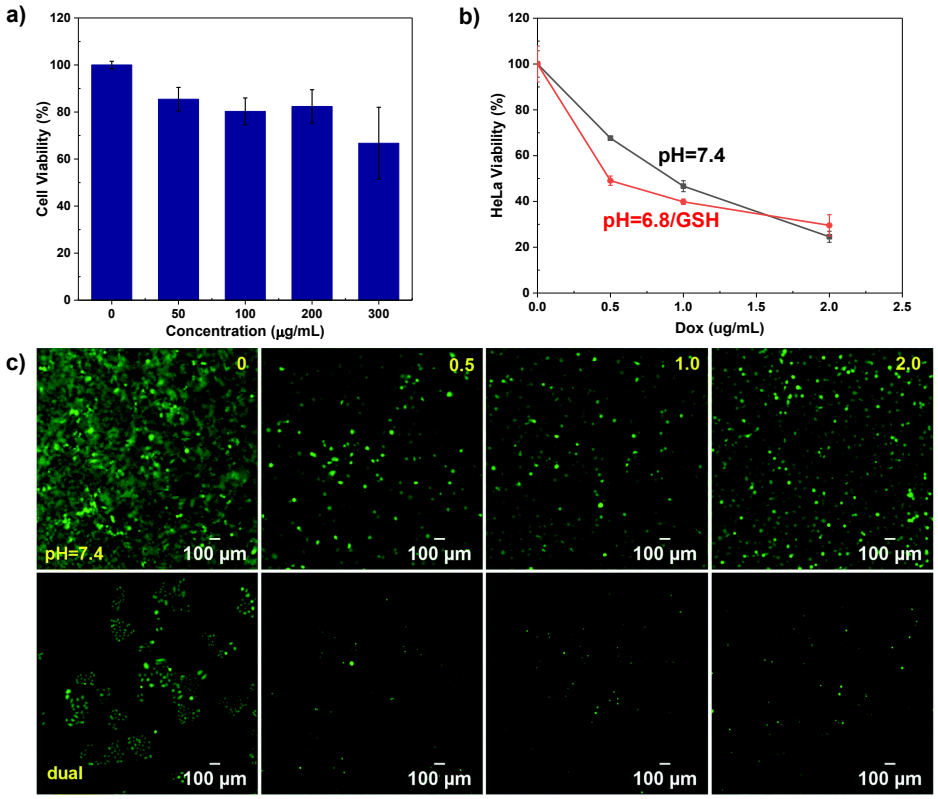

Figure 4.4. Hela cell viability in the presence of empty **P2** micelles **a)**, SRD based Dox release quantified by image analysis **b)** and fluorescence microscopy images of calcein AM stained HeLa cells **c)** treated with varying concentration of Dox-loaded **P2** micelles at pH = 7.4 or pH = 6.8/GSH-OEt.

4.3.3. Cytotoxicity and cellular uptake of P3

As seen in Figure 4.5.a, the **P3** nanogels demonstrated viability to be >85%, suggesting that they are not toxic to the cells up to a concentration of 400 µg/mL. Furthermore, the nanogels were examined for their intracellular tracking by epi-fluorescence microscopy. As seen in Figure 4.5.b, HeLa cells incubated with Dox and Dox-loaded **P3** nanogels show a strong fluorescence signal inside the cells and around the perinuclear region. This indicates that both Dox and Dox-loaded **P3** nanogels were taken up by the cells. In addition, a stronger Dox fluorescence signal from cells treated with Dox-loaded **P3** nanogels indicates that the micelles were taken up by the cells to a greater extent in comparison to free Dox.

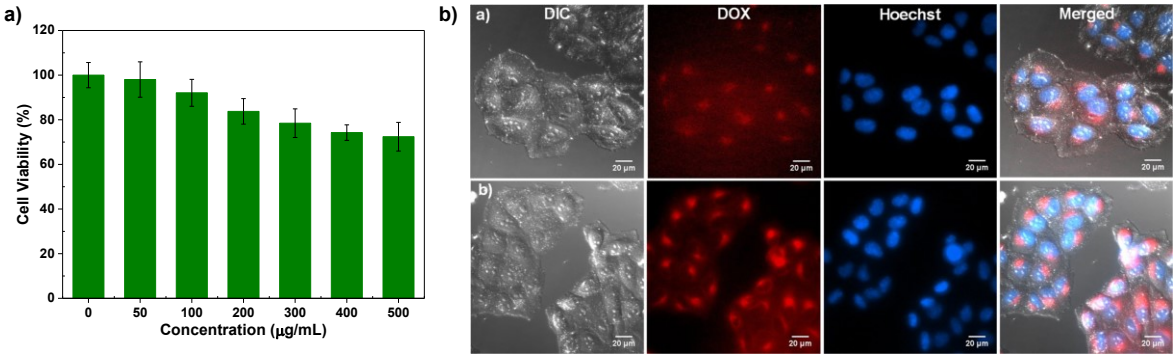

Figure 4.5. HeLa cell viability in the presence of empty **P3** nanogels **a)** and fluorescence microscope image of HeLa cells incubated with Dox and Dox-loaded **P3** nanogels **b)**.

4.3.4. Cytotoxicity and cellular uptake of P4

Upon evaluation of HeLa cells viability in the presence of these polymers, it was found that **P4** micelles showed > 75 % cell viability up to 200 µg/mL, as seen in Figure 4.6.a. Furthermore, the cellular uptake of **P4** micelles was evaluated by incubating either NR or NR-loaded **P4** micelles with HeLa cells and observing the localization using an epifluorescent microscope. The fluorescence microscopy images in Figure 4.6. shows a strong NR fluorescence signal inside the cells and around the perinuclear region which indicates that both NR and NR-loaded **P4** micelles were taken up by HeLa cells. However, NR-loaded **P4** micelles were taken up by the cells to a lower extent as compared to free NR.

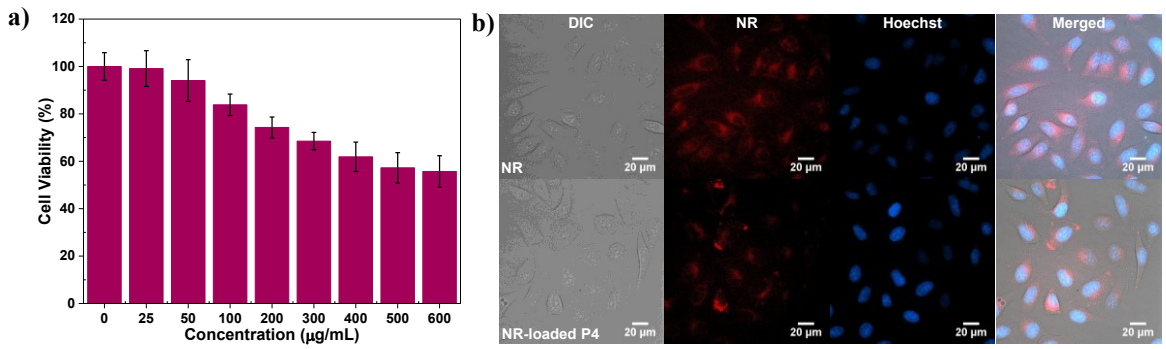

Figure 4.6. HeLa cell viability in the presence of empty **P4** nanogels **a)** and fluorescence microscope image of HeLa cells incubated with Dox and Dox-loaded **P4** nanogels **b)**.

4.4. Further methods to study cellular interaction

4.4.1. Cytotoxicity assays

Alamar blue assay

Despite being high-throughput, simple and rapid, the unavoidable cell death and need for crystal dissolution before spectroscopic measurement, makes MTT tedious and not suitable for real-time assays. In order to overcome these limitations of the MTT assay, a resazurin based assay i.e. Alamar blue assay was developed. Resazurin is a deep blue colored cell-permeable redox dye which in viable cells, forms pink-colored cell-permeable resorufin (Figure 4.7) upon being reduced by enzymes in mitochondria, microsome enzymes, the respiratory chain or by electron transfer agents such as N-methylphenazinium methosulfate (PMS) in the presence of NADH or NADPH. Both resazurin and resorufin absorb visible light; however, resazurin has an absorbance maximum at 600 nm whereas resorufin's is at 570 nm. Moreover, resazurin is non-fluorescent whereas resorufin is fluorescent with excitation at 560 nm and emission at 590 nm. Since resorufin is water-soluble, it eliminates the lengthy post-reaction processing step and allows for direct quantification of resorufin by spectroscopic methods. Resazurin based assays have been reported to be more sensitive and reliable than the MTT assay; however, a change in pH, temperature, and initial resazurin concentration can influence the reduction rate thereby influencing the final results. Thus, it is essential that these parameters must be kept constant when resazurin based assays are used. The procedure used in the Alamar blue assay is the same as that in MTT assay with the elimination of the post-incubation dissolution step.[184,185]

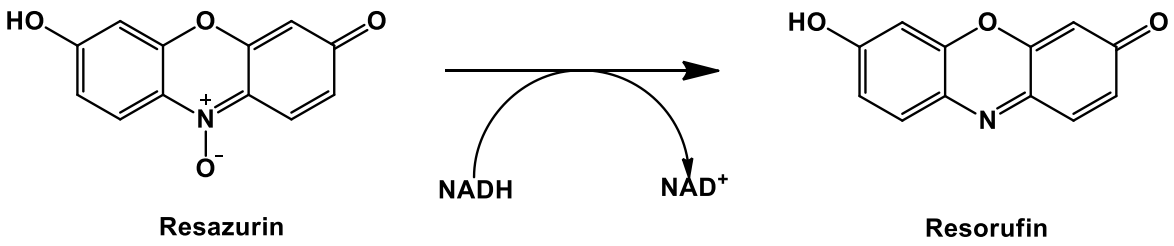

Figure 4.7. Enzymatic reduction of resazurin to resorufin using NADH as electron source.

ATP assay

Both tetrazolium and resazurin salt-based assays are simple and rapid assays that have been extensively used for high throughput screening. However, they both suffer from limitations such as the requirement of at least 4 hr incubation to generate detectable indicators; inaccurate results due to interference from chemical reducing agents; and cell death due to toxicity of tetrazolium and resazurin salts. ATP assay overcomes these limitations by measuring the widely accepted marker of viable cells, ATP. Viable cells are capable of synthesizing ATP and regulating its intracellular concentration. On the other hand, dead or dying cells lose their ability to synthesize ATP, and the consumption of available ATP by endogenous ATPase results in a rapid drop in intracellular ATP levels. Thus, the presence of ATP is associated only with live cells, and its quantification directly correlates to cell viability. Quantification of ATP can be accomplished by quantifying the photons generated as a result of ATP-dependant cleavage of luciferin by luciferase. Thus, ATP detection involves cell lysis, prevention of further ATP metabolism by inhibiting ATPase, and generation of a photon from cleavage of luciferin by luciferase. All these steps can be achieved by the addition of a single reagent and the generated luminescent signal stabilizes within a few minutes. This makes the ATP assay the fastest and most convenient cell viability assay. Since the photons can be generated only in the presence of ATP, there is a negligible chance of interference from sample components. Moreover, a low background signal enables a large signal to noise ratio. This makes ATP assay an extremely sensitive cell viability assay. These advantages make the ATP assay a gold standard for cell viability measurement.[186]

4.4.2. Cellular uptake

Cellular uptake of a nanocarrier plays an important role in its therapeutic efficacy and is affected by size, shape, surface charge, and composition. Thus, knowledge of the mechanism involved in cellular uptake plays a critical role in determining not only the fate and toxicity of the

nanocarrier but also aid in the design of modifications to its structure that will enhance interaction with cells. Cellular uptake, also known as endocytosis, can be classified into two categories: phagocytosis and pinocytosis. Phagocytosis differs from pinocytosis in terms of the size of the particle being taken up and the subsequent size of vesicle formed. Phagocytosis is involved in the uptake of particles with a size of ~ 250 nm; whereas pinocytosis is involved in fluid uptake or uptake of particles ranging in size from a few nanometres to hundreds of nm. Thus, pinocytosis is the major pathway involved in the uptake of nanocarriers. Pinocytosis can be further categorized into four types: clathrin-mediated endocytosis, caveolae-mediated endocytosis, clathrin- and caveolae-independent endocytosis and micropinocytosis.[187,188]

Cells obtain nutrients, iron, and plasma membrane components such as cholesterol primarily by clathrin-mediated endocytosis. This mechanism can be receptor-dependent or receptor-independent. Non-specific hydrophobic or electrostatic interaction with the cell membrane can initiate receptor-independent clathrin-mediated endocytosis. Clathrin-mediated endocytosis occurs on plasma membrane surfaces rich in clathrin and the particles are engulfed via clathrin-coated vesicles. Caveolae-mediated endocytosis involves caveolin-coated flask-shaped invaginations called caveolae responsible for uptake of particles 50-80 nm in size. This mode of endocytosis is responsible for cell signaling; and regulation of lipids, fatty acids, membrane proteins, and membrane tension. Particles entering the cells by caveolae-mediated endocytosis can evade lysosomal degradation and thus attempts are being made to exploit this pathway for nanocarrier-based therapeutic delivery. Cells lacking clathrin or caveolin uptake extracellular fluids, Interleukin-2, and growth hormones by clathrin- and caveolae-independent endocytosis. Particles entering cells via this pathway might also be capable of escaping lysosomal degradation. Macropinocytosis involves cytoskeletal rearrangements to form large membrane extensions which can engulf high volumes of extracellular fluid by forming a large vesicle (0.5–10 μm) called macropinosomes. Micron-sized particles can enter cells by taking advantage of this pathway. Nanocarriers made of PLA, poly(lactide-co-glycolide), and anionic particles were found to enter cells via both clathrin- or caveolae-dependent endocytosis. However, cationic nanocarriers were found to enter only via clathrin-dependent endocytosis. Moreover, folate-coated nanocarriers were found to utilize clathrin- and caveolae-independent endocytosis to gain cell entry.[187,188]

The most commonly employed method to determine and quantify nanocarrier uptake into cells is imaging techniques. Localization of fluorescently-labeled nanocarrier or nanocarrier

encapsulating fluorescent moieties can be visualized using fluorescence microscopy techniques.[189] Pre-treatment of cells by various drugs that inhibit different endocytosis pathways and subsequent visualization of nanocarrier localization can enable determination of the specific pathway employed by nanocarriers for cell entry. Some examples of the drugs are chlorpromazine and nocodazole to inhibit clathrin-dependent endocytosis; cytochalasin A and genistein to inhibit caveolae-dependent endocytosis [190,191]; and lovastatin to inhibit clathrin-dependent endocytosis, caveolae-dependent endocytosis, and micropinocytosis.[192] Other commonly employed methods include the use of electron microscopy (EM) techniques such as scanning EM, transmission EM, and focused ion beam EM.[189]

4.4.3. Hemocompatibility

Upon entering the bloodstream, nanocarriers come in contact with blood components such as red blood cells and serum proteins. Modifications have been incorporated into nanocarriers to prolong their circulation time causing enhanced accumulation of polymeric nanocarriers in tumor tissues. However, prolonged circulation time also increases the interaction of nanocarriers with blood components. Thus, it is imperative to determine the effect of nanocarrier size, shape, surface charge, and composition on its interaction with blood components.

Red blood cells, the major component of blood, are prone to lyse in the presence of foreign bodies such as nanocarriers. Upon cell lysis, also known as hemolysis, iron-containing protein hemoglobin leaks from the damaged red blood cells into the plasma. The possibility of life-threatening conditions, such as hemolytic anemia, jaundice, and renal failure, due to severe hemolysis makes it critical to evaluate the hemolytic activity of a nanocarrier. The hemolytic behavior of a nanocarrier can be evaluated by incubating the samples with either whole blood or purified RBC and quantifying the released hemoglobin using spectrophotometric methods.

Apart from red blood cells, nanocarriers can also interact with serum proteins, the minor component of blood. The interaction of nanocarriers with serum proteins can initiate a wide range of events ranging from induction of coagulation to activation of mononuclear phagocytic system due to adsorption of opsonin. These events can be detrimental to not only the human body but also the nanocarriers since it promotes the rapid clearance of nanocarriers.[193] Various methods have been developed for direct and indirect detection of protein adsorption. Frequently used direct methods involve visualization of adsorbed protein on nanocarrier using transmission EM after

negative staining; or quantifying the unbound protein by standard biochemical protein quantification assays, such as Bradford or BCA. Indirect methods measure protein adsorption by monitoring changes in the size, charge, density, mass, absorbance and fluorescence of the nanocarrier upon interaction with protein. Some examples of indirect methods include scanning EM, transmission EM, DLS and the fluorescence quenching assay.[194]

4.5. Conclusion

Cytotoxicity and cellular uptake of four amphiphilic block copolymers exhibiting dual acid/glutathione-responsive degradation and enhanced drug release were investigated. **P1**, a polymer-based on biocompatible and biodegradable polylactide polymer, was found to be non-cytotoxic up to the tested concentration which suggests that polymers based on biologically compatible materials would result in polymers with superior biological performance. **P2**, **P3,** and **P4** are examples of methacrylate-based block copolymers that have the same hydrophobic unit i.e. HMssEt, but different hydrophilic units. The hydrophilic unit is composed of PEG for **P2**, POEOMA for **P4** and both PEG and POEOMA for **P3**. **P2** and **P4** exhibited similar cell viability and cellular uptake, thus indicating that PEG and POEOMA have a similar influence on the cytotoxicity and uptake of the polymer. However, **P3** showed enhanced cell viability and cellular uptake which suggests that when incorporated together, PEG and POEOMA could enhance cell viability and uptake of the micelle. Furthermore, apart from composition, **P3** differs from **P4** and **P2** in terms of polymer architecture. The hydrophilic corona of **P2** and **P4** is composed of PEG and POEOMA respectively, whereas, in the case of **P3**, PEG forms the hydrophilic corona but POEOMA forms the part of the core. This structural difference could also be the reason for enhanced cell viability and cellular uptake of **P3** micelles compared to **P2** and **P4** micelles. Thus, our preliminary results suggest that the composition and architecture of the copolymers are important design parameters that significantly influence the cellular interactions.

Chapter 5

Conclusion and Future Gene Carrier Strategy

5.1. Conclusion

Cationic polymers have been widely explored for the delivery of nucleic acids, however there still exists several challenges to be addressed to improve their properties as nanocarriers including: poor stability, high cytotoxicity, and low gene transfection efficiency. My Master's research main objective was the exploration of stimuli-responsive degradation and hydrophobic modification in the synthesis of a novel cationic block copolymer for controlled gene delivery. As a proof of concept, a novel cationic amphiphilic block copolymer PEG-AC-P(HMssEt-co-DMAEMA) (PDss) was synthesized by ATRP of a mixture of DMAEMA and HMssEt in the presence of an acid-labile acetal-labeled PEG-AC-Br macroinitiator. At a N/P ratio >2, PDss was able to condense dsDNA through electrostatic interactions of the positively-charged tertiary amine groups of the DMAEMA units with negatively-charged dsDNA. Such complexation resulted in the formation of nanometre-sized micelleplexes containing acetal groups at the core/corona interfaces and disulfide linkages in the cores. A micelleplex fabricated at a N/P ratio = 10 was subjected to a thiol-disulfide exchange reaction to form a colloidally stable core-crosslinked micelleplex (xM-PDss) with a diameter = 83 nm and ζ-potential = -1.2 ± 0.5 mV. In the presence of both endogenous acidic pH and GSH, xM-PDss was destabilized, releasing dsDNA from the micelleplexes. PDss was shown to be non-cytotoxic to HeLa cells with > 95 % cell viability up to 0.9 mg/mL. siRNA containing xM-PDss was capable of escaping from endosomes and demonstrated enhanced silencing of the EGFP gene in the presence of 10 mM GSH. These combined results suggest that the incorporation of stimuli-responsive degradation and hydrophobic modifications into the design of cationic block copolymers is an effective approach to enhance colloidal stability, improve cytotoxicity, and enhance gene transfection efficiency.

Further, another objective of my master's research was to study the cellular interactions of stimuli-responsive degradable polymeric nanoassemblies. Particularly, cell viability and cellular uptake were evaluated for four block copolymer nanoassemblies exhibiting dual-acid/reduction responsive degradation with different chemical composition and architecture. Backbone multi-

cleavable nano-assemblies containing PLA were non-cytotoxic throughout the concentration range evaluated. Methacrylate-based polymers show cytotoxicity and cellular uptake that is dependent on the composition and architecture of the polymer. Further, PEG and POEOMA were found to be similar in their cytotoxic nature; however, when incorporated together they enhanced the cytotoxicity and cellular uptake of the nanocarrier. Moreover, the arrangement of PEG and POEOMA in the polymer block could play a role in enhancing the cellular interaction of nanocarriers. These preliminary results suggest that the composition and architecture of polymer are important parameters that significantly influence the cellular interaction of nanocarriers.

5.2. Proposed strategy: Development of acid-responsive PEG-detachable and reduction-responsive backbone cleavable nanocarriers of gene delivery

My master's research explored a promising platform of DL-DSRD combined with a hydrophobic modification to synthesize a novel cationic block copolymer for effective gene delivery. The copolymer was designed to contain an acetal group at the block junction and pendant disulfide linkages in the hydrophobic block. The results showed that this platform enhanced colloidal stability, reduced cytotoxicity, and improved GSH-induced gene silencing efficiency. However, further modifications will be required to improve gene silencing efficiency. First, a methyl-substituted acetal linkage used in my study displayed slow hydrolysis at a tumor extracellular pH = 6.5 – 6.8 and even endosomal pH = 5.5. Second, the cleavage of pendant disulfide linkages in the core failed to significantly enhance gene release. This is could be attributed to reduced reductive cleavage and the resultant effect on the release of nucleic acids due to relatively strong electrostatic interactions between DNA and DMAEMA moieties. Finally, the degraded products generated from the SRD process have limited solubility in the aqueous environment. The large aggregates that form could be problematic as they could pose a challenge for elimination from the body.

Figure 5.1 illustrates our proposed design and chemical structure of a robust cationic block copolymer for effective gene delivery. First, a cyclic acetal linkage present at the block junction can be anticipated to undergo rapid hydrolysis at acidic pH. Second, the presence of disulfide linkages in the backbone would be beneficial to generate small molecular weight degraded products. Third, pendant disulfides attached to tertiary amino groups could facilitate gene release upon their cleavage in the GSH-rich cytosol of cancer cells. Eventually, our approach allows us to

explore a new mechanism for gene release over the acidic pH-induced endosomal escape mechanism.

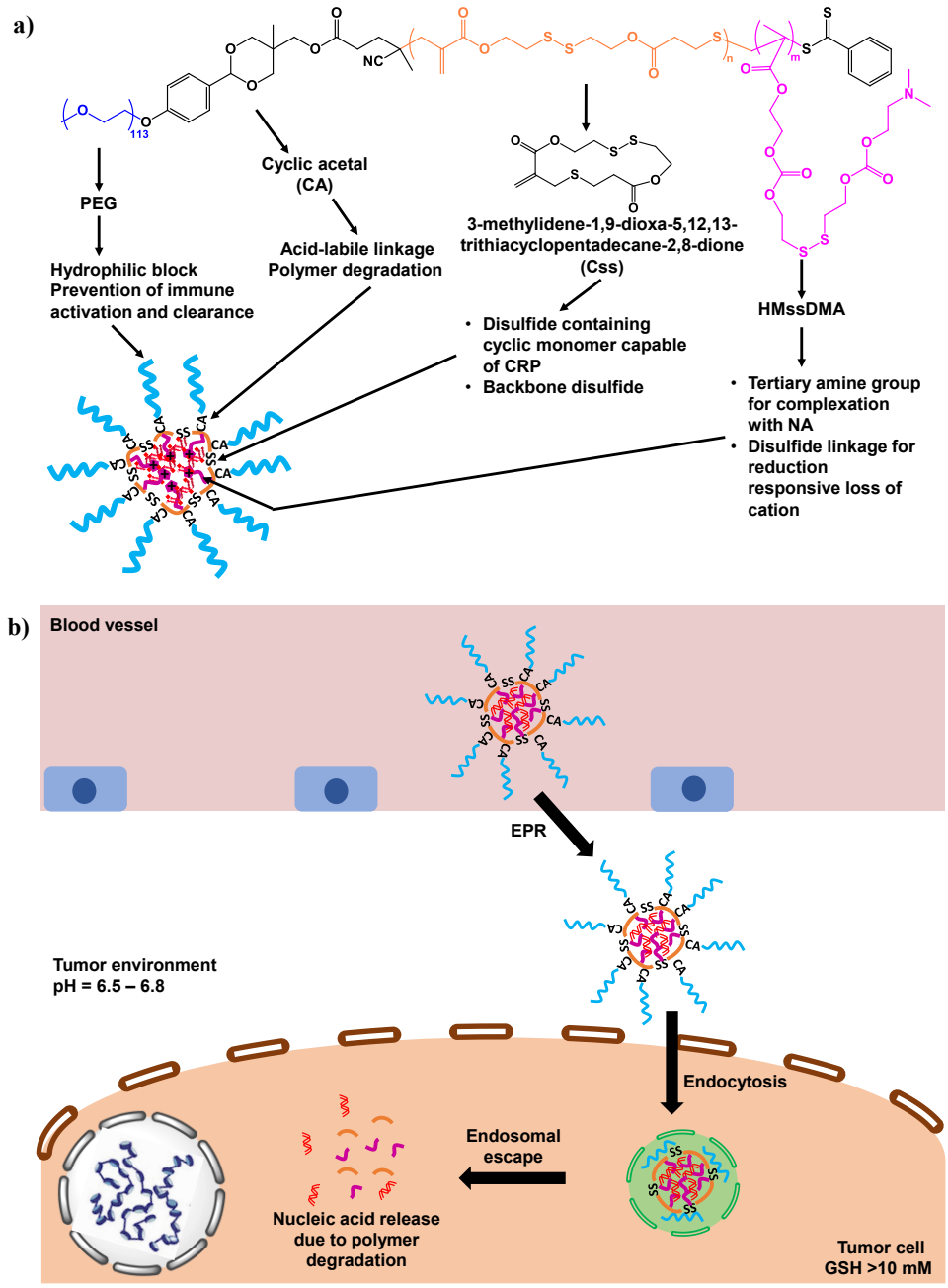

Figure 5.1. Design strategy for a novel nucleic acid carrier and the role of each component **a)** and schematic illustration of intracellular release of nucleic acid in presence of GSH. Accumulation of micelleplex in the tumor tissue by EPR effect is followed by endocytosis into the tumor cell. After endosomal escape, the degradation of polymer backbone in presence of intracellular GSH results in complete nucleic acid release **b)**.

5.2.1. Progress up to now

Synthesis of PEG-CA-RAFT

Figure 5.2.a shows the reaction scheme for the synthesis of PEG-CA-OH. The first step is the synthesis of PEG-mesylate (PEG-Ms).[195] Briefly, methane sulfonyl chloride (MsCl, 0.46 g, 4 mmol) diluted in DCM (5 mL) was added dropwise to a solution consisting of azeotropically dried PEG (5000 g/mol, 4 g, 0.8 mmol) and triethylamine (Et_3N, 0.24 g, 2.4 mmol) dissolved in DCM (15 mL) under vigorous stirring in an ice bath. The reaction mixture was stirred overnight at room temperature, washed four times with a 1:1 solution of HCl (0.1 M) and brine, dried over anhydrous sodium sulfate and precipitated from diethyl ether. The ^{1}H-NMR spectrum of the purified PEG-Ms in Figure 5.2.b shows signals corresponding to methoxy protons (a) at 3.38 ppm, PEG protons (b) at 3.48 – 3.8 ppm, methylene protons (c) next to the mesylate group at 4.38 ppm and methyl protons (d) attached to mesylate at 3.08 ppm. The next step is the synthesis of PEG-benzaldehyde by reaction of PEG-Ms with 4-hydroxybenzaldehyde (0.2 g, 39.4 µmol) in the presence of potassium carbonate (K_2CO_3, 0.109 g, 0.8 mmol).[196] The reaction was performed in THF overnight under reflux. The product was purified by precipitation from diethyl ether. The ^{1}H-NMR spectrum of the purified PEG-benzaldehyde in Figure 5.2.c contains signals corresponding to a para-substituted benzene (e and f) at 7 and 7.8 ppm and aldehyde proton (g) at 9.9 ppm. The last step is the synthesis of PEG-CA-OH by the reaction of 1,1,1-tris(hydroxymethyl)ethane (TME, 16 g, 0.14 mol) with PEG-benzaldehyde (1 g, 0.2 mmol) in the presence of HCl (0.2 mmol).[197] The reaction was performed in THF at 60 °C for 30 mins, followed by the addition of Et_3N to neutralize HCl. The residue was dissolved in chloroform and insoluble components were removed by filtration. After purification by precipitation from diethyl ether, PEG-CA-OH was characterized by ^{1}H-NMR (Figure 5.2.d). The disappearance of the signal corresponding to the aldehyde proton (g) and appearance of additional signals corresponding to an acetal proton (h) at 5.38 ppm and cyclized TME protons (i, j, k) at 4.02, 3.07 and 0.81 ppm indicate the successful synthesis of PEG-CA-OH. The synthesized PEG-CA-OH will be subjected to conjugation with 4-cyano-4-(phenylcarbonothioylthio)pentanoic acid (RAFT) to form PEG-CA-RAFT macroinitiator bearing an acid-labile cyclic acetal linkage.

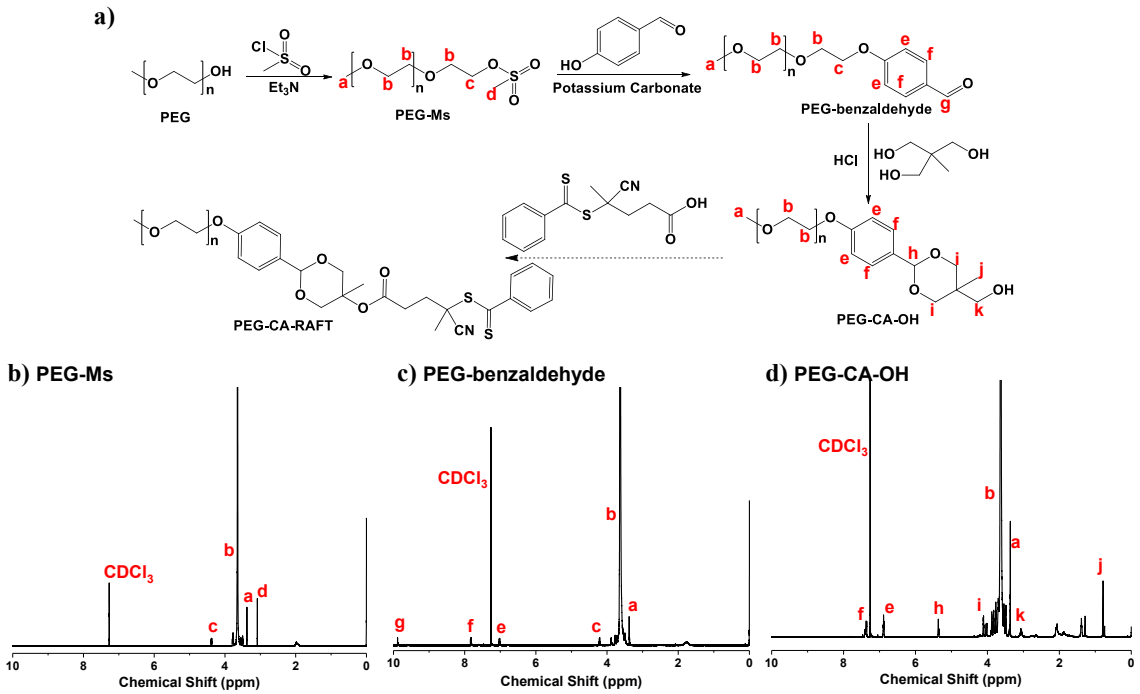

Figure 5.2. Synthesis scheme for PEG-CA-RAFT **a)** and ^{1}H-NMR spectra of PEG-Ms **b)**, PEG-benzaldehyde **c)** and PEG-CA-OH **d)**.

Synthesis of HMssDMA

HMssDMA is designed to have a pendant disulfide and tertiary amino group. As depicted in Figure 5.3.a., the first step to synthesize HMssDMA is the reaction of 2-hydroxyethyl disulfide (2 g, 13 mmol) with 1,1′-carbonyldiimidazole (CDI, 8.41 g, 52 mmol) in acetonitrile (200 mL) for 2 hrs. Water was used to neutralize excess CDI. The product was extracted in chloroform (100 mL) five times, washed with water (100 mL) and brine (100 mL), dried over sodium sulfate and evaporated. The ss-diCDI product was isolated as a white solid and analysed by ^{1}H-NMR (Figure 5.3.b). The spectrum contains signals at 7.09, 7.44 and 8.15 ppm corresponding to protons a, b and c of the imidazole ring with the ring nitrogen atom comprising a carbamate group. Also present in the spectrum are signals for methylene protons (d) at 4.70 ppm which are attached to a carbamate group and methylene protons (e) at 3.10 ppm connected to a disulfide group. The next step in the synthesis involves reaction of ss-diCDI (8.88 g, 25.9 mmol), 2-hydroxyethyl methacrylate (HEMA, 1 g, 6.5 mmol) and 1,8-diazabicyclo(5.4.0)undec-7-ene (DBU, 0.074 g, 0.5 mmol) in THF (10 mL) under vigorous stirring in an ice bath. After 4 hrs, the product was purified by column chromatography using 6/4 v/v ethyl acetate/hexane as the eluent. The ^{1}H-NMR spectrum (Figure

5.3.c) shows the appearance of new signals corresponding to a pair of methylene protons at 4.68 ppm (f) connected to the oxygen atoms of carbonate and ester groups. Also present were signals at 1.95 ppm corresponding to methyl protons (i) attached to a vinyl group, and signals at 6.13 and 5.6 ppm (g, h) for the vinyl protons. The final step to prepare HMssDMA will involve reaction of HMssCDI with 2-dimethylaminoethanol (DMA) in the presence of a catalytic amount of DBU.

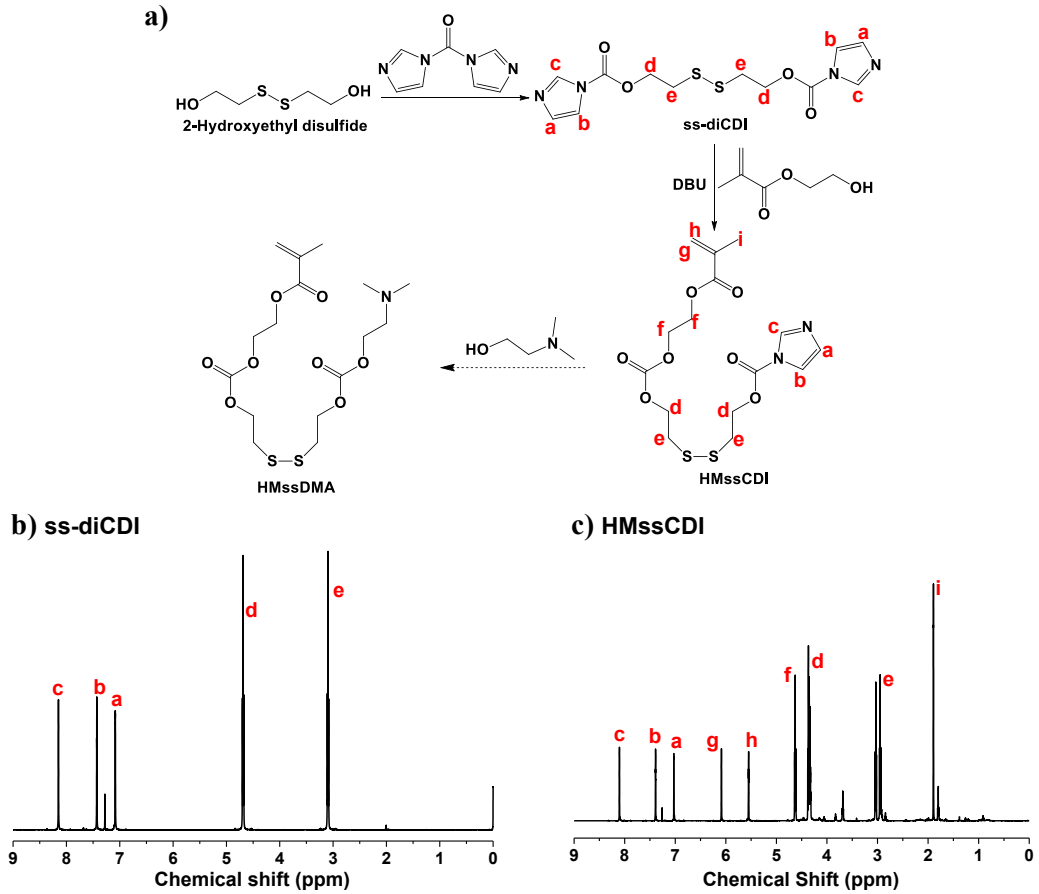

Figure 5.3. Synthesis scheme for HMssDMA **a)** and ^{1}H-NMR spectrum of ss-diCDI **b)** and HMssCDI **c)**.

References

1. Hanahan, D. and Weinberg, R.A., The Hallmarks of Cancer. *Cell*, **2000**. *100*, 57-70.
2. Sudhakar, A., History of Cancer, Ancient and Modern Treatment Methods. *Journal of Cancer Science & Therapy*, **2009**. *01*, 1-4.
3. Corrie, P.G., Cytotoxic chemotherapy: clinical aspects. *Medicine*, **2008**. *36*, 24-28.
4. Bassal, M., Mertens, A.C., Taylor, L., Neglia, J.P., Greffe, B.S., Hammond, S., Ronckers, C.M., Friedman, D.L., Stovall, M., Yasui, Y.Y., Robison, L.L., Meadows, A.T., and Kadan-Lottick, N.S., Risk of Selected Subsequent Carcinomas in Survivors of Childhood Cancer: A Report From the Childhood Cancer Survivor Study. *Journal of Clinical Oncology*, **2006**. *24*, 476-483.
5. Brenner, D.R., Weir, H.K., Demers, A.A., Ellison, L.F., Louzado, C., Shaw, A., Turner, D., Woods, R.R., and Smith, L.M., Projected estimates of cancer in Canada in 2020. *CMAJ*, **2020**. *192*, 199-205.
6. Panchal, R.G., Novel Therapeutic Strategies to Selectively Kill Cancer Cells. *Biochemical Pharmacology*, **1998**. *55*, 247-252.
7. Sheikhi, M.A., Ebadi, A., Talaeizadeh, A., and Rahmani, H., Alternative Methods to Treat Nausea and Vomiting from Cancer Chemotherapy. *Chemotherapy Research and Practice*, **2015**. *2015*, 1-6.
8. Jemal, A., Bray, F., Center, M.M., Ferlay, J., Ward, E., and Forman, D., Global cancer statistics. *CA: A Cancer Journal for Clinicians*, **2011**. *61*, 69-90.
9. Ferlay, J., Colombet, M., Soerjomataram, I., Mathers, C., Parkin, D.M., Piñeros, M., Znaor, A., and Bray, F., Estimating the global cancer incidence and mortality in 2018: GLOBOCAN sources and methods. *International Journal of Cancer*, **2018**. *144*, 1941-1953.
10. Ferlay, J., Soerjomataram, I., Dikshit, R., Eser, S., Mathers, C., Rebelo, M., Parkin, D.M., Forman, D., and Bray, F., Cancer incidence and mortality worldwide: Sources, methods and major patterns in GLOBOCAN 2012. *International Journal of Cancer*, **2015**. *136*, E359-E386.
11. Hornberg, J.J., Bruggeman, F.J., Westerhoff, H.V., and Lankelma, J., Cancer: A Systems Biology disease. *Biosystems*, **2006**. *83*, 81-90.
12. Seyfried, T. and Shelton, L., Cancer as a metabolic disease. *Nutrition & Metabolism*, **2010**. *7*, 1-22.
13. Vogelstein, B. and Kinzler, K.W., Cancer genes and the pathways they control. *Nature Medicine*, **2004**. *10*, 789-799.
14. Harrington, K.J., Biology of cancer. *Medicine*, **2008**. *36*, 1-4.
15. Merdana, T., Kopecek, J., and Kissel, T., Prospects for cationic polymers in gene and oligonucleotide therapy against cancer. *Advanced Drug Delivery Reviews*, **2002**. *54*, 715-758.
16. Mulligan, R.C., The basic science of gene therapy. *Science*, **1993**. *260*, 926-932.
17. McMenamin, M.M., Translational benefits of gene therapy to date. *Clinical Oncology and Cancer Research*, **2011**. *8*, 10-15.
18. Yin, H., Kanasty, R.L., Eltoukhy, A.A., Vegas, A.J., Dorkin, J.R., and Anderson, D.G., Non-viral vectors for gene-based therapy. *Nature Reviews Genetics*, **2014**. *15*, 541-555.

19. Dominguez, A.A., Lim, W.A., and Qi, L.S., Beyond editing: repurposing CRISPR–Cas9 for precision genome regulation and interrogation. *Nature Reviews Molecular Cell Biology*, **2015**. *17*, 5-15.
20. Ortiz, R., Melguizo, C., Prados, J., Álvarez, P.J., Caba, O., Rodríguez-Serrano, F., Hita, F., and Aránega, A., New Gene Therapy Strategies for Cancer Treatment: A Review of Recent Patents. *Recent Patents on Anti-Cancer Drug Discovery*, **2012**. *7*, 297-312.
21. Cross, D. and Burmester, J., Gene Therapy for Cancer Treatment: Past, Present and Future. *Clinical Medicine & Research*, **2006**. *4*, 218-227.
22. McCormick, F., Cancer Gene Therapy: Fringe or Cutting Edge? *Nature Reviews Cancer*, **2001**. *1*, 130-141.
23. Das, S.K., Menezes, M.E., Bhatia, S., Wang, X.-Y., Emdad, L., Sarkar, D., and Fisher, P.B., Gene Therapies for Cancer: Strategies, Challenges and Successes. *Journal of Cellular Physiology*, **2015**. *230*, 259-271.
24. Amer, M., Gene therapy for cancer: present status and future perspective. *Molecular and Cellular Therapies*, **2014**. *2*, 1-19.
25. Vile, R.G., Russell, S. J. and Lemoine, N. R. , Cancer gene therapy hard lessons and new courses. *Gene Therapy*, **2000**. *7*, 2-8.
26. Lächelt, U. and Wagner, E., Nucleic Acid Therapeutics Using Polyplexes: A Journey of 50 Years (and Beyond). *Chemical Reviews*, **2015**. *115*, 11043-11078.
27. Lin, G., Zhang, H., and Huang, L., Smart Polymeric Nanoparticles for Cancer Gene Delivery. *Molecular Pharmaceutics*, **2015**. *12*, 314-321.
28. Miyata, K., Nishiyama, N. and Kataoka, K., Rational design of smart supramolecular assemblies for gene delivery: chemical challenges in the creation of artificial viruses. *Chemical Society Reviews*, **2012**. *41*, 2562–2574.
29. Wu, J., Chen, J., Feng, Y., Tian, H., and Chen, X., Tumor microenvironment as the "regulator" and "target" for gene therapy. *The Journal of Gene Medicine*, **2019**. *21*, e3088.
30. Whiteside, T.L., The tumor microenvironment and its role in promoting tumor growth. *Oncogene*, **2008**. *27*, 5904-5912.
31. Weber, C.E. and Kuo, P.C., The tumor microenvironment. *Surgical Oncology*, **2012**. *21*, 172-177.
32. Jhaveri, A.M. and Torchilin, V.P., Multifunctional polymeric micelles for delivery of drugs and siRNA. *Frontiers in Pharmacology*, **2014**. *5*, 77.
33. Baban, D.F. and Seymour, L.W., Control of tumour vascular permeability. *Advanced Drug Delivery Reviews*, **1998**. *34*, 109-119.
34. Maeda, H., Wu, J., Sawa, T., Matsumura, Y., and Hori, K., Tumor vascular permeability and the EPR effect in macromolecular therapeutics: a review. *Journal of Controlled Release*, **2000**. *65*, 271-284.
35. Du, J., Lane, L.A., and Nie, S., Stimuli-responsive nanoparticles for targeting the tumor microenvironment. *Journal of Controlled Release*, **2015**. *219*, 205-214.
36. Upreti, M., Jyoti, A., and Sethi, P., Tumor microenvironment and nanotherapeutics. *Transl Cancer Res*, **2013**. *2*, 309-319.
37. Pelicano, H., Carney, D., and Huang, P., ROS stress in cancer cells and therapeutic implications. *Drug Resistance Updates*, **2004**. *7*, 97-110.
38. de Sá Junior, P.L., Câmara, D.A.D., Porcacchia, A.S., Fonseca, P.M.M., Jorge, S.D., Araldi, R.P., and Ferreira, A.K., The Roles of ROS in Cancer Heterogeneity and Therapy. *Oxidative Medicine and Cellular Longevity*, **2017**. *2017*, 1-12.

39. Vazquez, A., Kamphorst, J.J., Markert, E.K., Schug, Z.T., Tardito, S., and Gottlieb, E., Cancer metabolism at a glance. *Journal of Cell Science*, **2016**. *129*, 3367-3373.
40. Sreedhar, A. and Zhao, Y., Dysregulated metabolic enzymes and metabolic reprogramming in cancer cells (Review). *Biomedical Reports*, **2017**. *8*, 3-10.
41. Finger, E.C. and Giaccia, A.J., Hypoxia, inflammation, and the tumor microenvironment in metastatic disease. *Cancer and Metastasis Reviews*, **2010**. *29*, 285-293.
42. Mathew, A., Cho, K.-H., Uthaman, S., Cho, C.-S., and Park, I.-K., Stimuli-Regulated Smart Polymeric Systems for Gene Therapy. *Polymers*, **2017**. *9*, 152.
43. Robbins, P.D. and Ghivizzani, S.C., Viral Vectors for Gene Therapy. *Pharmacology & Therapeutics*, **1998**. *80*, 35-47.
44. Hardee, C., Arévalo-Soliz, L., Hornstein, B., and Zechiedrich, L., Advances in Non-Viral DNA Vectors for Gene Therapy. *Genes*, **2017**. *8*, 65.
45. Husain, S.R., Han, J., Au, P., Shannon, K., and Puri, R.K., Gene therapy for cancer: regulatory considerations for approval. *Cancer Gene Therapy*, **2015**. *22*, 554-563.
46. Xiao, Y., Shi, K., Qu, Y., Chu, B., and Qian, Z., Engineering Nanoparticles for Targeted Delivery of Nucleic Acid Therapeutics in Tumor. *Molecular Therapy - Methods & Clinical Development*, **2019**. *12*, 1-18.
47. Seow, Y. and Wood, M.J., Biological Gene Delivery Vehicles: Beyond Viral Vectors. *Molecular Therapy*, **2009**. *17*, 767-777.
48. Brown, M.D., Schatzlein, A.G., and Uchegbu, I.F., Gene delivery with synthetic (non viral) carriers. *International Journal of Pharmaceutics*, **2001**. *229*, 1-21.
49. De Laporte, L., Cruz Rea, J., and Shea, L.D., Design of modular non-viral gene therapy vectors. *Biomaterials*, **2006**. *27*, 947-954.
50. Park, T., Jeong, J., and Kim, S., Current status of polymeric gene delivery systems. *Advanced Drug Delivery Reviews*, **2006**. *58*, 467-486.
51. Li, Y., Gao, J., Zhang, C., Cao, Z., Cheng, D., Liu, J., and Shuai, X., Stimuli-Responsive Polymeric Nanocarriers for Efficient Gene Delivery. *Topics in Current Chemistry*, **2017**. *375*, 27.
52. Lee, Y. and Kataoka, K., Delivery of Nucleic Acid Drugs. **2011**. *249*, 95-134.
53. Kabanov, A.V., Taking polycation gene delivery systems from in vitro to in vivo. *Pharmaceutical Science & Technology Today*, **1999**. *2*, 365-372.
54. Zhang, P. and Wagner, E., History of Polymeric Gene Delivery Systems. *Topics in Current Chemistry*, **2017**. *375*, 26.
55. Pouton, C.W. and Seymour, L.W., Key issues in non-viral gene delivery. *Advanced Drug Delivery Reviews*, **2001**. *46*, 187-203.
56. Jones, C.H., Chen, C.-K., Ravikrishnan, A., Rane, S., and Pfeifer, B.A., Overcoming Nonviral Gene Delivery Barriers: Perspective and Future. *Molecular Pharmaceutics*, **2013**. *10*, 4082-4098.
57. Bus, T., Traeger, A., and Schubert, U.S., The great escape: how cationic polyplexes overcome the endosomal barrier. *Journal of Materials Chemistry B*, **2018**. *6*, 6904-6918.
58. Ogris, M. and Wagner, E., Targeting tumors with non-viral gene delivery systems. *Drug Discovery Today*, **2002**. *7*, 479-485.
59. Gonçalves, S.d.Á. and Vieira, R.P., Current status of ATRP-based materials for gene therapy. *Reactive and Functional Polymers*, **2020**. *147*, 104453.
60. Elsabahy, M. and Wooley, K.L., Design of polymeric nanoparticles for biomedical delivery applications. *Chemical Society Reviews*, **2012**. *41*, 2545-2561.

61. Xu, F.J. and Yang, W.T., Polymer vectors via controlled/living radical polymerization for gene delivery. *Progress in Polymer Science*, **2011**. *36*, 1099-1131.
62. Chu, D.S.H., Schellinger, J.G., Shi, J., Convertine, A.J., Stayton, P.S., and Pun, S.H., Application of Living Free Radical Polymerization for Nucleic Acid Delivery. *Accounts of Chemical Research*, **2012**. *45*, 1089-1099.
63. Heath, W.H., Senyurt, A.F., Layman, J., and Long, T.E., Charged Polymers via Controlled Radical Polymerization and their Implications for Gene Delivery. *Macromolecular Chemistry and Physics*, **2007**. *208*, 1243-1249.
64. Liu, Z., Zhang, Z., Zhou, C., and Jiao, Y., Hydrophobic modifications of cationic polymers for gene delivery. *Progress in Polymer Science*, **2010**. *35*, 1144-1162.
65. Chen, J., Wang, K., Wu, J., Tian, H., and Chen, X., Polycations for Gene Delivery: Dilemmas and Solutions. *Bioconjugate Chemistry*, **2018**. *30*, 338-349.
66. Kost, J. and Langer, R., Responsive polymeric delivery systems. *Advanced Drug Delivery Reviews*, **2012**. *64*, 327-341.
67. Ganta, S., Devalapally, H., Shahiwala, A., and Amiji, M., A review of stimuli-responsive nanocarriers for drug and gene delivery. *Journal of Controlled Release*, **2008**. *126*, 187-204.
68. Lind, M.J., Principles of cytotoxic chemotherapy. *Medicine*, **2011**. *39*, 711-716.
69. Dash, T.K. and Konkimalla, V.B., Poly-ϵ-caprolactone based formulations for drug delivery and tissue engineering: A review. *Journal of Controlled Release*, **2012**. *158*, 15-33.
70. Lombardo, D., Kiselev, M.A., and Caccamo, M.T., Smart Nanoparticles for Drug Delivery Application: Development of Versatile Nanocarrier Platforms in Biotechnology and Nanomedicine. *Journal of Nanomaterials*, **2019**. *2019*, 1-26.
71. Patra, J.K., Das, G., Fraceto, L.F., Campos, E.V.R., Rodriguez-Torres, M.d.P., Acosta-Torres, L.S., Diaz-Torres, L.A., Grillo, R., Swamy, M.K., Sharma, S., Habtemariam, S., and Shin, H.-S., Nano based drug delivery systems: recent developments and future prospects. *Journal of Nanobiotechnology*, **2018**. *16*, 71.
72. Dhanka, M., Shetty, C., and Srivastava, R., Injectable methotrexate loaded polycaprolactone microspheres: Physicochemical characterization, biocompatibility, and hemocompatibility evaluation. *Materials Science and Engineering: C*, **2017**. *81*, 542-550.
73. Dhanka, M., Shetty, C., and Srivastava, R., Methotrexate loaded alginate microparticles and effect of Ca 2+ post-crosslinking: An in vitro physicochemical and biological evaluation. *International Journal of Biological Macromolecules*, **2018**. *110*, 294-307.
74. Dhanka, M., Shetty, C., and Srivastava, R., Methotrexate loaded gellan gum microparticles for drug delivery. *International Journal of Biological Macromolecules*, **2018**. *110*, 346-356.
75. Mailander, V., and Landfester, K., Interaction of Nanoparticles with Cells. *Biomacromolecules*, **2009**. *10*, 2379–2400.
76. Hoshyar, N., Gray, S., Han, H., and Bao, G., The effect of nanoparticle size on in vivo pharmacokinetics and cellular interaction. *Nanomedicine (Lond)*, **2016**. *11*, 673–692.
77. Wei, Y., Quan, L., Zhou, C., and Zhan, Q., Factors relating to the biodistribution & clearance of nanoparticles & their effects on in vivo application. *Nanomedicine (Lond.)* **2018**. *13*, 1495–1512.

78. Jindal, A.B., The effect of particle shape on cellular interaction and drug delivery applications of micro- and nanoparticles. *International Journal of Pharmaceutics*, **2017**. *532*, 450-465.
79. Tannock, I.F. and Rotin, D., Acid pH in Tumors and Its Potential for Therapeutic Exploitation. *Perspectives in Cancer Research*, **1989**. *49*, 4373-4384.
80. Griffiths, J.R., Are cancer cells acidic? *British Journal of Cancer*, **1991**. *64*, 425-427.
81. Kato, Y., Ozawa, S., Miyamoto, C., Maehata, Y., Suzuki, A., Maeda, T., and Baba, Y., Acidic extracellular microenvironment and cancer. *Cancer Cell International*, **2013**. *13*, 89.
82. Kocak, G., Tuncer, C., and Bütün, V., pH-Responsive polymers. *Polymer Chemistry*, **2017**. *8*, 144-176.
83. Jazani, A.M. and Oh, J.K., Development and disassembly of single and multiple acid-cleavable block copolymer nanoassemblies for drug delivery. *Polymer Chemistry*, **2020**. *11*, 2934-2954.
84. Park, I.-K., Singha, K., Arote, R.B., Choi, Y.-J., Kim, W.J., and Cho, C.-S., pH-Responsive Polymers as Gene Carriers. *Macromolecular Rapid Communications*, **2010**. *31*, 1122-1133.
85. Guan, X., Guo, Z., Wang, T., Lin, L., Chen, J., Tian, H., and Chen, X., A pH-Responsive Detachable PEG Shielding Strategy for Gene Delivery System in Cancer Therapy. *Biomacromolecules*, **2017**. *18*, 1342-1349.
86. Yang, Y.-Y., Hu, H., Wang, X., Yang, F., Shen, H., Xu, F.-J., and Wu, D.-C., Acid-Labile Poly(glycidyl methacrylate)-Based Star Gene Vectors. *ACS Applied Materials & Interfaces*, **2015**. *7*, 12238-12248.
87. Leber, N., Kaps, L., Aslam, M., Schupp, J., Brose, A., Schäffel, D., Fischer, K., Diken, M., Strand, D., Koynov, K., Tuettenberg, A., Nuhn, L., Zentel, R., and Schuppan, D., SiRNA-mediated in vivo gene knockdown by acid-degradable cationic nanohydrogel particles. *Journal of Controlled Release*, **2017**. *248*, 10-23.
88. Kim, J., Lee, Y.M., Kim, H., Park, D., Kim, J., and Kim, W.J., Phenylboronic acid-sugar grafted polymer architecture as a dual stimuli-responsive gene carrier for targeted anti-angiogenic tumor therapy. *Biomaterials*, **2016**. *75*, 102-111.
89. Tang, H., Zhao, W., Yu, J., Li, Y., and Zhao, C., Recent Development of pH-Responsive Polymers for Cancer Nanomedicine. *Molecules*, **2018**. *24*, 4.
90. Varkouhi, A.K., Scholte, M., Storm, G., and Haisma, H.J., Endosomal escape pathways for delivery of biologicals. *Journal of Controlled Release*, **2011**. *151*, 220-228.
91. Ye, M., Wang, Y., Zhao, Y., Xie, R., Yodsanit, N., Johnston, K., and Gong, S., Double-Network Nanogel as a Nonviral Vector for DNA Delivery. *ACS Applied Materials & Interfaces*, **2019**. *11*, 42865-42872.
92. Cheng, Y., Sellers, D.L., Tan, J.-K.Y., Peeler, D.J., Horner, P.J., and Pun, S.H., Development of switchable polymers to address the dilemma of stability and cargo release in polycationic nucleic acid carriers. *Biomaterials*, **2017**. *127*, 89-96.
93. Cheng, Y., Yumul, R.C., and Pun, S.H., Virus-Inspired Polymer for Efficient In Vitro and In Vivo Gene Delivery. *Angewandte Chemie (International Ed.)*, **2016**. *55*, 1-6.
94. Guo, A., Wang, Y., Xu, S., Zhang, X., Li, M., Liu, Q., Shen, Y., Cui, D., and Guo, S., Preparation and evaluation of pH -responsive charge-convertible ternary complex FA-PEI-CCA/PEI/DNA with low cytotoxicity and efficient gene delivery. *Colloids and Surfaces B: Biointerfaces*, **2017**. *152*, 58-67.

95. Ooi, Y.J., Wen, Y., Zhu, J., Song, X., and Li, J., Surface Charge Switchable Polymer/DNA Nanoparticles Responsive to Tumor Extracellular pH for Tumor-Triggered Enhanced Gene Delivery. *Biomacromolecules*, **2020**. *21*, 1136-1148.
96. Quinn, J.F., Whittaker, M.R., and Davis, T.P., Glutathione responsive polymers and their application in drug delivery systems. *Polymer Chemistry*, **2017**. *8*, 97-126.
97. Russo, A., DeGraff, W., Friedman, N., and Mitchell, J.B., Selective Modulation of Glutathione Levels in Human Normal versus Tumor Cells and Subsequent Differential Response to Chemotherapy Drugs. *Basic Sciences*, **1986**. *46*, 2845-2848.
98. Kuppusamy, P., Li, H., Ilangovan, G., Cardounel, A.J., Zweier, J.L., Yamada, K., Krishna, M.C., and Mitchell, J.B., Noninvasive imaging of tumor redox status and its modification by tissue glutathione levels. *Cancer research*, **2002**. *62*, 307-312.
99. Saito, G., Swanson, J.A., and Lee, K.D., Drug delivery strategy utilizing conjugation via reversible disulfide linkages: role and site of cellular reducing activities. *Advanced Drug Delivery Reviews*, **2003**. *55*, 199-215.
100. Kim, T.-i. and Kim, S.W., Bioreducible polymers for gene delivery. *Reactive and Functional Polymers*, **2011**. *71*, 344-349.
101. Ullah, I., Zhao, J., Rukh, S., Muhammad, K., Guo, J., Ren, X.-k., Xia, S., Zhang, W., and Feng, Y., A PEG-b-poly(disulfide-l-lysine) based redox-responsive cationic polymer for efficient gene transfection. *Journal of Materials Chemistry B*, **2019**. *7*, 1893-1905.
102. Peng, Y.-Y., Diaz-Dussan, D., Kumar, P., and Narain, R., Tumor Microenvironment-Regulated Redox Responsive Cationic Galactose-Based Hyperbranched Polymers for siRNA Delivery. *Bioconjugate Chemistry*, **2019**. *30*, 405-412.
103. Gao, Y., Böhmer, V.I., Zhou, D., Zhao, T., Wang, W., and Paulusse, J.M.J., Main-chain degradable single-chain cyclized polymers as gene delivery vectors. *Journal of Controlled Release*, **2016**. *244*, 375-383.
104. Kang, Y., Lu, L., Lan, J., Ding, Y., Yang, J., Zhang, Y., Zhao, Y., Zhang, T., and Ho, R.J.Y., Redox-responsive polymeric micelles formed by conjugating gambogic acid with bioreducible poly(amido amine)s for the co-delivery of docetaxel and MMP-9 shRNA. *Acta Biomaterialia*, **2018**. *68*, 137-153.
105. Jiang, Z., Cui, W., Prasad, P., Touve, M.A., Gianneschi, N.C., Mager, J., and Thayumanavan, S., Bait-and-Switch Supramolecular Strategy To Generate Noncationic RNA–Polymer Complexes for RNA Delivery. *Biomacromolecules*, **2018**. *20*, 435-442.
106. Wang, Y., Ma, B., Abdeen, A.A., Chen, G., Xie, R., Saha, K., and Gong, S., Versatile Redox-Responsive Polyplexes for the Delivery of Plasmid DNA, Messenger RNA, and CRISPR-Cas9 Genome-Editing Machinery. *ACS Applied Materials & Interfaces*, **2018**. *10*, 31915-31927.
107. Wang, G., Zhu, D., Zhou, Z., Piao, Y., Tang, J., and Shen, Y., Glutathione-Specific and Intracellularly Labile Polymeric Nanocarrier for Efficient and Safe Cancer Gene Delivery. *ACS Applied Materials & Interfaces*, **2020**. *12*, 14825-14838.
108. Perillo, B., Di Donato, M., Pezone, A., Di Zazzo, E., Giovannelli, P., Galasso, G., Castoria, G., and Migliaccio, A., ROS in cancer therapy: the bright side of the moon. *Experimental & Molecular Medicine*, **2020**. *52*, 192-203.
109. Yang, H., Villani, R.M., Wang, H., Simpson, M.J., Roberts, M.S., Tang, M., and Liang, X., The role of cellular reactive oxygen species in cancer chemotherapy. *Journal of Experimental & Clinical Cancer Research*, **2018**. *37*, 266.

110. Aggarwal, V., Tuli, H.S., Varol, A., Thakral, F., Yerer, M.B., Sak, K., Varol, M., Jain, A., Khan, M.A., and Sethi, G., Role of Reactive Oxygen Species in Cancer Progression: Molecular Mechanisms and Recent Advancements. *Biomolecules*, **2019**. *9*, 735.
111. Li, S., Chen, B., Qu, Y., Yan, X., Wang, W., Ma, X., Wang, B., Liu, S., and Yu, X., ROS-Response-Induced Zwitterionic Dendrimer for Gene Delivery. *Langmuir*, **2018**. *35*, 1613-1620.
112. Fang, H., Chen, J., Lin, L., Liu, F., Tian, H., and Chen, X., A Strategy of Killing Three Birds with One Stone for Cancer Therapy through Regulating the Tumor Microenvironment by H2O2-Responsive Gene Delivery System. *ACS Applied Materials & Interfaces*, **2019**. *11*, 47785-47797.
113. Lincet, H. and Icard, P., How do glycolytic enzymes favour cancer cell proliferation by nonmetabolic functions? *Oncogene*, **2014**. *34*, 3751-3759.
114. Dong, H., Pang, L., Cong, H., Shen, Y., and Yu, B., Application and design of esterase-responsive nanoparticles for cancer therapy. *Drug Delivery*, **2019**. *26*, 416-432.
115. Kessenbrock, K., Plaks, V., and Werb, Z., Matrix Metalloproteinases: Regulators of the Tumor Microenvironment. *Cell*, **2010**. *141*, 52-67.
116. Qiu, N., Liu, X., Zhong, Y., Zhou, Z., Piao, Y., Miao, L., Zhang, Q., Tang, J., Huang, L., and Shen, Y., Esterase-Activated Charge-Reversal Polymer for Fibroblast-Exempt Cancer Gene Therapy. *Advanced Materials*, **2016**. *28*, 10613-10622.
117. Zhang, H., Huang, J.-J., Wang, J., Hu, M., Chen, X.-c., Sun, W., Ren, K.-f., and Ji, J., Surface-Mediated Stimuli-Responsive Gene Delivery Based on Breath Figure Film Combined with Matrix Metalloproteinase-Sensitive Hydrogel. *ACS Biomaterials Science & Engineering*, **2019**. *5*, 6610-6616.
118. Fischer, D., Li, Y., Ahlemeyer, B., Krieglstein, J. and Kissel, T., In vitro cytotoxicity testing of polycations: influence of polymer structure on cell viability and hemolysis. *Biomaterials*, **2003**. *24*, 1121-1131.
119. Incani, V., Lavasanifar, A., and Uludağ, H., Lipid and hydrophobic modification of cationic carriers on route to superior gene vectors. *Soft Matter*, **2010**. *6*, 2124-2138.
120. Fan, X., Jiang, S., Li, Z., and Loh, X.J., Conjugation of poly(ethylene glycol) to poly(lactide)-based polyelectrolytes: An effective method to modulate cytotoxicity in gene delivery. *Materials Science and Engineering: C*, **2017**. *73*, 275-284.
121. Cheng, H., Fan, X., Wu, C., Wang, X., Wang, L.-J., Loh, X.J., Li, Z., and Wu, Y.-L., Cyclodextrin-Based Star-Like Amphiphilic Cationic Polymer as a Potential Pharmaceutical Carrier in Macrophages. *Macromolecular Rapid Communications*, **2019**. *40*, 1800207.
122. Nelson, C.E., Kintzing, J.R., Hanna, A., Shannon, J.M., Gupta, M.K., and Duvall, C.L., Balancing Cationic and Hydrophobic Content of PEGylated siRNA Polyplexes Enhances Endosome Escape, Stability, Blood Circulation Time, and Bioactivity in Vivo. *ACS Nano*, **2013**. *7*, 8870-8880.
123. Werfel, T.A., Jackson, M.A., Kavanaugh, T.E., Kirkbride, K.C., Miteva, M., Giorgio, T.D., and Duvall, C., Combinatorial optimization of PEG architecture and hydrophobic content improves ternary siRNA polyplex stability, pharmacokinetics, and potency in vivo. *Journal of Controlled Release*, **2017**. *255*, 12-26.
124. Teo, P.Y., Yang, C., Hedrick, J.L., Engler, A.C., Coady, D.J., Ghaem-Maghami, S., George, A.J.T., and Yang, Y.Y., Hydrophobic modification of low molecular weight polyethylenimine for improved gene transfection. *Biomaterials*, **2013**. *34*, 7971-7979.

125. Thapa, B., Plianwong, S., Remant Bahadur, K.C., Rutherford, B., and Uludağ, H., Small hydrophobe substitution on polyethylenimine for plasmid DNA delivery: Optimal substitution is critical for effective delivery. *Acta Biomaterialia*, **2016**. *33*, 213-224.
126. Wilson, R.C. and Doudna, J.A., Molecular Mechanisms of RNA Interference. *Annual Review of Biophysics*, **2013**. *42*, 217-239.
127. Wittrup, A. and Lieberman, J., Knocking down disease: a progress report on siRNA therapeutics. *Nature Reviews Genetics*, **2015**. *16*, 543-552.
128. Kozielski, K.L., Tzeng, S.Y., and Green, J.J., Bioengineered nanoparticles for siRNA delivery. *Wiley Interdisciplinary Reviews: Nanomedicine and Nanobiotechnology*, **2013**. *5*, 449-468.
129. Kanasty, R., Dorkin, J.R., Vegas, A., and Anderson, D., Delivery materials for siRNA therapeutics. *Nature Materials*, **2013**. *12*, 967-977.
130. Castanotto, D. and Rossi, J.J., The promises and pitfalls of RNA-interference-based therapeutics. *Nature*, **2009**. *457*, 426-433.
131. Oliveira, S., Storm, G., and Schiffelers, R.M., Targeted Delivery of siRNA. *Journal of Biomedicine and Biotechnology*, **2006**. *2006*, 1-9.
132. Wagner, E., Polymers for siRNA Delivery: Inspired by Viruses to be Targeted, Dynamic, and Precise. *Accounts of Chemical Research*, **2011**. *45*, 1005-1013.
133. Verma, I.M. and Somia, N., Gene therapy—promises, problems and prospects. *Nature* **1997**. *389*, 239–242.
134. Thomas, C.E., Ehrhardt, A., and Kay, M.A., Progress and problems with the use of viral vectors for gene therapy. *Nature Reviews Genetics*, **2003**. *4*, 346-358.
135. Gao, K. and Huang, L., Nonviral Methods for siRNA Delivery. *Molecular Pharmaceutics*, **2008**. *6*, 651-658.
136. David, S., Pitard, B., Benoît, J.-P., and Passirani, C., Non-viral nanosystems for systemic siRNA delivery. *Pharmacological Research*, **2010**. *62*, 100-114.
137. Pack, D.W., Hoffman, A.S., Pun, S., and Stayton, P.S., Design and development of polymers for gene delivery. *Nature Reviews Drug Discovery*, **2005**. *4*, 581-593.
138. De Smedt, S.C., Demeester, J., and Hennink, W.E., Cationic Polymer Based Gene Delivery Systems. *Pharmaceutical Research*, **2000**. *17*, 113–126.
139. Gary, D.J., Puri, N., and Won, Y.-Y., Polymer-based siRNA delivery: Perspectives on the fundamental and phenomenological distinctions from polymer-based DNA delivery. *Journal of Controlled Release*, **2007**. *121*, 64-73.
140. Kim, W.J. and Kim, S.W., Efficient siRNA Delivery with Non-viral Polymeric Vehicles. *Pharmaceutical Research*, **2008**. *26*, 657-666.
141. Nishikawa, M. and Huang, L., Nonviral Vectors in the New Millennium: Delivery Barriers in Gene Transfer. *HUMAN GENE THERAPY*, **2001**. *12*, 861–870.
142. Wagner, E., Polymers for Nucleic Acid Transfer—An Overview. **2014**. *88*, 231-261.
143. Fang, J., Sawa, T., and Maeda, H., *Factors and Mechanism of "EPR" Effect and the Enhanced Antitumor Effects of Macromolecular Drugs Including SMANCS*, in *Polymer Drugs in the Clinical Stage. Advances in Experimental Medicine and Biology* H. Maeda, et al., Editors. 2004, Springer: Boston, MA.
144. Greish, K., Fang, J., Inutsuka, T., Nagamitsu, A., and Maeda, H., Macromolecular Therapeutics Advantages and Prospects with Special Emphasis on Solid Tumour Targeting. *Clinical Pharmacokinetics*, **2003**. *42*, 1089-1105.

145. Maeda, H., The enhanced permeability and retention (EPR) effect in tumor vasculature: the key role of tumor-selective macromolecular drug targeting. *Advances in Enzyme Regulation*, **2001**. *41*, 189-207.
146. Luten, J., van Nostrum, C.F., De Smedt, S.C., and Hennink, W.E., Biodegradable polymers as non-viral carriers for plasmid DNA delivery. *Journal of Controlled Release*, **2008**. *126*, 97-110.
147. Pannier, A.K. and Shea, L.D., Controlled release systems for DNA delivery. *Molecular Therapy*, **2004**. *10*, 19-26.
148. Shim, M.S. and Kwon, Y.J., Stimuli-responsive polymers and nanomaterials for gene delivery and imaging applications. *Advanced Drug Delivery Reviews*, **2012**. *64*, 1046-1059.
149. Rapoport, N., Physical stimuli-responsive polymeric micelles for anti-cancer drug delivery. *Progress in Polymer Science*, **2007**. *32*, 962-990.
150. Kaur, S., Prasad, C., Balakrishnan, B., and Banerjee, R., Trigger responsive polymeric nanocarriers for cancer therapy. *Biomaterials Science*, **2015**. *3*, 955-987.
151. Islam, M.A., Park, T.E., Singh, B., Maharjan, S., Firdous, J., Cho, M.-H., Kang, S.-K., Yun, C.-H., Choi, Y.J., and Cho, C.-S., Major degradable polycations as carriers for DNA and siRNA. *Journal of Controlled Release*, **2014**. *193*, 74-89.
152. Zhang, Q., Aleksanian, S., Noh, S.M., and Oh, J.K., Thiol-responsive block copolymer nanocarriers exhibiting tunable release with morphology changes. *Polym. Chem.*, **2013**. *4*, 351-359.
153. Maruya-Li, K., Shetty, C., Moini Jazani, A., Arezi, N., and Oh, J.K., Dual Reduction/Acid-Responsive Disassembly and Thermoresponsive Tunability of Degradable Double Hydrophilic Block Copolymer. *ACS Omega*, **2020**. *5*, 3734-3742.
154. Yañez-Macias, R., Alvarez-Moises, I., Perevyazko, I., Lezov, A., Guerrero-Santos, R., Schubert, U.S., and Guerrero-Sanchez, C., Effect of the Degree of Quaternization and Molar Mass on the Cloud Point of Poly[2-(dimethylamino)ethyl methacrylate] Aqueous Solutions: A Systematic Investigation. *Macromolecular Chemistry and Physics*, **2017**. *218*, 1700065.
155. Mislick, K.A. and Baldeschwieler, J.D., Evidence for the role of proteoglycans in cation-mediated gene transfer. *Proceedings of the National Academy of Sciences*, **1996**. *93*, 12349-12354.
156. Behr, J.P., Gene Transfer with Synthetic Cationic Amphiphiles: Prospects for Gene Therapy. *Bioconjugate Chemistry*, **1994**. *5*, 382-389.
157. Papagiannopoulos, A., Vlassi, E., Pispas, S., and Jafta, C.J., Tuning the solution organization of cationic polymers through interactions with bovine serum albumin. *Physical Chemistry Chemical Physics*, **2017** *19*, 18471-18480.
158. Parhamifar, L., Larsen, A.K., Hunter, A.C., Andresenc, T.L., and Moghimi, S.M., Polycation cytotoxicity: a delicate matter for nucleic acid therapy - focus on polyethylenimine. *Soft Matter*, **2010**. *6*, 4001-4009.
159. Thomas, M. and Klibanov, A.M., Non-viral gene therapy: polycation-mediated DNA delivery. *Applied Microbiology and Biotechnology*, **2003**. *62*, 27-34.
160. Martens, T.F., Remaut, K., Demeester, J., De Smedt, S.C., and Braeckmans, K., Intracellular delivery of nanomaterials: How to catch endosomal escape in the act. *Nano Today*, **2014**. *9*, 344-364.

161. Ma, D., Enhancing endosomal escape for nanoparticle mediated siRNA delivery. *Nanoscale*, **2014**. *6*, 6415.
162. Gong, J., Chen, M., Zheng, Y., Wang, S., and Wang, Y., Polymeric micelles drug delivery system in oncology. *Journal of Controlled Release*, **2012**. *159*, 312-323.
163. Lu, Y. and Park, K., Polymeric micelles and alternative nanonized delivery vehicles for poorly soluble drugs. *International Journal of Pharmaceutics*, **2013**. *453*, 198-214.
164. Mikhail, A.S. and Allen, C., Block copolymer micelles for delivery of cancer therapy: Transport at the whole body, tissue and cellular levels. *Journal of Controlled Release*, **2009**. *138*, 214-223.
165. Masood, F., Polymeric nanoparticles for targeted drug delivery system for cancer therapy. *Materials Science and Engineering: C*, **2016**. *60*, 569-578.
166. Guo, X., Wang, L., Wei, X., and Zhou, S., Polymer-based drug delivery systems for cancer treatment. *Journal of Polymer Science Part A: Polymer Chemistry*, **2016**. *54*, 3525-3550.
167. Duncan, R., The dawning era of polymer therapeutics. *Nature Reviews Drug Discovery*, **2003**. *2*, 347-360.
168. Wang, C.E., Stayton, P.S., Pun, S.H., and Convertine, A.J., Polymer nanostructures synthesized by controlled living polymerization for tumor-targeted drug delivery. *Journal of Controlled Release*, **2015**. *219*, 345-354.
169. Rodrigues, P.R. and Vieira, R.P., Advances in atom-transfer radical polymerization for drug delivery applications. *European Polymer Journal*, **2019**. *115*, 45-58.
170. Li, M.-H. and Keller, P., Stimuli-responsive polymer vesicles. *Soft Matter*, **2009**. *5*, 927-937.
171. Mura, S., Nicolas, J., and Couvreur, P., Stimuli-responsive nanocarriers for drug delivery. *Nature Materials*, **2013**. *12*, 991-1003.
172. Stuart, M., Huck, W., Genzer, J., Müller, M., Ober, C., Stamm, M., Sukhorukov, G., Szleifer, I., Tsukruk, V., Urban, M., Winnik, F., Zauscher, S., Luzinov, I., and Minko, S., Emerging applications of stimuli-responsive polymer materials. *Nature Materials*, **2010**. *9*, 101-113.
173. Wei, M., Gao, Y., Li, X., and Serpe, M.J., Stimuli-responsive polymers and their applications. *Polymer Chemistry*, **2017**. *8*, 127-143.
174. Yuan, D., He, H., Wu, Y., Fan, J., and Cao, Y., Physiologically Based Pharmacokinetic Modeling of Nanoparticles. *Journal of Pharmaceutical Sciences*, **2019**. *108*, 58-72.
175. Bawa, K.K., Jazani, A.M., Shetty, C., and Oh, J.K., PLA-Based Triblock Copolymer Micelles Exhibiting Dual Acidic pH/Reduction Responses at Dual Core and Core/Corona Interface Locations. *Macromolecular Rapid Communications*, **2018**. *39*, 1800477.
176. Uhrich, K.E., Cannizzaro, S.M., Langer, R.S., and Shakesheff, K.M., Polymeric Systems for Controlled Drug Release. *Chemical Reviews*, **1999**. *99*, 3181-3198.
177. Dechy-Cabaret, O., Martin-Vaca, B. and Bourissou, D., Controlled Ring-Opening Polymerization of Lactide and Glycolide. *Chemical Reviews*, **2004**. *104*, 6147-6176.
178. Jazani, A.M., Arezi, N., Shetty, C., Hong, S.H., Li, H., Wang, X., and Oh, J.K., Tumor-targeting intracellular drug delivery based on dual acid/reduction-degradable nanoassemblies with ketal interface and disulfide core locations. *Polymer Chemistry*, **2019**. *10*, 2840-2853.
179. Präbst, K., Engelhardt, H., Ringgeler, S., and Hübner, H., Basic Colorimetric Proliferation Assays: MTT, WST, and Resazurin, in *Cell Viability Assays: Methods and Protocols*, D.F. Gilbert, and Friedrich, O., Editor, Springer Nature.

180. Riss, T.L., Moravec, R.A., Niles, A.L., Duellman, S., Benink, H.A., Worzella, T.J., and Minor, L., Cell Viability Assay, in *Assay Guidance Manual*, C.N. Sittampalam G.S., Brimacombe K., et al., Editor. 2013, Eli Lilly & Company and the National Center for Advancing Translational Sciences: Bethesda (MD).
181. Li-Ying Chan, L., McCulley, K. J. and Kessel, S. L., Assessment of Cell Viability with Single-, Dual-,and Multi-Staining Methods Using Image Cytometry, in *Cell Viability Assays: Methods and Protocols*, D.F. Gilbert, and Friedrich, O., Editor, Springer Nature.
182. Decherchi, P., Cochard, P., and Gauthier, P., Dual staining assessment of Schwann cell viability within whole peripheral nerves using calcein-AM and ethidium homodimer. *Journal of Neuroscience Methods*, **1997**. *71*, 205-213.
183. Adjei, I.M., Sharma, B., and Labhasetwar, V., Nanoparticles: Cellular Uptake and Cytotoxicity, in *Nanomaterial. Advances in Experimental Medicine and Biology*, C.Y. Capco D., Editor. 2014, Springer: Dordrecht. p. 73-91.
184. Goegan, P., Johnson, G. and Vincent, R., Effects of Serum Protein and Colloid on the AlamarBlue Assay in Cell Cultures. *Toxic. in Vitro*, **1995**. *9*, 257-266.
185. Aslantürk, Ö.S., In Vitro Cytotoxicity and Cell Viability Assays: Principles, Advantages, and Disadvantages, in *Genotoxicity - A Predictable Risk to Our Actual World*, Larramendy, M. L. and Soloneski, S., Editor. 2018, IntechOpen.
186. Riss, T.L., Moravec, R.A., and Niles, A.L., Cytotoxicity Testing: Measuring Viable Cells, Dead Cells, and Detecting Mechanism of Cell Death. **2011**. *740*, 103-114.
187. Behzadi, S., Serpooshan, V., Tao, W., Hamaly, M.A., Alkawareek, M.Y., Dreaden, E.C., Brown, D., Alkilany, A.M., Farokhzad, O.C., and Mahmoudi, M., Cellular uptake of nanoparticles: journey inside the cell. *Chemical Society Reviews*, **2017**. *46*, 4218-4244.
188. Foroozandeh, P. and Aziz, A.A., Insight into Cellular Uptake and Intracellular Trafficking of Nanoparticles. *Nanoscale Research Letters*, **2018**. *13*, 339.
189. Drasler, B., Vanhecke, D., Rodriguez-Lorenzo, L., Petri-Fink, A., and Rothen-Rutishauser, B., Quantifying nanoparticle cellular uptake: which method is best? *Nanomedicine (Lond)*, **2017**. *12*, 1095–1099.
190. Schnur, J.M., dos Santos, T., Varela, J., Lynch, I., Salvati, A., and Dawson, K.A., Effects of Transport Inhibitors on the Cellular Uptake of Carboxylated Polystyrene Nanoparticles in Different Cell Lines. *PLoS ONE*, **2011**. *6*, e24438.
191. Vercauteren, D., Vandenbroucke, R.E., Jones, A.T., Rejman, J., Demeester, J., De Smedt, S.C., Sanders, N.N., and Braeckmans, K., The Use of Inhibitors to Study Endocytic Pathways of Gene Carriers: Optimization and Pitfalls. *Molecular Therapy*, **2010**. *18*, 561-569.
192. Rejman, J., Oberle, V., Zuhorn, S. I., and Hoekstra, D., Size-dependent internalization of particles via the pathways of clathrin- and caveolae-mediated endocytosis. *Biochemical Journal*, **2004**. *377*, 159-169.
193. Simpson, Smith, Thurecht, and Such, Engineered Polymeric Materials for Biological Applications: Overcoming Challenges of the Bio–Nano Interface. *Polymers*, **2019**. *11*, 1441.
194. Carrillo-Carrion, C., Carril, M., and Parak, W.J., Techniques for the experimental investigation of the protein corona. *Current Opinion in Biotechnology*, **2017**. *46*, 106-113.
195. Edward Semple, J., Sullivan, B., Vojkovsky, T., and Sill, K.N., Synthesis and facile end-group quantification of functionalized PEG azides. *Journal of Polymer Science Part A: Polymer Chemistry*, **2016**. *54*, 2888-2895.

196. Liu, M., Kono, K., and Frechet, J.M.J., Water-soluble dendritic unimolecular micelles: Their potential as drug delivery agents. *Journal of Controlled Release*, **2000**. *65*, 121-131.
197. Dong, J.-L., Yu, L.-S.-H., and Xie, J.-W., A Simple and Versatile Method for the Formation of Acetals/Ketals Using Trace Conventional Acids. *ACS Omega*, **2018**. *3*, 4974-4985.

Appendix A

Supporting Information and Figures for Chapter 3

A1. Synthesis of PEG-AC-Br

Figure A1.a shows the scheme for the synthesis of acid-labile acetal labeled PEG-AC-Br macroinitiator. In the first step, 2-vinyloxyethyl 2-bromoisobutyrate (VEBr) was synthesized by esterification of ethylene glycol vinyl ether (4 g, 45.3 mmol) with α-bromoisobutyryl bromide (11.5 g, 50 mmol) in presence of triethylamine (Et_3N, 5.5 g, 54.5 mmol) in DCM (200 mL). After a 5 hr reaction under vigorous stirring, the white precipitate was filtered and the organic solution was washed with brine (3 times). After washing, DCM was dried over anhydrous sodium sulfate followed by complete evaporation of solvent to afford a yellow oil. This step enabled the synthesis of VEBr with a high yield of about 98%. ^{1}H-NMR (Figure A1.c) shows signals corresponding to methyl protons (a) attached to the tertiary carbon at 1.93 ppm, methylene proton (b) next to the carboxyl group at 4.4 ppm, methylene proton (c) next to ether group at 3.94 ppm, vinyl protons (d, e, f) at 6.4-6.5, 4.0 and 4.2 ppm.

In the next step, PEG-AC-Br was synthesized by the reaction of the purified VEBr with PEG in the presence of pyridinium p-toluenesulfonate (PPTS). PEG (2 g, 0.4 mmol) purified by azeotropic distillation in anhydrous toluene (0.2 g/mL) was dissolved in anhydrous DCM (10 mL) along with PPTS (12 mg, 50 μmol). VEBr (2.844 g, 12 mmol) diluted with anhydrous DCM (5 mL) was then added dropwise into the above solution under vigorous stirring in an ice-bath. After stirring at room temperature for 48 hr, the reaction was terminated by the addition of Et_3N (0.14 mmol), and DCM (200 mL) was added to the reaction mixture. The reaction mixture was further washed 3 times with PBS. This step enabled the synthesis of PEG-AC-Br with a yield of about 78%. ^{1}H-NMR (Figure A1.b) shows the disappearance of signals corresponding to vinyl protons (d, e, f) and appearance of new signals corresponding to acetal protons (d', g) at 4.8 and 1.32 ppm, PEO (h) at 3.62 ppm and methoxy group (i) at 3.37 ppm.

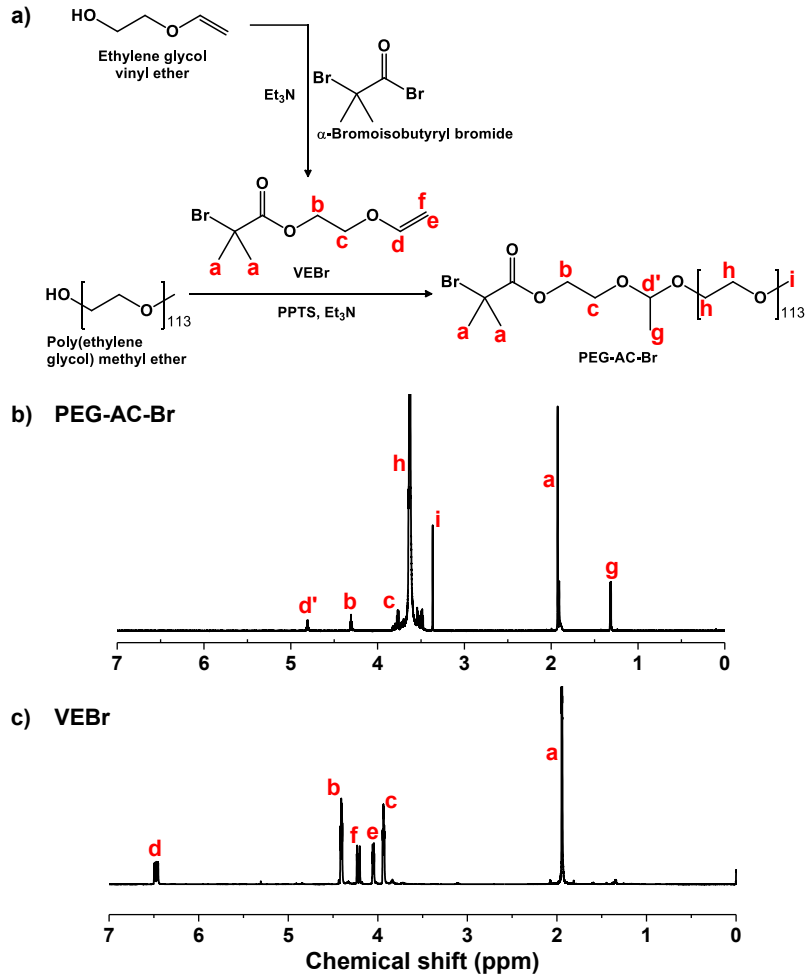

Figure A1. Synthesis **a)** and ^{1}H-NMR spectrum of PEG-AC-Br **b)**, compared with its precursor VEBr **c)**.

A2. Thermoresponsive nature of PDss

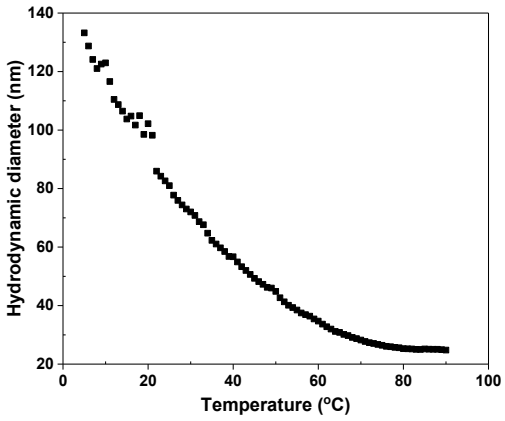

Figure A2. Thermoresponsive nature of PDss analysed by DLS.

Appendix B

Acid-labile Block Copolymer for Gene Delivery

B1. Synthesis of PEG-AC-PDMAEMA (PD) and its thermoresponsive nature

Figure B1.a shows the scheme for synthesis of PEG-AC-PDMAEMA (PD) by ATRP. Briefly, PEG-AC-Br (0.3 g, 57 μmol), DMAEMA (1 g, 6.87 mmol), $Cu(II)Br_2$/TPMA complex (1.5 mg, 3 μmol), TPMA (2.5 mg, 9 μmol) were dissolved in anisole (4.8 g) in a 10 mL Schlenk flask. The mixture was deoxygenated by purging under nitrogen for 1 hr and then placed in an oil bath preheated at 50 °C. A nitrogen pre-purged solution of $Sn(II)(EH)_2$ (9.3 mg, 0.23 mmol) dissolved in anisole (0.5 g) was injected to initiate polymerization and purged further for 30 mins. After 3 hrs, polymerization was stopped by cooling the reaction mixture in an ice bath and exposing it to air. For purification, the as-prepared polymer solutions were precipitated from hexane. The precipitate was then dissolved in THF and passed through a basic alumina column to remove residual copper species. After the removal of organic solvent by rotary evaporation at room temperature, the product was dried in a vacuum oven set at 50 °C for 12 hrs. The ^{1}H-NMR spectrum (Figure B1.b) shows signals corresponding to EO protons from PEO block at 3.6 - 3.7 ppm and methyl protons in the PDMAEMA units at 2.3 ppm. Using their integration ratios with the DP of PEG block = 113, the DP was found to be 86 for PDMAEMA. The GPC chromatograph (Figure B1.c) of PD shows a shift of molecular weight distribution to higher molecular weight region with no significant residual of PEG-AC-Br initiator.

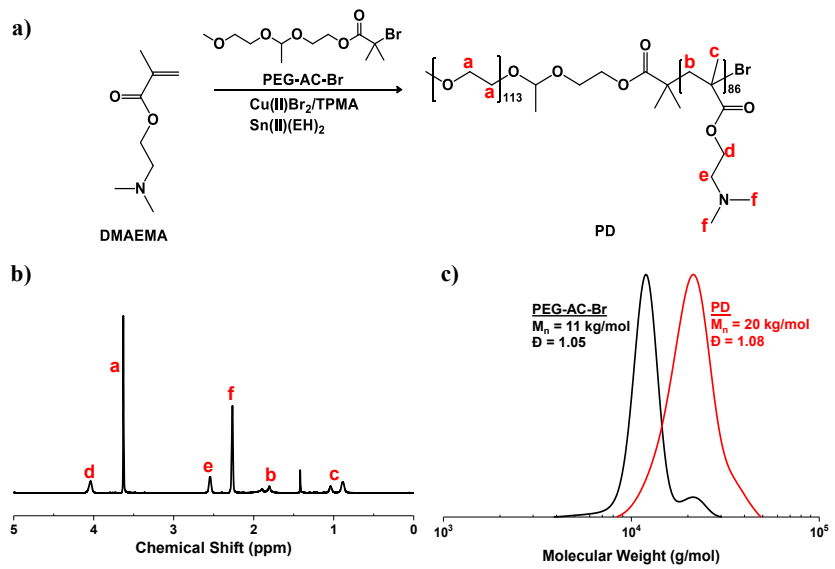

Figure B1. Synthesis by ATRP **a)**, ^{1}H-NMR spectra in $CDCl_3$ **b)**, and GPC trace **c)** of PD.

PBS solutions (1 mL) consisting of different amounts of PD (0.5, 1 and 3 mg) were transferred to a quartz cuvette and then sealed with a Teflon stopper. DLS was used to monitor a change in light scattering intensity at an increment of 1 °C/min in the temperature range of 25 - 90 °C. As seen in Figure B2.a, for PD (1 mg/mL) the normalized count rate stayed constant up to ~ 50 °C and then increased sharply at 56.4 °C, indicating the hydrophilic to hydrophobic transition of PDMAEMA block. Further, the temperature required for onset of transition was found to increase with a decrease in PD concentration (Figure B2.b).

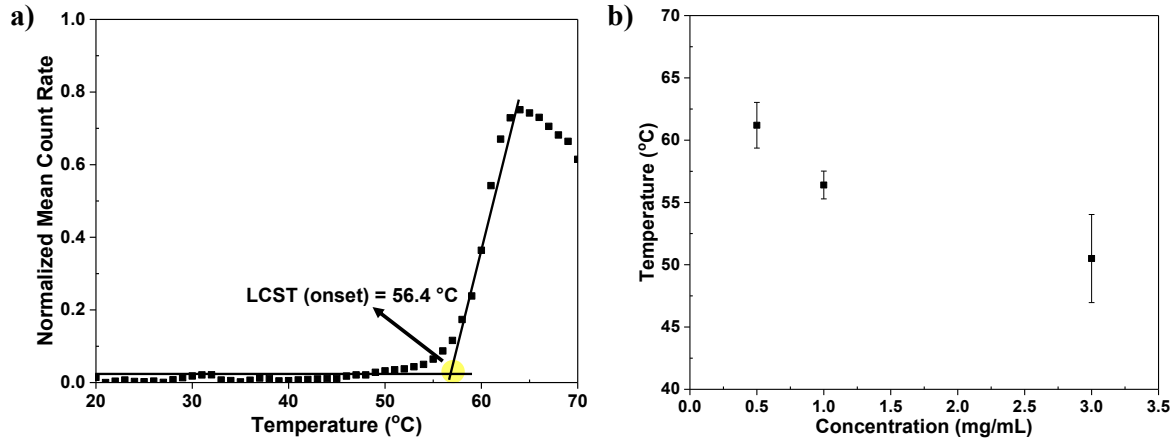

Figure B2. Evolution of light scattering intensity over temperature for PD (1 mg/mL) **a)** and LCST over PD concentration **b)** by DLS.

B2. Quaternization of PD with methyl iodide

Further, PD was partially quaternized by adding methyl iodide (30.3 mg, 0.2 mmol) diluted in THF (1 mL) to a solution of PD (100 mg, 6.3 µmol) in THF (2 mL) under stirring (Figure B3.a). The reaction was stirred overnight and the product was purified by evaporating the solvent to obtain a brown solid. ^{1}H-NMR spectrum (Figure B3.b) shows the appearance of new signals corresponding to methylene group (g) at 4.37 ppm and methyl groups (h) attached to quaternized amine at 3.24 ppm and thus confirms successful quaternization of PD. However, the GPC chromatograph (Figure B3.c) shows a shift of molecular weight distribution to lower molecular weight region coinciding with PEG-AC-Br. This suggests that acetal in unstable in the presence of methyl iodide leading to separation of two blocks. In order to verify if the acetal group could cleave in presence of methyl iodide, PEG-AC-Br (30 mg, 5.7 µmol) was dissolved in DMSO-d_6 and methyl iodide (0.19 mmol) was added dropwise to the above solution under stirring. After an overnight reaction, the product was characterized by ^{1}H-NMR, which showed a decrease in signal corresponding to the acetal proton and thereby confirming the instability of the acetal in the presence of methyl iodide.

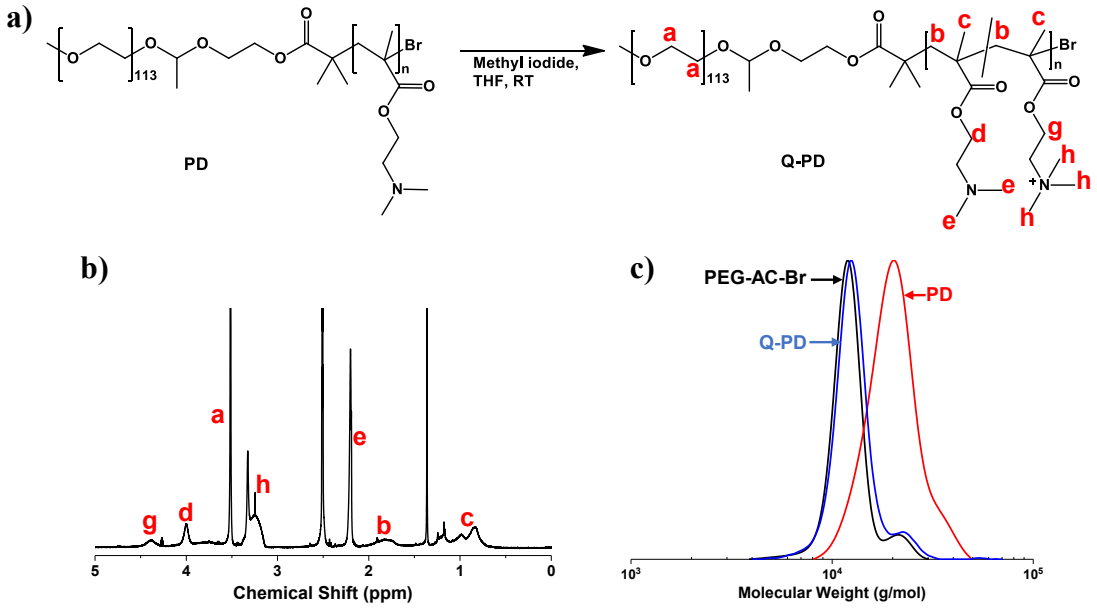

Figure B3. Scheme for quaternization of PD using methyl iodide **a)**, ^{1}H-NMR spectrum in DMSO-d_6 **b)** and GPC chromatograph **c)** of Q-PD.

B3. Complexation with nucleic acid

PD polyplexes were prepared in a similar way as PDss micelleplexes. Briefly, a series of aqueous dispersion containing different amounts of PD were mixed with an aqueous solution of dsDNA (0.36 nmol) in acetate buffer (3 μL, 10 mM, pH = 5) for 30 mins, and then PBS (3 μL, 20 mM, pH = 7.4) for 1 hrs under stirring, yielding a series of aqueous M-PD dispersions with various N/P ratios of 0.8, 1, 2, 4, 6, 8 and 10 at pH = 7.4. Their aliquots (8 μL) were mixed with glycerol (8 μL) for the electrophoresis assay. As shown in Figure B4, at N/P ratios ≥ 2/1, no stained band equivalent to free dsDNAs was present, suggesting that most dsDNA molecules are condensed to M-PD.

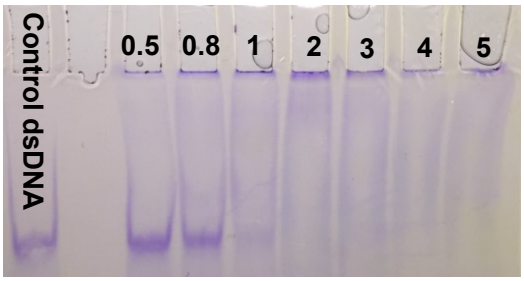

Figure B4. Evaluation of optimum N/P ratio for complete complexation by gel electrophoresis.

B4. Cytotoxicity and Endosomal escape

HeLa cells (10,000 cells/well) were seeded into a 96-well plate and incubated at 37 °C for 24 hrs. Cells were then treated with DMEM (100 μL) containing different concentrations of PD. Untreated cells were used as controls. After 48 hrs, the media was replaced with DMEM (100 μL) containing 10% Alamar Blue dye (0.15 mg/mL) and incubated at 37 °C for 4 hrs. Absorbance at 570 nm and 600 nm were recorded to calculate the cell viability. PD was found to be non-cytotoxic up to 150 μg/mL and cell viability decreased significantly above this concentration (Figure B5.a).

HeLa cells (50,000 cells/well) were seeded into a 4-well glass bottom plate and incubated at 37°C for 24 hrs. They were then incubated with Alexa Fluor-488 labelled dsDNA (100 nM) complexed with PD at N/P 10, then mixed with DMEM and added to each well. After 24 hrs, the media was replaced with phenol red free DMEM containing Lysotracker (75 nM) and Hoechst 33342 (36 μM). The cells were incubated in the dark for 1 hr before imaging with a Nikon Eclipse TiE inverted epifluorescence microscope. The captured images were processed using ImageJ software. As shown in Figure B5.b, M-PD was taken up by the cell, however the merging of Alexa

Fluor's green fluorescence with LysoTracker's red fluorescence suggests that M-PD were unable to escape the endosome.

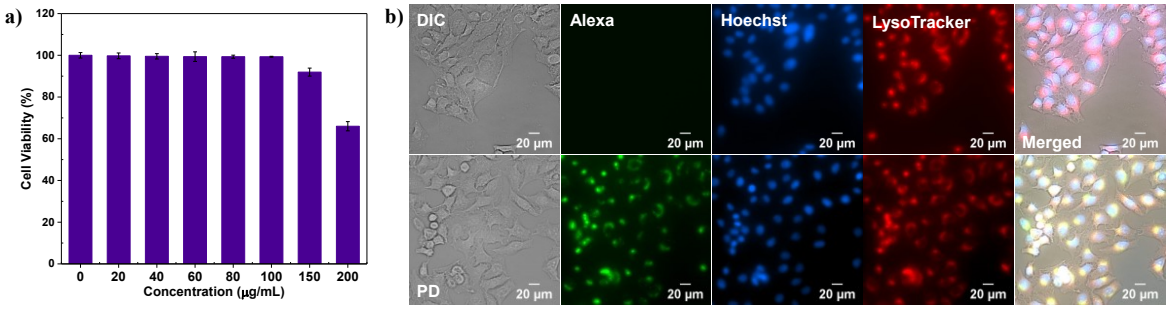

Figure B5. HeLa cell viability in presence of different concentrations of PD **a)** and fluorescence microscopy images of HeLa cells incubated with M-PD containing Alexa Fluor 488 tagged dsDNA (100 nM) compared to free Alexa Fluor tagged dsDNA after 24 hr **b).**